Flying V Landing Gear

The Kinematic Design and Weight Estimation of a Flying V Main Landing Gear

Marko Rehbein

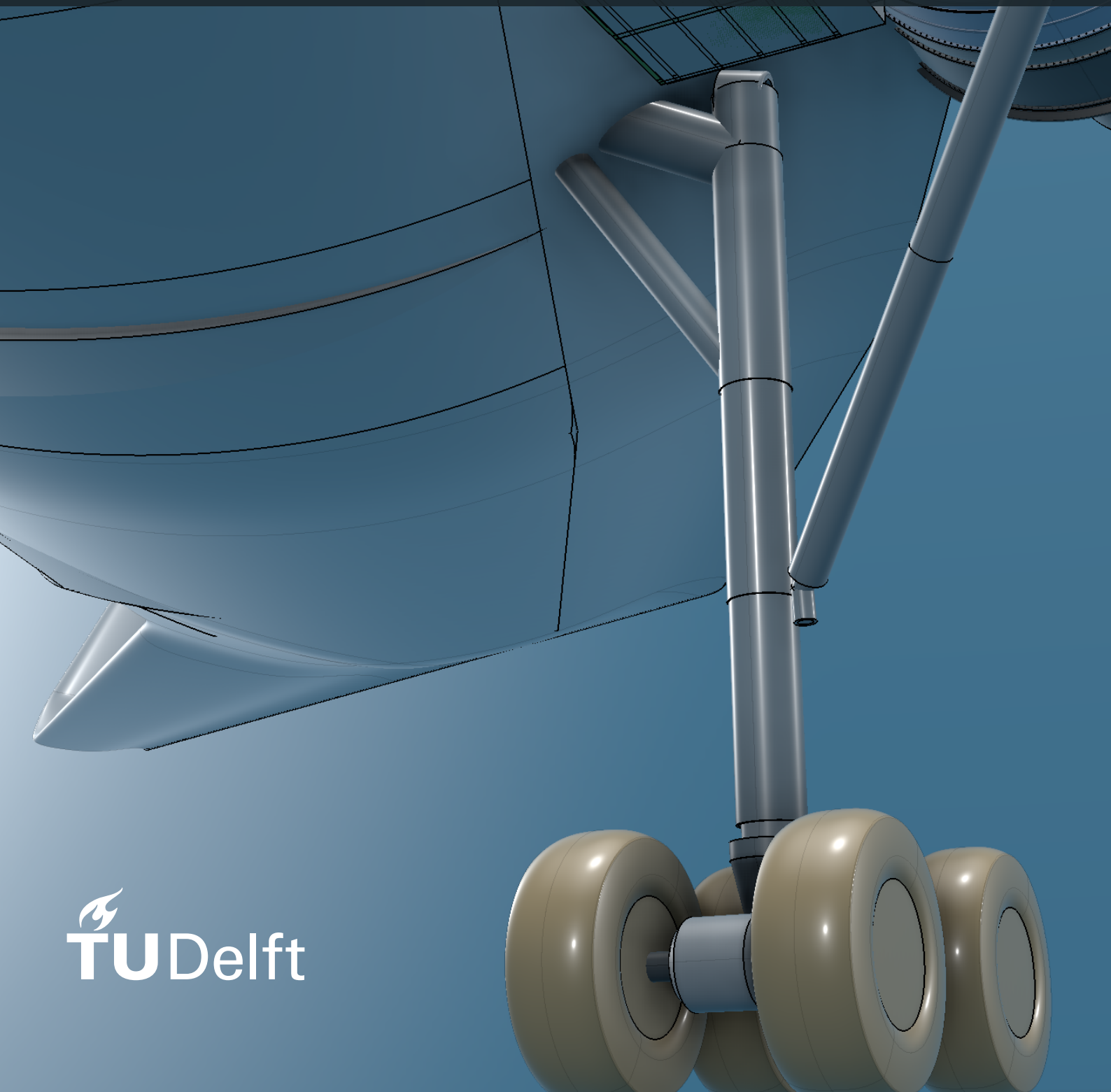

TU Delft

Flying V Landing Gear

The Kinematic Design and Weight Estimation of a Flying V Main Landing Gear

Thesis report

by

Marko Rehbein

to obtain the degree of Master of Science
at the Delft University of Technology
to be defended publicly on November 23, 2023 at 13:30

Supervisors:	Akira Ikenaga	(Airbus, Future Projects Office)
	Dr.ing. J. Benad	(TU Delft)
	Dr.ir. R. Vos	(TU Delft)
Thesis committee:		
Chair:	Dr.ir. R. Vos	(TU Delft)
External examiners:	Dr.ir. M.F.M. Hoogreef	(TU Delft)
	Dr.ir. JMJF van Campen	(TU Delft)
	Akira Ikenaga	(Airbus, Future Projects Office)
Place:	Faculty of Aerospace Engineering, Delft	
Project Duration:	March, 2022 - November, 2023	
Student number:	4460936	

An electronic version of this thesis is available at `http://repository.tudelft.nl/`.

Airbus Future Projects Office · Faculty of Aerospace Engineering · Delft University of Technology

Summary

At a time when there is a distinct drive for accelerated sustainability the Flying V is a promising new aircraft configuration with the potential for significantly higher efficiency than the current state-of-the-art. Since its inception in 2015, the Flying V aerodynamic and structural models have evolved to such depth as to enable detailed studies of system-level components such as the outer wing, winglets, cockpit and engine mounting structures among others. Up until this point the Landing Gear layout has been investigated at an aircraft-level yet there is limited knowledge on the systems integration with the surrounding environment. Given that the landing gear is a safety-critical component that makes up to 5% of the MTOW, the parameters which drive the weights effects must be understood as they can influence the design choices of connected disciplines. On top of that, redesigning a landing gear at late development stages can pose serious cost or performance implications. Therefore, industry practices and collaboration is crucial to make sure that there is strong basis for design in a direction that will eventually converge to an operationally-feasible gear.

The need for a more accurate weight estimation of the landing gear therefore leads to the aim of this thesis which is to increase the fidelity of the weight estimation of an operationally-feasible main landing gear by maximising the use of physics-based calculations. The model development is performed at the Airbus Future Projects Office in Hamburg in order to collaborate on a weight estimation module capable of rapidly sizing landing gear geometries while gaining understanding of the unique kinematic considerations that might arise from unconventional future aircraft.

In order to arrive at a more representative first weight estimate the previous landing gear topology is first refined in order to address certain complexities in the kinematic design which do not align with typical commercial operations. The existing gear height and wheel positions of the FV-1000 is adopted and a CAD-based design process is followed to arrive at a refined landing gear mechanism. Similar to the old design, the new baseline gear is forward retracting to enable gravity-assisted extension during power failure. However, the folding main strut is replaced by a skewed hinge at the top of the main strut which positions the bogie parallel to the rear spar. A kink is added to the bottom of the main strut which enables the wheel assembly to stow flat beneath upper surface of the wing. This significantly reduces size of the lower wing fairing and reduces the added bogie rotation in the previous design. The primary components of mechanism are deemed operationally feasible yet certain components like the torque link, actuation systems and locks need to be added before a complete kinematic simulation can take place.

The resulting stick diagram is discretized and the internal forces are generated using an existing numerical 1-Dimensional FEM class available at FPO. These are fed into the developed Landing Gear Mass Module (LGMM) to obtain critical stress and buckling values. A minimization function is run in order to size the thickness of each tubular element based on the given beam properties and selected sizing ground loads. Using the obtained convergence and geometry data the critical load cases and mass for each beam can be derived. In line with Class 2.5 estimation methods, the secondary components are calculated using empirical relations. A single main landing gear is estimated to weigh 6 tons and the total main landing gear weight amounts to 13.2 tons which is 5.09 % of MTOW. This value aligns with classic literature but is significantly higher than the known ”structurally-efficient” landing gears of state-of-the-art aircraft that have values of 3.7 - 4%. During validation it was also observed that the estimation method under sizes certain components like the sidestay.

The physics-based weight estimation is 8% higher than previous empirical calculations. Such a discrepancies fall within expected estimation errors in literature but the overall trend suggest that Flying V landing gear is heavier than conventional aircraft. The sensitivity study concludes that the landing gear length is a linear driving mass factor. The sidestay and crossbrace components are less influenced by geometry changes but weight effects should be expected when changing their attachment locations. The unknown weight effects which need to be investigated in the future are components specific to the Flying V which include the bogie design (and actuation), the shock-absorber and the pintle attachment.

Preface

When I first started my masters journey I did not think I would have the incredible opportunity finish it working on the Flying V (which I thought was the most captivating research project at the Faculty) and doing it right at the heart of the aviation industry. Having just come back from an internship at Airbus I could not wait to get back into an environment full of passion and of course, airplanes. As my time as a student comes to an end I would like to take the moment to thank everyone who made this journey and this thesis possible.

First I would like to thank Akira Ikenega, my daily supervisor, for his genuine support and guidance throughout the entire process at the Future Projects Office. Thank you for going above and beyond to be involved in the project whether it was clarifying concepts, evoking discussions, offering words of encouragement or tackling unexpected IT issues. I would also like to thank Klaus Bender for sharing his incredible knowledge from everything from wings to the German rail network and for helping get to grips with the FEM class. Finally, thank you to the entire FPO and especially the Filton and Hamburg teams for making me feel like part of the team. I was inspired by everyone's passion and look back at memorable moments like watching the A321XLR maiden flight, Munich and many more.

At the same time I would like to thank all the support I received from my TU Delft supervisors. Justus Benad for sharing your Flying V vision and all the encouragement along the way and Roelof Vos for seamlessly organizing this collaboration. I am grateful to be involved in such a meaningful project with other master students and people passionate about future aviation.

It also goes without saying that there are so many people, friends and family who behind the scenes have been an amazing support whether in Hamburg, Augsburg or Delft. Thank you for being the study partners, project partners, travel partners and everything in between. My attention will soon turn to another adventure across the Ocean. Yet I'm very curious how this masters experience will influence my continued passion for working sustainable projects alongside inspiring people!

Marko Rehbein
Delft, November 2023

Contents

Nomenclature

List of Abbreviations

ACN	Aircraft Classification Number
ACR	Aircraft Classification Rating
CAD	Computer-Assisted Design
CG	Center of Gravity
FEM	Finite Element Method
FPO	Future Projects Office
FWD	Forward
LGMM	Landing Gear Mass Module
MLG	Main Landing Gear
MTOW	Maximum take-off weight
NLG	Nose Landing Gear
PCN	Pavement Classification Number
PCR	Pavement Classification Rating

List of Symbols

d_i	inner tube diameter
d_o	outer tube diameter
E	modulus of elasticity material
K_{bogie}	bogie calibration factor as a function of MTOW
$K_{correction}$	Correction factor to calibrate calculated raw weight
K_{mp}	1.126 for kneeling main gear; 1.0 otherwise
K_{np}	1.15 for kneeling nose gear; 1.0 otherwise
L	unsupported column length (m)
L_m	extended length of main landing gear (in.)
L_n	extended length of nose landing gear (in.)
N_l	ultimate landing load factor
N_{mss}	number of main gear shock struts
N_{mw}	number of main wheels
N_{nw}	number of nose wheels
r	critical stress of a column
r	radius of gyration
R_b	Buckling stress ratio
R_s	Von Mises stress ratio
SF_t	target safety factor
t	tube thickness
V_{stall}	stall speed (ft/s)
W_l	landing design gross weight (lb)
W_{bogie}	combined weight of bogie structure and rolling stock
W_{LGMM}	raw mass computed by the mass module of the upper structural primary components
$W_{secondary}$	total weight of secondary structural components
$W_{structure}$	combined primary and secondary structural weight

List of Figures

List of Tables

1 Introduction

1.1. Introduction problem

Over the last years designing for sustainability has been a main driver for the next generation of aircraft. The continuous projected growth of the aviation sector, combined with climate-conscious travel and enforcement of fuel-taxes has caused an increased focus on sustainability [1]. Manufacturers and operators alike are therefore more motivated than ever to develop the next generation of sustainable aircraft and infrastructure. The Flying V, is a novel aircraft configuration founded by Benad while at Future Projects Office in Airbus, designed to consume 20% less fuel than an equivalent state-of-art tube-and-wing A350 [2]. Primarily this is achieved through decreased wetted area and a more efficient structure which aims for a higher lift-over-drag ratio. Since the initial concept in 2015, the aircraft design has been continuously investigated and refined through research conducted at TU Delft and industry partners. Much attention in recent years has revolved around the two main efficiency drivers of the Flying V to improve the aerodynamic and structural models and thus better predict aircraft performance. With research now implementing Multidisciplinary Design problems and focusing on more component level design choices such as the sizing of rudders, cockpits and winglets.

With an increasing focus on system-level design and multi-disciplinary investigations a need arises for more accurate weight estimations because they are key to constructing more representative structural and aerodynamic models [3, 4]. Additionally, more accurate accurate weight estimations would provide more insight of weight effects when making system-level design choices. The integration of the landing gear into the structure is also so crucial at an early stage in order to avoid costly re-designs which can be detrimental to costs and performance [4, 5, 6]. As of now physics-based weight estimations have been obtained for the Flying V fuselage, outerwing and most recently the engine mount box-structure. The landing gear which on conventional aircraft typically accounts for up to 8% of MTOW has up until now only been calculate using empirical equations derived from historical aircraft data, thus is critical missing piece.

In the first ever study on Flying V landing gear the initial gear layout and kinematics was proposed by Bourget [7]. The comprehensive investigation was conducted on an aircraft-level and thus certain component-level considerations were not investigated in detail. One example is the weight estimation which was calculated using empirical formulas. These formulas are based on data from past conventional tube-and-wing aircraft and are potentially not applicable to unconventional configurations like the Flying V. These needs led to a research objective to be defined capable of tackling both the weight estimation and implicit geometric refinement. It reads as follows:

Research Objective

"To refine the proposed LG architecture of the Flying V while considering operational & design requirements by developing a rapid LG sizing method capable of increasing the fidelity of the landing gear mass estimate at a conceptual level."

The research objective was consulted with the Wing and Landing Gear department at the Future Project Office in Hamburg. The office specializes in conceptualizing, sizing, evaluating and trading-off future wing and landing gear designs. In line with a collaboration aimed at fostering knowledge on new landing gear configurations the following research question was devised:

Research Question

How can an analytical rapid weight estimation tool be implemented to evaluate an operationally suitable landing gear for the Flying V at a conceptual level?

To structure the tasks in a chronological order as is inspired by the workflow at Airbus, the research questions was broken into the following sub-questions which would guide the process.

Sub-questions

- How can an operational-suitable landing gear kinematic design be realized at the conceptual level considering the unique considerations of the Flying V?
- What are the critical ground load cases for each structural component of the landing gear?
- What are the weight effects of the landing gear design choices at a component level on the weight estimation?

The sub questions are roughly characterized by the kinematic design process, the weight methodology process and finally the implications of the results. Together they aim to answer the overall research question.

1.2. Report structure

The report first summarizes relevant part of the literature review which introduces the reader to the background of the Flying V with a focus on the relevant airframe-engine-landing gear integration environment, requirements of landing gears, unconventional mechanisms and weight estimation methodologies. Thereafter, the kinematic design process is covered which explains how a kinematic mechanism was built starting with a baseline aircraft. The final results of kinematic design are included in the final results sections. After the kinematic design process, the main weight estimation methodology is presented which includes a description of the geometry generation, critical loads sizing and mass generation methods. Thereafter, the verification and validation chapter covers the steps taken to verify the methods described earlier and the steps taken to validate the overall model against a conventional aircraft landing gear. The results of both the kinematic design and weight estimation methodology are then presented and evaluated. Finally, the conclusion wraps up the results and future recommendations are proposed to build on the current study and learn from potential limitations.

2

Literature Review

2.1. Flying V background

Over the years a large number of studies have investigated various aspects of the Flying V to determine the size, weight and location of top-level aircraft components like the fuselage, cabin and outer wing. More recently, however studies are investigating the design choices on level deeper at a system or component level such as rudders, split flaps and winglets. The landing gear is a major system that depends on and influences other aircraft disciplines. As mentioned in the introduction it was determined that knowledge of variables governing the design space of the landing gear and surrounding environments has not yet caught up with the later stages of design observable at overall aircraft level. Therefore, an understanding needs to be presented of where the current landing gear design process stands and what the objective of the thesis aims to bring it to. This drives the content researched in the literature study as well as the criteria used to evalute the fidelity of the refined landing gear design. The chronological definition of a typical transport aircraft development process is visualized in Figure 2.1. According to Raymer the end of the conceptual design is marked when the overall wing and fuselage geometry are define and when the equipment, engine and landing gear are chosen [8]. It can be seen that the landing gear initial layout and initial analysis has been performed by Bourget. To progress towards a more defined conceptual design, the landing gear needs to be revised with additional analysis into substructures and subsystems. By approaching the kinematic design at component level the thesis aims to gain more understanding of those interactions.

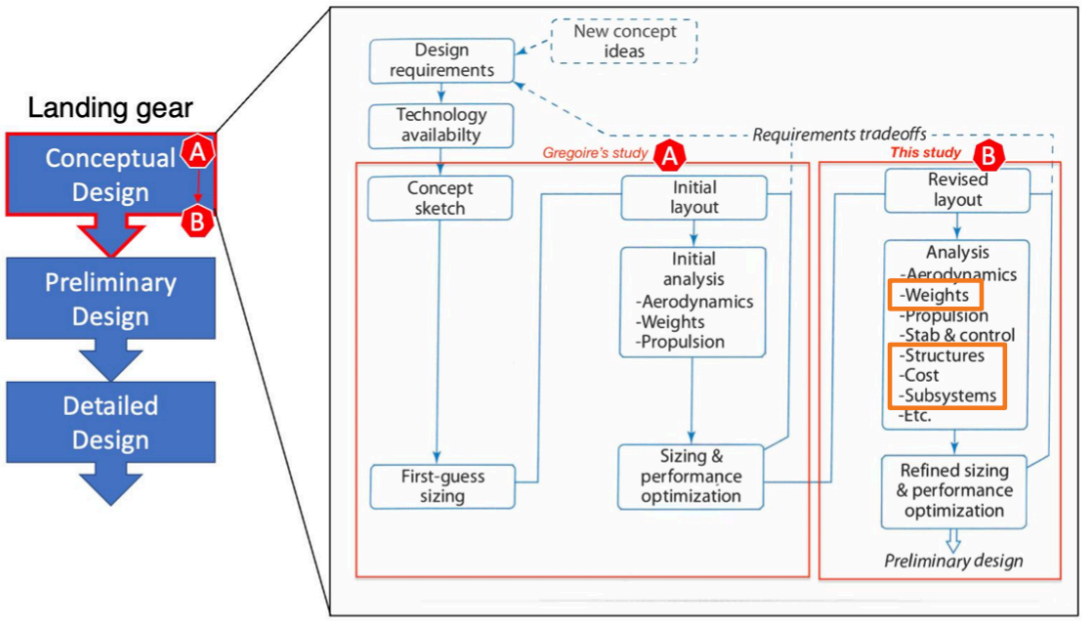

Figure 2.1: Research objective

2.1.1. Earlier landing gear studies

Prior to this study, there has only been one previous study dedicated to the Landing Gear of the Flying V. The work by Bourget set out to determine a suitable landing gear configuration for the Flying-V and study the effects of its implementation on the lateral stability derivatives, maneuverability and other metrics [7]. A conventional tri-cycle bogied configuration was selected and checked for typical operational requirements such as turnover angle, turn radius, tipback angle and rotation ability. Through this process, the height of the landing gear was identified as an important design variable driving influencing rotation ability, fairing drag and stability derivatives. Landing gear height had to be increased to satisfied the pitch and roll requirements which led to a heavier landing gear than the reference A350-900. A solution to reduce landing gear height was to increase the wing dihedral at the cost of decrease lateral stability. Three gear lengths with different wing dihedrals and outriggers were proposed and compared as in Figure 2.2

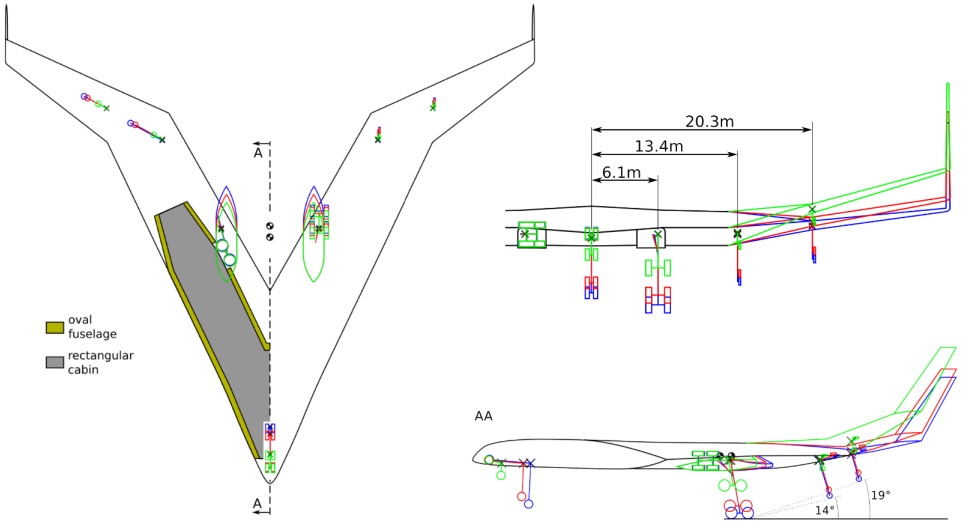

Figure 2.2: Three-view drawing of the propoself landing gear configurations Floor 5.5 (red), Default (blue), Max dihedral (green) [7]

The landing gear weight was estimated using a statistical equation by Raymer, resulting LG weights of 12.8, 12.3 and 9.62 for gear heights for MLG lengths 6.03, 5.3 and 2.65 respectively. Lastly a kinematic mechanism was proposed to retract the landing gear as seen in Figure 2.3

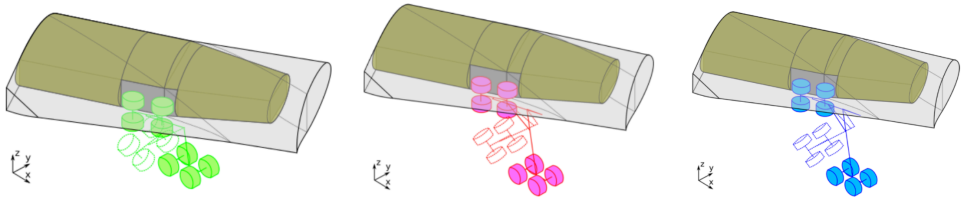

Figure 2.3: Proposed retraction mechanism by Bourget [9]

For this study, it was observed that proposed kinematic mechanism includes several complications which are not typical on modern commercial airlines. These include the bogie rotating about the leg and a folding main fitting. In line with the research objective simplification of the kinematic mechanism is required in addition to increased component-level definition of structural attachments and stowage. Finally, through the use of analytical methods in this study better understanding of the accuracy of the weight estimation obtained by Bourget should be attained. Essentially, the current study aims to go one level deeper at the LG component-level whereas Bourget's investigation concerned the LG at aircraft-level.

2.1.2. Landing gear stowage

The study by Voeten was the first study to investigate the structural integration of the engine, landing gear and airframe [10]. Voeten re-evaluated Bourget's landing gear kinematic mechanism while keeping the tri-cycle configuration. Relevant, for this study however is the new "Box-structure" which provides the structural connection between the engine and the airframe. The volume inside the structure serves as the the new allocated landing gear stowage volume for this study.

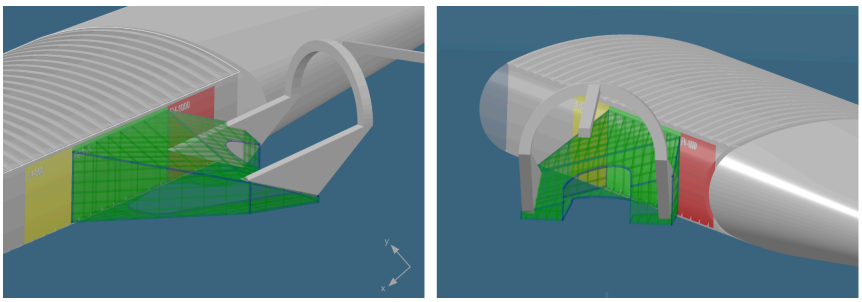

Figure 2.4: Voetens engine mount "box-structure" [10]

This study also provided the most up-to-date Engine location thereby further increasing the fidelity of the 3D model used for the kinematic design in the current study. Voeten also added a landing gear different from Bourgets design in order to generate a load path for the FEM model and focused mainly on shock-absorber characteristics. The kinematic design and structural attachments were noted in the report to serve as placeholders and that more refinement was desired.

2.1.3. Overall aircraft parameters

Designing a landing gear requires up-to-date and consistent overall-aircraft parameters to avoid costly-redesigns [5, 6]. With a continuously evolving aircraft such as the Flying V it was therefore important to establish a baseline that best represents the current state including parameters such as Maximum Take off Weight, CG-range, Mean Aerodynamic-Chord and thrust. These are necessary to calculate accurate loads.

In the comprehensive work on Flying V Flight Performance, Zoeten created a model that used the relevent aircraft parameters to simulate take-off and landing performance for Flying-V [11]. These are phases of flight relevant to the landing gear. Zoeten compiled all the various CG-ranges available and eventually adopted the CG and MTOW related parameters first presented by Cappuyns [12]. It was observed that the center-of-gravity range plays an important role on take-off and landing distance while concluding that the tail-strike angle dictates the minimum unstick speed. While recommendations of Zoeten to implement Multi-Body Physics to better understand shock-damper - LG interactions is out of scope of this study, there is a benefit in adopting Zoeten's parameters as it keeps parameters consistent for future studies on landing gears and field performance. At the time of this study the Flying V Family Design by Oosterom provided the most most up-to-date aircraft planform, length and naming. The FV-800, -900 and -1000 are the result of multidisciplinary optimisation that looked into fuel burn and also estimated group component weights. The landing gear weight of 11.1t here was also estimated using statistical methods and the layout of Bourget was adopted. Designing a landing gear with changes in MTOW is important therefore the planform by Oosterom is selected.

2.1.4. Addressing the knowledge gap

As a result of the literature review which investigated landing-gear related literature both for overall aircraft and the Flying V specifically, a list of needs was identified. These are summarized and listed in Table 2.1. The benefits are the foreseen improvements as a result of addressing the needs.

Table 2.1: The identified needs and potential benefits

The need	The benefit
A more suitable quasi-analytical weight estimation method for unconventional landing gears	To bridge the gap between unsuitable statistical Class II methods and costly fully-physics-based Class III methods
More accurate component group weights for the Flying V	To better understand the effect of component level design choices on aircraft performance
Improved operational characteristics of landing gear (including outriggers) within the boundaries of safety regulations	To ensure suitable ground operations and feasible kinematic solutions
A more detailed representation of the environment surrounding the landing gear, engine and airframe structure	To enable more detailed studies on fuel tank and airframe integration
A continued focus on family design philosophy	To improve Flying-V attractiveness in the eyes of operators and manufacturers.

2.2. Landing gear requirements

At its core the landing gear is the system on a aircraft which connects an aircraft in its natural habitat, to the ground. At the same time each landing gear is unique to the aircraft it was designed for and to the environment it is operating in. Therefore, the Flying-V landing gear needs to be able to perform a common list of functions [3, 5, 13]. These functions are:

1. To absorb the landing loads by dissipating the kinetic energy due to vertical velocity
2. To enable steering capability for manoeuvres such as taxiing, landing-roll, take-off roll, loading and unloading
3. To provide braking capability by absorbing forward energy and holding the aircraft at the gate
4. To protect the airfield surface
5. To protect the aircraft components from damage from coming into contact with the ground

What all of these functions have in common is safety as an overarching theme. In fact, much of landing gear design is driven by regulations and safety requirements. Since a large part of the research objective is to design an operationally-suitable gear, it is important to introduce some of the key operational and design requirements that are relevant to the study. Operational requirements are driven by the needs of operators, customers and regulatory bodies and concern the influence of the landing gear on the overall aircraft. Design requirements, on the other hand, concern the landing gear on a system level and thus typically cover specific structural, loading and aerodynamic considerations. Often these design and operational requirements can be conflicting but ultimately they must be balanced to result in a safe landing gear [3, 5].

Numerous landing gear requirements are prescribed the European Aviation Safety Agency (EASA) and include requirements concerning landing gear loads, system functions, testing and crash-worthiness amongst others. For this thesis, the so-called ”bookcase” loads are of particular relevance since they are required to apply realistic loads for the structural analysis. Additionally, important risk and LG system-level requirements are explained as they are relevant to the kinematic design philosophy. Otherwise, for access to all requirements the full descriptions can be consulted in the Acceptable Means of Compliance (AMC) section of the CS25 handbook [14].

Ground Loads

Even though landing gears evoke an image of tires making impact on a runway during landing, ground-loads are equally important. Within industry and in literature ground loads are considered sizing loads and can be more accessible at a preliminary stage of design [15, 5]. This can be attributed to the fact

that ground loads apply when an aircraft is at it's maximum take off weight. Furthermore, multiple sources agree that landing gear loads are critical for fatigue failure with some even claiming that over 80% fatigue failures are associated with Taxi loads [16]. Fatigue loads are not subject of this study but these values do present evidence to the importance of ground loads. The ground loads specified in CS25 include:

- **CS 25.489** Ground-handling conditions
- **CS 25.4** Taxi, takeoff and landing roll
- **CS 25.483** Braked roll conditions
- **CS 25.485** Tail-wheel yawing
- **CS 25.487** Nose-wheel yaw and steering
- **CS 25.489** Pivoting
- **CS 25.485** Reverse braking
- **CS 25.487** Towing loads
- **CS 25.489** Ground loads: unsymmetrical loads on multiple wheels
- **CS 25.489** Jacking and tie-down provisions

Of these only Taxi, Braked-Roll, Pivoting and Turning are used for load calculations since they have been identified by experts as the most critical ground loads. Since these ground loads are considered static the shock-absorber is assumed to be in the static configuration and the loads depend on static load per leg, F_s, as seen in the relevant equation in Figure 2.5. Typically, the main landing gears take up 93-95% of the total aircraft weight. The exact static balance depends on the required steering power desired on the nose landing gear and the braking requirements on the main landing gear [17, 3]

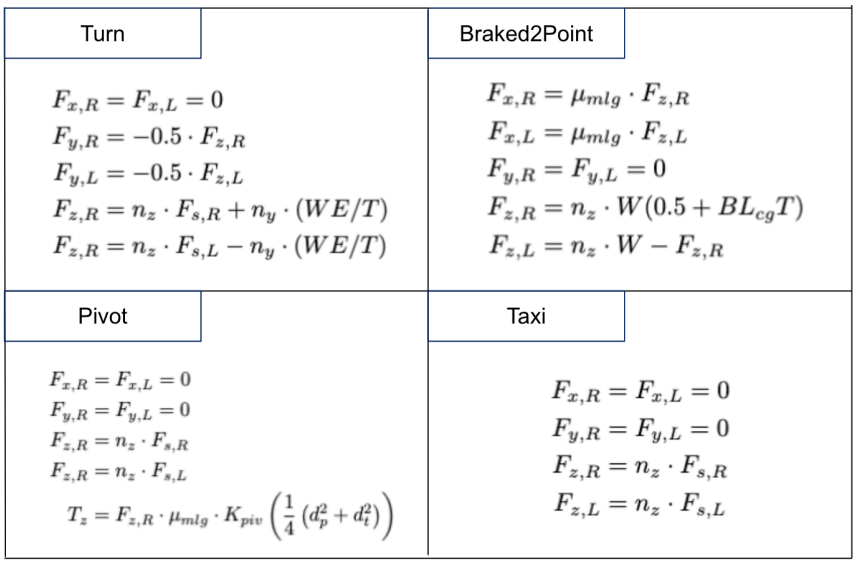

Figure 2.5: Equations for selected ground loads[18]

The load factors, n_z and n_y as well as the friction coefficient μ_{mlg} above are derived from statistics. However, current ground maneuvering requirements are deemed to be realistic for many types of different aircraft [16, 5]. Furthermore, ground maneuvering load cases are also considered strength and stiffness cases [19]. These point to the fact that they are sensible loads to be used in a preliminary structural study in the absence of of detailed knowledge of or access to multi-body simulation models which are required for dynamic loads.

2.2.1. Dynamic & landing loads

Dynamic loads, which are often associated with landing are also clearly a significant aspect of landing gear design. Dynamic loads are not included as loadcases in this thesis and therefore they won't be covered in

detail. However, the inclusion and placement of components related to dynamic loads such as the shock-absorber are qualitatively considered during the kinematic design process. For the future, it is important to note that shock-absorber characteristics and the critical loadcases are influenced by parameters such as roll, rate, sink, tire deflection as well as phenomena like spin-up [**niu**, 20, 21, 17]. Especially, the latter is relevant for future studies since vibration issues have been in the past been recognized in supersonic airliners who employed more slender landing gears and thus higher structural flexibility [22].

2.2.2. Safe-life design

The landing gear must be designed to handle both landing and dynamic loads according to safe-life philosophy dictated in CS 25.721. Components can be considered safe-life when the crack-growth can be detected during normal inspection intervals or predicted [3]. The strict nature of this requirement is also why typically most conventional landing gears look similar since a single defined load-path is easier to inspect routinely. This is rather unique to the general weight-saving philosophy in the aerospace industry that makes use of a fail-safe philosophy with multiple loadpaths.

The safe-life design also affects the kinematic design and structural considerations of a landing gear. In line with crash-worthiness requirements a landing must detach as a unit in the event of a catastrophic malfunction to prevent larger damage to the structure. An example, of this requirement in action can be seen in whereby the 777 main landing weighing more than 6 tons breaks cleanly upon impact.

Figure 2.6: Asiana Flight 214 Crash in San Francisco

Figure 2.7: Clean detach of B777-300ER landing gear

2.2.3. Tire failure modes

Tire failure modes are another key safety requirement to be evaluated when designing a landing gear for an entirely new aircraft configuration. **CS25.734** stipulates the need to protect the aircraft and landing gear against tyre failures. This consideration has not yet been explored for the Flying-V. Safe operation of must be ensured against:

- Tyre debris
- Wheel flange debris
- Flailing tyre strip
- Tyre burst pressure

For each failure mode EASA defined zones of vulnerability which need to identified on the aircraft and landing gear. The hazards then need to be mitigated according to the acceptable means of compliance by for example segregating vulnerable systems, shielding or including redundancies where possible [14, 5]. One notable example of a configuration vulnerable to this requirement is the Concorde which was brought down after runway debris caused tire debris to impact the fuel tank.

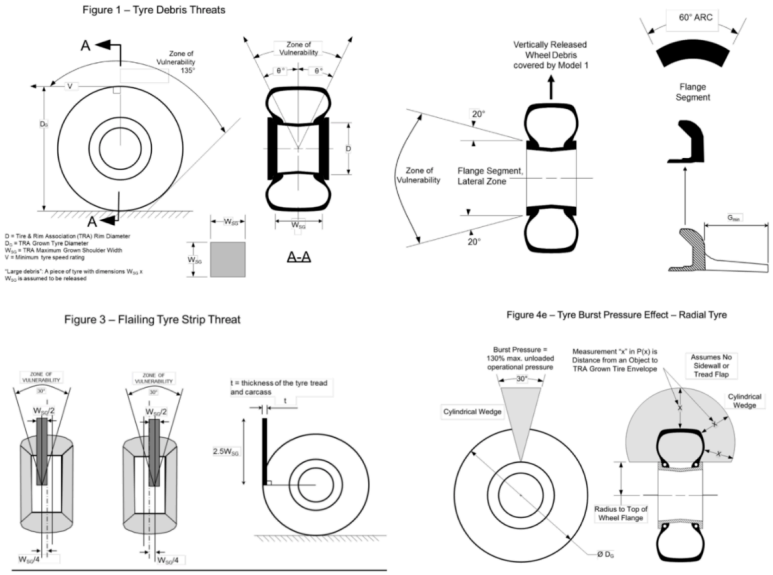

Figure 2.8: Tire failure modes

2.3. Kinematic design

The Kinematic design process of the Flying V is a significant portion of the thesis therefore the functions of a feasible mechanism, important considerations and past designs are presented to introduce the reader to the terminology and designs of the past. A kinematic mechanism shall:

- Retract the landing gear safely into the body of the aircraft while minimizing airframe drag by minimizing the disruptions to the outer contour of the wing or airframe [17, 5].
- Interfere as little as possible with the surrounding structure [23]
- Include a redundant capability of extending the landing gear in the event of power/hydraulic loss [14, 6]
- Ensure positive locking of the mechanism [14]

At the same time landing gear designers stress the absolute importance of incorporating simplicity in the design [5, 3, 17, 13]. It is even argued that complexity of kinematics has more influence on cost than weight due to increased maintenance and risk of malfunctions [24, 3]. Evidently, this is not always possible and thus lessons can be taken from past designs on what has worked and what hasn't.

2.3.1. A conventional landing gear mechanism

In order to evaluate the kinematic design of the Flying V landing gear there must be understanding on what a conventional landing gear looks like on modern commercial transport aircraft with wing-mounted engines. The landing gear picture in Figure 2.9 is classified as a "Bogied" gear because there are multiple wheel axes connected to a bogie beam. The beam is in turn connected to the main gear leg via the fork at Point E which typically serves as the origin for describing a landing gear geometry. The piston or shock-absorber is the component which absorbs most of the kinetic energy during landings and slides within the so-called "main fitting' which is considered the main structural component. The sidestay is designed to carry the sideloads and in different literature may also be referred to as a sidebrace, brace or just stay. Aircraft may also have two sidestays that share the loads as is present on the A350 and 787. Finally, one of the most important terms important to the kinematic design of the landing gear is the "pintle". The term can be used interchangeable with pivot axis or retraction axis, but it essentially marks the main axis about which the LG pivots in order to retract.

Figure 2.9: A330/340 landing gear

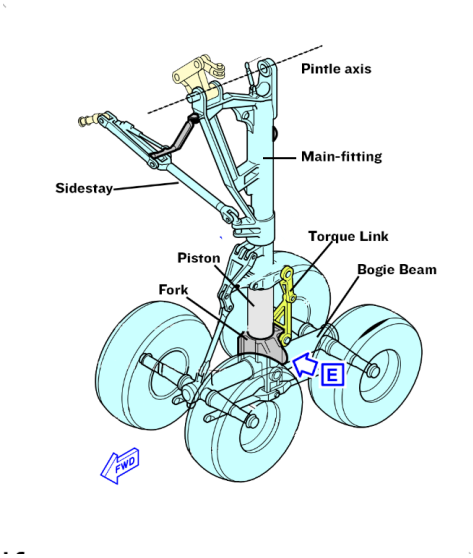

Figure 2.10: A330/340 landing gear component terminology

Understanding the different types of joints found on landing gears is also important as this gives an idea on what type of joints are feasible. Two common types of joints are the revolute joint commonly found in planar folding mechanisms and universal joints. Universal joints are essentially two revolute joints combined thereby allowing two degrees of rotation. The A330 bogie above, as well as most sideways retracting gear use this configuration. The pintle attachment points are typically spherical joints as can be seen

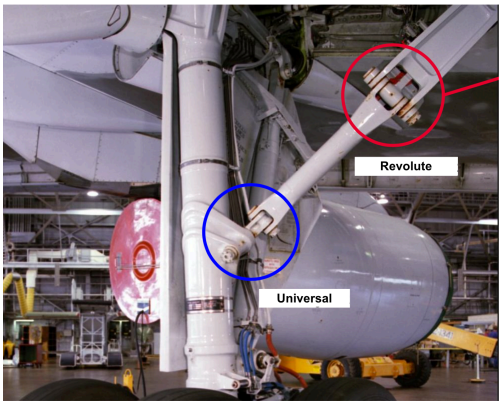

Figure 2.11: Example of a revolute and universal joint

Figure 2.12: Spherical joint on 767 pintle attachment [25]

2.3.2. Unconventional landing gear mechanism

Since Flying-V is an unconventional aircraft at this stage from a LG perspective the following sections will briefly touch on landing gear mechanism with unconventional features to demonstrate that landing gear mechanisms are influenced by their unique aircraft configurations. It can be noticed that the following aircraft are all characterized as rather high from the ground which is a known conclusion of the latest study by Bourget.

Concorde

The Sideway retracting concorde landing gear from afar resembles that of conventional airliners. While the retraction concept is conventional, the mechanism at a component-level is heavily influenced by the shape of the fuselage, wing which has certain implications. Given the need for a certain area-ratio to

reduce wave-drag, the belly fairing had to be minimized. As a result smaller tires were selected and thus smaller brakes which caused overheating and increased the risk of tyrefailure as a result of which wheel cooling fans were added. Furthermore, given due to the underwing engines and the operational tailstrike requirements the landing gears had to be made longer. The gear legs were longer than the belly fairing and so a shortening mechanism had to be introduced which added complexity. The concorde example demonstrates how requirements from other disciplines such as aerodynamics can influence the landing gear mechanism.

B58 Hustler
The B58 hustler was a millitary aircraft with noticably long landing gear which were required in order to fullfill operation requirements when carrying underbelly payloads. The kinematic mechanism features a forward retracting landing gear which was desired to minimize the disturbance of the contours of the thin delta wing, which is another example of aerodynamics influencing design choices. Furthermore, the mechanism adds complexity in that it uses a folding main fitting, which allows for more compact storage. Finally, the aircraft features an unconventional bogie design, whereby a the bogie is packed flat which is enable by the addition of a kink below the piston.

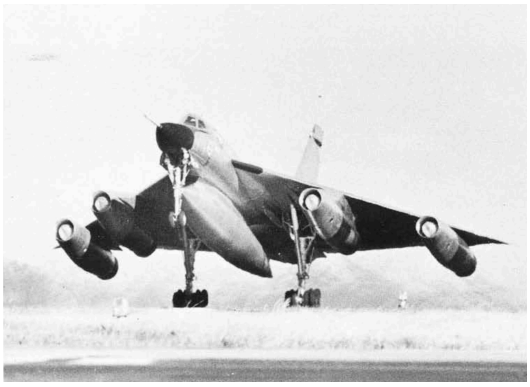

Figure 2.13: B-58 Hustler take-off [26]

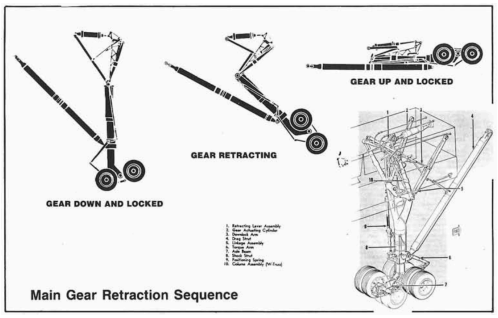

Figure 2.14: B-58 Hustler retraction mechanism [26]

Vulcan
The Avro Vulcan is another millitary aircraft with long landing gear legs and a delta wing. It features a folding main fitting with a similar concept to that of the B-58 Hustler. Two noticable difference however, is that the landing gear retracts afts which could be due to numerous reasons such as structural attachment points, payload requirements or cg effects. However, the biggest difference lies in the bogie design, which features an ”exposed” shock absorber in a semi-levered design. This was implemented due to the type of special nitrogen gas used. What this mechanism demonstrates is that even highly tailored landing gear designs draw similarities based on overall aircraft characteristics such as the planform shape.

2.3.3. Unconventional bogie designs
Unconventional bogies have been implemented in the past by designers to integrate landing gears with aircraft that have unique requirements for such an added layer of complexity. Given that the Flying V boasts a unique fuselage these bogies were studied in preparation for the kinematic design process. Figure 2.15 pictures a collection of unconventional bogies for both military and commercial aircraft categorized according to their direction of articulation.

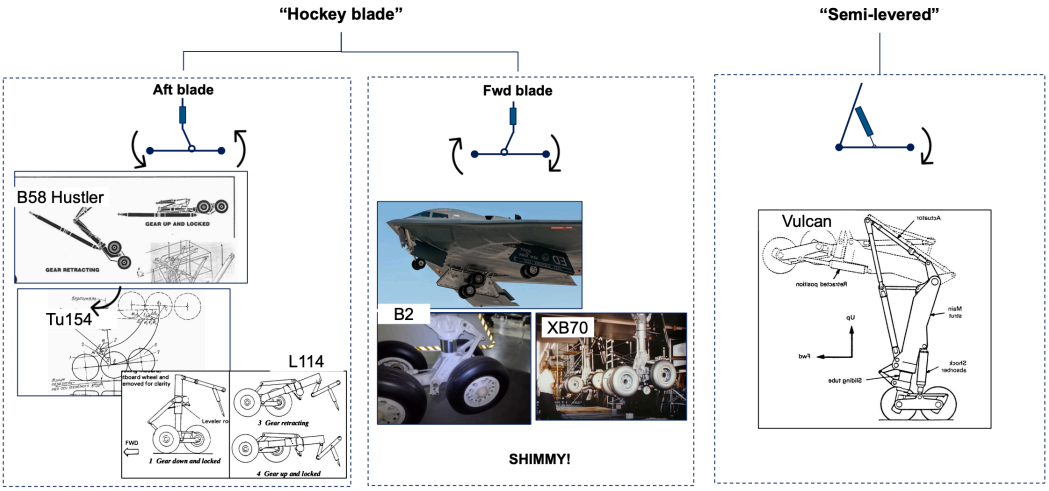

Figure 2.15: Types of unconventional bogies implemented on existing landing gears [3, 13]

2.4. Weight estimation

Good knowledge of weight effects is necessary for making good design decision. Different weight estimation methods are typically categorized into four "classes" [**empty citation**] which are considered classic. In recent times the emergence of so called hybrid classes has emerged which combine lower order methods with higher accuracy. These are briefly introduced below

Class I: Class 1 methods are typically implemented at the start of a conceptual design when only top-level requirements such as speed, range and maximum take-off weights are known to designers [27]. They purely based on regression-based statistics, involve no simulatino or volumetric sizing [28]. They are often found in popoular handbooks by Raymer, Roskam and Torenbeek [8, 13, 29]

Class II: Class 2 methods still rely on statistical historical data but semi-epirical equations can be used to size component group weights based on the knowledge of baseline geometry, volumes and load factors. The weight estimation by Bourget and Oosterom can be considered a Class 2 method.

Class III: Class 3 weight estimations take a physics-based approach and make use of component specific knowledge including density and volume. Finite Element Analysis (FEA) is typically the tool of choice as it is considered high fidelity, high-accuracy method when implemented correctly. The results of a Class 3 weight estimations are also used in MDO as sufficient knowledge of the parameters and rules is available.

Class 2.5: These are so-called hybrid methods because they use fundamental physics to analyze primary structure and semi-empirical rules for secondary structures. A notable example is the tool EMWET developed by Elham estimate the weight of primary wing structures like ribs, spars and skins using physics and secondary structures like joints, slats and flaps using rules. Elham addressed accuracies of an oversimplified geometry in Class 2 methods and removing the reliance on tuning coefficients. The result was an average 2% error compared to 25% previously, while keeping the computational time significantly lower than a Class 3 method.

2.5. Past Class 2.5 methods for landing gears

Class 2.5 methods for landing gears for conventional aircraft have been developed in the past. The two methods from which are the most referenced is the work by Kraus and the method by Chai and Mason [30, 24]. The need for this method arose with the knowledge that statistical equations are not sensitive enough to drastic configuration changes which arise during changes in geometry, design requirements or performance requirements [30]. Kraus set a strong basis for analytical weight estimation of landing gear which was improved upon by Chai and Mason who added the capability of more geometries and refined input assumptions. Both methods follow a similar approach as characterized in this flow diagram.

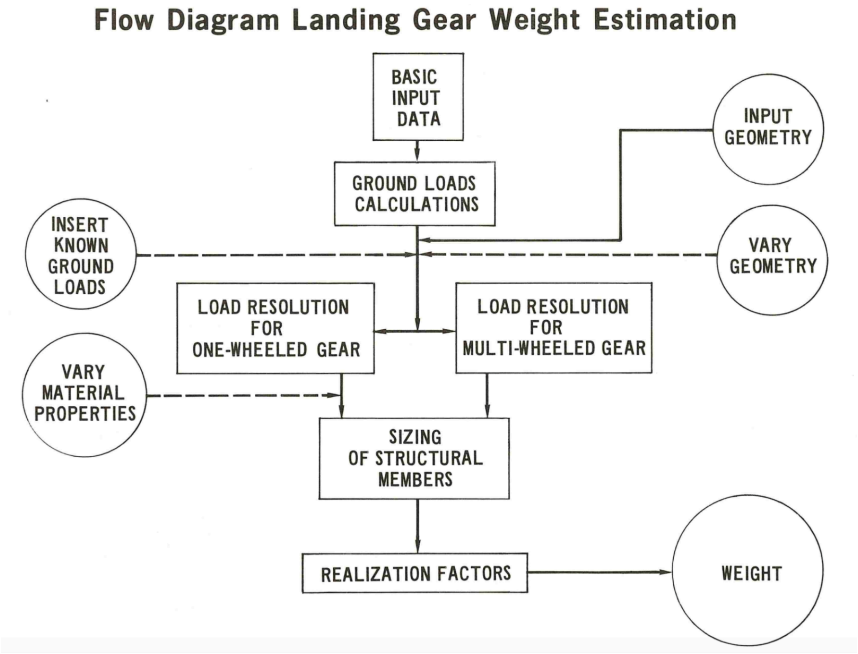

Figure 2.16: Kraus method flow diagram [30]

.

The method by Chai and Mason is refined in order to integrate into an MDO framework and as such the kinematic design is computed numerically. This differs from the graphic kinematic method selected for this study which favour exploration as the rules of the aircraft configuration are not fully developed. On the otherhand, Chai and Mason use Euler Beam Theory to resolve external loads into internal forces, whereas this thesis implements a numerical 1DFEM method.

Empirical relations

As is common for Class 2.5 methods, secondary structures are calculated using empirical relations or statistical equations. It is expected that these relationships will also be used in the weight estimation of the Flying V landing gear. One of the most respected landing gear handbooks by Currey provides a detailed breakdown of component weights as a percentage of overall MLG weight. It can be seen that rolling stock which includes, wheels, tires, brakes accounts for over a third of the total weight. The structure accounts of half, and the remainder is allocated to controls.

	Business Jets		Transports			
Breakdown	JetStar	Gulfstream	Small B737	Medium B727	Large B707	Jumbo L-1011
Main gear	80	81	88	85	92	89
Roll. stock	44	30	34	34	35	32
Wheels	11	8	7	7	8	6
Tires	12	11	11	10	11	10
Brakes	21	11	16	15	16	16
Misc.				2		
Structure	26	35	43	42	46	50
Sh. strut	24	28	22	21	27	32
Fittings	2	4	15	15	14	12
Braces		3	5	5	4	5
Misc.			1	1	1	1
Controls	10	16	11	9	11	7

Figure 2.17: Typical Component Breakdown, % [17]

.

2.5.1. 1D Finite Element Method

Finite Element Analysis describes a broad numerical method that is available for engineers to approximate solutions to structural problems and is also used in wider engineering applications such as fluid flow and heat transfer. Typically, the Finite Element Method (FEM) is implemented when working with complex geometries and boundary conditions, which are difficult or cumbersome to solve analytically. That is why it is typically used in Class 3 weight estimations for landing gear where for example joints, holes and fillets are too complex to using only equilibrium equations. Nevertheless, FEM still relies on the basis of solving for equilibrium but rather than solving for equilibrium equations directly on a continous element it relies on breaking up a component into finite defined elements, which is called discretization. Elements are connected at nodes and equilibrium needs only to be satisfied for a finite number of elements rather than continously along the whole component. There many different type of elements from 1D lines to 3D volumes, and these depend on the problem at hand. For this thesis solely line elements are considered because the geometry of the landing gear at this stage is only available as a stick diagram. More specifically the line element is referred to as a beam which can carry axial, bending, shear and torsional loads. As opposed to a rod that only carries axial forces. The main objective of the numerical method is to solve for displacement from which stress and strain can be derived. Each displacement whether translational or rotational is called a degree of freedom. For a 3D beam there are 6 degrees of freedom per node. For each element a linear equation is solved

$$f = [k]u \tag{2.1}$$

The element stiffness matrix in Python is derived using the Direct Method meaning that the shear and moments are derived from the following classic relationships.

$$EI\frac{d^3v}{dx^3} = V(x) \tag{2.2}$$

$$EI\frac{d^2v}{dx^2} = M(x) \tag{2.3}$$

Once the square element stiffness matrices are obtained they can be combined into a global stiffness matrix, K. At this stage the boundary conditions and forces acting on the nodes can be applied. The boundary conditions are determined based on the the type of joint used in the landing gear, as explained earlier. Contrary to most commercial solvers that deal with higher order elements, the 1DFEM module used in this thesis computes the displacements by inversing the stiffness matrix. For more complex shapes this would be computationally inefficient [31].

3

Kinematic Design

There are practically endless possibilities when it comes to developing a retraction mechanism [3]. Starting with a blank canvas, the following chapter explains the steps taken to arrive at an operationally feasible landing gear design for the Flying V. First, the constraints and considerations used to guide the process are explained. Thereafter, the kinematic design choices and the final design is evaluated and its implications discussed.

3.1. Kinematic design process

As explained in the introduction, the previous kinematic mechanism proposed by Bourget came with several challenges relating to complexity and structural efficiency. As a result, it was decided refine the design with a fresh perspective while including up-to-date aircraft parameters and newly developed interfaces such as the engine attachment structure proposed by Voeten [10]. It was determined that the design space was still too broad and the engine-airframe-landing gear interactions still too undefined to take full advantage of fully automated methods such as ParaPy to design a kinematic. In order to start building knowledge while using common industry practices, a more ”hands-on” approach was selected. The kinematic design process roughly follows these 4 steps:

1. Initiate Kinematic design
2. Build up a parametric CAD model
3. Implement desired kinematic concept
4. Assess mechanism with operational constraints and design considerations

The objective of the kinematic design process is to arrive at a feasible first-pass topology that can be used as an input for the mass estimation tool.

3.1.1. Design Considerations

In line with the research objective to design an operationally suitable landing gear for a commercially viable aircraft, a set of design considerations were defined. These considerations, summarized in Table 3.1, act as pillars throughout this process.

Table 3.1: The guiding Flying V Kinematic Design considerations

Consideration	Objective	Effect
Compactness	Disturbance of the Flying V upper surface wing contour shall be minimized	Reduces aerodynamic drag and propulsive efficiency due to more uniform flow at the inlet
Complexity	Number of joints and actuators shall be minimized	Reduces weight and maintenanance costs
Structural efficiency	Load introduction efficiency shall be maximised	Reduces weight and maintenance costs
Interfaces	Number of interfaces with other aircraft systems shall be minimized	Reduces design costs and increase family commonality
Risk	Risk shall be minimized	Reduces certification costs

Unlike the design requirements introduced later in the chapter, the design considerations are more qualitative in nature. In other words, design choices can not be blocked by these considerations but they can be used to compare and evaluate design choices. As more knowledge is gained it is expected that in future studies these considerations can evolve into well-defined requirements in order to perform measurable trade-offs.

3.1.2. Requirements

Design constraints refer to the requirements used to constrain the design and arrive at an objectively feasible gear. A distinction was made between operation requirements and design requirements. Operational requirements refer to the ”standard” landing gear requirements that are commonly found in literature. These are applicable more at an aircraft-level and are also important for engineers from other departments. On the other hand, design requirements relate to the landing gear at component-level. These are more specific to the design tasks at hand and take into account expert recommendations and industry practices.

Table 3.2: Thesis Design requirements

Category	Requirement
Folding angles	Primary structure folding angles shall be greater than 20 degrees
	Torque link folding angles shall be less than 135 degrees
Clearance	LG wheels or structure shall not penetrate the upper wing top surface
	Tires shall have a prescribed minimum clearance with the upper wing surface
	Tires shall have a prescribed minimum clearance with the rear spar
Shock absorber (SA)	The stroke shall be greater than a prescribed length
	SA maximum pressure shall be less than 6000 psi
Rake	Rake angle shall be less than 10 degrees

Table 3.3: Thesis Operational requirements

Category	Requirement
Loadshare	The NLG load shall be within 5-15% MTOW over the entire CG range
Stability	Lateral turnover angle shall be less than 57 degrees
	Longitudinal tipback angle shall be greater than pitch angle
Maneuvers	Wing tips shall be protected during critical pitch and roll maneuvers
	Gear layout shall be compatible with Type 4E airports
	Gear layout shall enable a turn width less than or equal to the A350-900
Risk	The kinematics shall enable down-lock
	There shall be sufficient clearance with stowage bay
	The kinematics shall allow for emergency free-fall

Certain requirements such loadshare and lateral turnover were calculated quantitatively at the start of the kinematic process. Maneuver requirements are related to the Bogie design. Finally, since full crashworthiness study was out of the scope of the thesis, the Risk is to be assessed throughtout the process. Design requirements were evaluated at regular intervals and during review sessions with experts at Future Projects Office.

3.2. Kinematic design initiation

The kinematic design process does not have a standard approach because every landing gear on every aircraft requires a tailored solution. For the Flying V it was initially proposed to design the kinematics using a rule-based approach on Para-Py, however the lack of knowledge on the relationship between

parameters in the design space make it difficult to create suitable rules. Therefore, a more hands-on approach was chosen using a parametric CAD model. This process flow is shown in Figure 3.1.

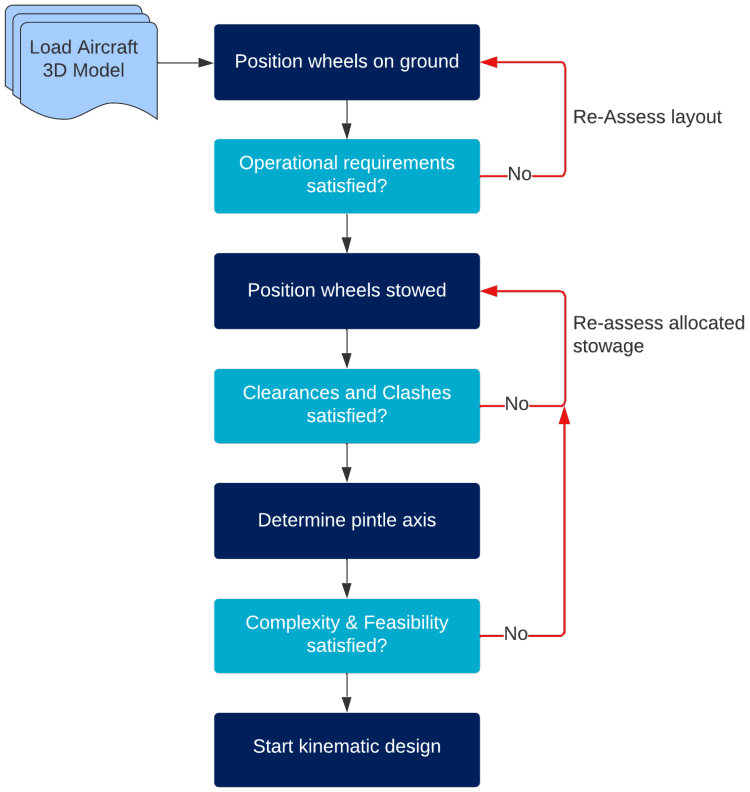

Figure 3.1: Kinematic design initiation

1. **Wheels-on-ground:** The wheels must be positioned on the ground as this is the starting point of the retraction sequence. Furthermore, this is also an opportunity for the designer to confirm that the turnover angle, static load and other important operational requirements are satisfied before committing to a potentially lengthy kinematic design process.
2. **Stowage volume:** Next the wheels can be moved to their fully retracted positions within the allocated stowage region. This can be achieved by 3D sketching and rotating a rough stick model between the wheels on ground and the stowed location. At this stage it also important to identify any obvious clearance issues or clashes with main structural components.
3. **Pintle axis:** Next the pintle axis needs to be derived. The pintle is the main hinge axis about which the landing gear pivots in order to transition from its extended state to its retracted state. Determining the natural pintle axis can already reveal multiple attributes of the design such as the sweep path, obstructions and structural attachment points.
4. **Kinematic Design:** Before continuing with the kinematic design, a designer should try and foresee whether the resulting hinge location promotes a simple and feasible design. If significant additional structure is required to support the joints at the hinge line or if the gear requires additional rotations to end up in its desired location, then the position of the wheels stowed should be revisited.

3.3. Baseline aircraft for design

Following the review of past Flying-V, a baseline aircraft was selected. The FV-1000 3D ParaPy model was obtained from Oosterom and imported into CATIAV5 [32]. Furthermore, the engine and engine-box structure obtained from Voeten's 3DEXPERIENCE model was selected as it represents the latest iteration of the interface region which is relevant to the study [10]. Finally, the overall-aircraft mass and CG parameters were selected as referenced by Zoeten, which inturn originally originated from Cappuyns [11]. The tailstrike angle and floor-to-ground height were selected from Bourget's study [7]. Note that the ground angle of -3 is not taken into account in the kinematic design or the weight estimation. Details on why these baseline parameter were chosen are recapped in Chapter 2.

Table 3.4: Baseline Aircraft parameters entering kinematic design process

Aircraft - Level				
Variable	**Value**	**Unit**	**Source**	**Reference**
3D Model	FV-1000	ParaPy	Oosterom	Zoeten
MTOW	260	10^3 kg	Cappuyns	Zoeten
MRW	260.9	10^3 kg	Cappuyns	Zoeten
MLW	210	10^3 kg	Cappuyns	Zoeten
Length	57	m	Oosterom	Zoeten
Span	65	m	Oosterom	Zoeten
FWD CG	45	% MAC	Cappuyns	Zoeten
AFT CG	57.7	% MAC	Cappuyns	Zoeten
X-pos FWD CG	29.3	m	Cappuyns	Zoeten
X-pos AFT CG	31.7	m	Cappuyns	Zoeten
CG Range	2.34	m	Cappuyns	Zoeten
Thrust	770	kN	Cappuyns	Zoeten
Tailstrike angle	19.2	°	Bourget	Zoeten
X-pos engine	31.0	m	R. Voeten	[-]
Y-pos engine	4.275	m	R. Voeten	[-]
Z-pos engine	0.8	m	R. Voeten	[-]
h_{hfdz}	6625	mm	[-]	[-]
cabin-ground height	5.5	m	G.Bourget	[-]
x_{mlg}	32.4	m	G.Bourget	[-]
x_{nlg}	6.5	m	G.Bourget	[-]

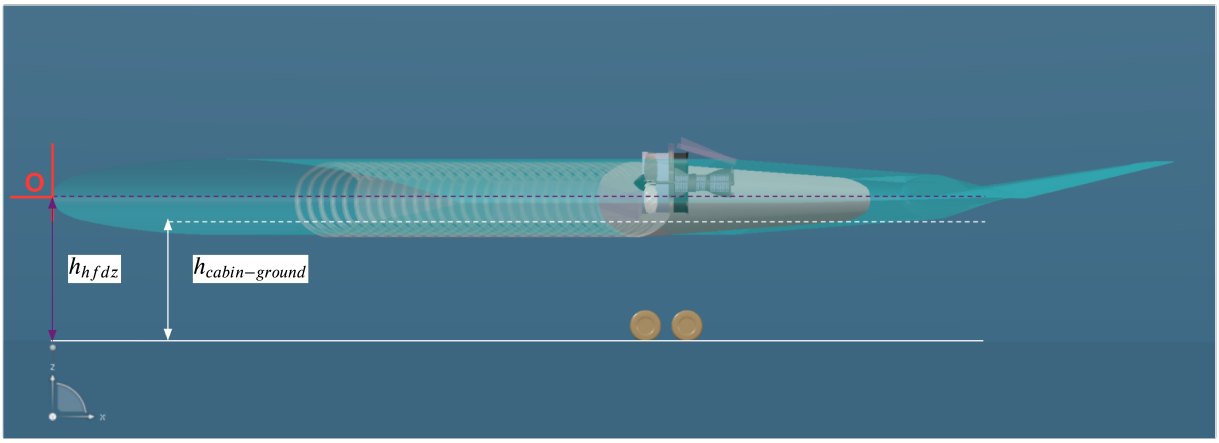

Figure 3.2: Terminology definition

3.3.1. Bogie dimensions

Tire size and spacing are key drivers at beginning of the kinematic design because they dictate the available stowage volume. The previous study by Bourget selected an A350-900 bogie with the assumption that the Flying V, given its lower MTOW, will be ground-compatible by default through the use of a bogie configuration of an inherently heavier aircraft [7]. However, during the current kinematic design process, the question of bogie sizing was re-evaluated in light of the increased emphasis on minimising the landing gear fairing. In other words, the design requirements called for reducing the stowage volume taken up by the bogie. Given the complexity of designing an entirely custom bogie and validating its flotation it was decided to look into existing alternatives. The A330 family is the closest Airbus aircraft with a two-strut/4 wheeled bogie gear configuration and its tighter bogie was chosen for further investigation. The goal was to estimate the ground compatibility of a fictional A330-900 with a MRW of 260.9 tons, equaling the MRW of the Flying V, and compare it to the ground compatibility of an A350-900 of the same weight, to see if tighter bogie arrangement is suitable.

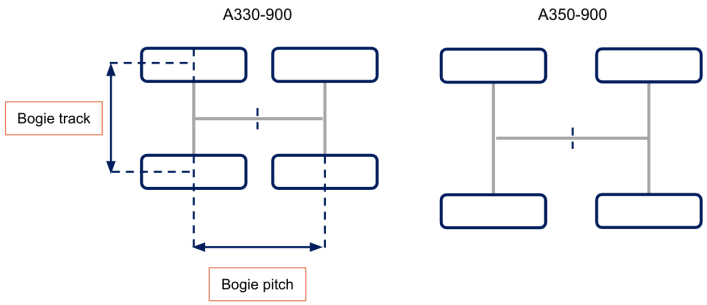

Figure 3.3: Comparison of A330 and A350 bogies

For this, the Aircraft Classification Number - Pavement Classification Number (ACN-PCN) system was used. The ACN indicates the structural ”damage” that an aircraft imparts on the runway while the PCN indicates the load-carry capacity of the runway. If the unique ACN of an aircraft, at a given % CBR subgrade, is lower than the PCN of a runway, then the Aircraft is suitable for unrestricted operations on that runway [33]. The ACN-PCN method demonstrates a somewhat linear relationship between ACN number and aircraft weight as it's derived from a static calculation using the Derived Single Wheel Load [33]. Therefore in early stages of design it is possible to interpolate an ACN value for a fictional A330 bogie with relative confidence knowing that ACN values are also conservative in nature [34].

The Weight Variant WV920 is the heaviest A330 with a maximum ramp weight (MRW) of 251.9 tons. With this in mind, Table 3.5 shows that for a fictional A330, 9 tons heavier than WV903, the interpolated ACN increases by 3.17 units from 74 to 77* (rounded). Applying this ratio to a weight increase from 251.9 to 260.9, it is possible to extrapolate that an A330 with the the same weight as the Flying V is estimated to have an ACN value of $80 + 3.17 \approx 83^{**}$.

Table 3.5: Interpolated A330 ACN value and bogie dimensions, A330 data [35]

Aircraft	Variant	MRW [t]	Bg. track [mm]	Bg. pitch [mm]	ACN [6% CBR]
A330-900	WV903	234.9	1397	1981	74
A330-900*	+$\Delta 9t$	243.9	1397	1981	77*
A330-900	WV920	251.9	1397	1981	80
A330-900**	+$\Delta 9t$	260.9	1397	1981	83**

It is therefore assumed that a 260t Flying V with an A330 bogie also has an ACN of 83. Looking at Table 3.6 it is now possible to evaluate the new ground compatibility by comparing against the reference A350-900 with equal MRW. Finally, it must be noted that ACN-PCN method will by replaced by an improved version of the method and re-named as the ACR-PCR method by 2024 as mandated by ICAO [36].

Table 3.6: Ground compatibility approximation of the Flying V compared to the A350-900 [37]

Aircraft	Variant	MRW [t]	Bg. track [mm]	Bg. pitch [mm]	ACN [-]
A350-900	WV004	260.9	1735	2040	78
FV (A330 Bogie)	260t	260.9	1397	1981	83*
A350-900	WV023	280.9	1735	2040	83

As expected a 260t A350-900 has a lower ACN than the Flying V due to a higher wheel spacing and thus more load distribution on the runway. The main takeaway however is that the Flying V with an A330 bogie has the same structural effects on a runway as an 280.9 ton variant of the A350-900. Although conservative, this value indicates that any significant increase in Flying V MTOW will increase the ACN value of the aircraft past 83, possibly putting it at a disadvantage in the eyes of an airport as it would cause more runway damage than the heaviest A350-900.

Nonetheless, the Flying V at it's current weight would be able to operate equally to a fully loaded A350-900. For example, both the A350-900 and the Flying V with A330 bogie spacing would be allowed to operate unrestricted in Schiphol since all runways have a PCN classification of 89 [38]. However, it must still be noted that a fully-loaded Flying V with tighter bogie spacing may not be able to operate at the same airports as an equivalent A350-900.

3.3.2. Tire dimensions

It is assumed that the tires on the A330 bogie are still suitable for the Flying V landing gear given that they are part of the same rolling stock assembly. In fact, the A330 and A350 tires have the same dimensions which are the *1400 x 530 R23* model. Where 1400 is nominal diameter (mm), 530 is the nominal section width (mm), R stands for "Radial" and 23 is the nominal wheel/rim diameter. The only difference is that the A350 tires have a 42 Ply-rating (PR) and the A330 tires have a 36PR. This simply means that the A350 tires can carry heavier loads and thus are heavier tires. It is recommended to use 42PR tires for the Flying V to allow a margin for future increase in load-bearing capacity, however since the tire dimensions are the same this difference does not affect the kinematic design.

What does affect the kinematic design however, is properly modelling the tires in CATIA. The tire catalogue dimensions correspond to "new" tires. However, when considering clearance the spinning contour should be used as a worst case since the centrifugal forces push the material outwards and expand the tire.

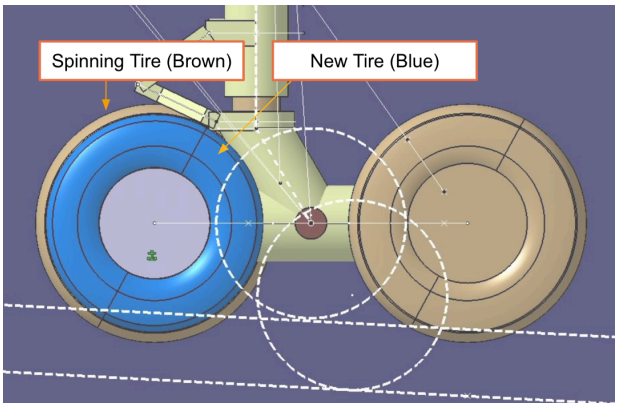

Figure 3.4: 3D model of new and spinning A330/A350 tires

3.4. Kinematic concept selection process

The following section explains the decision process of selecting the final kinematic mechanism. Figure 3.5 summarizes the mechanism concepts that were explored during the kinematic design process starting at a more aircraft-level and moving down to component-level. The grey boxes signify concepts that were

discarded while the green concepts were pursued further. The over-arching design path is inline with the research objective and industry recommendation to simplify the kinematic mechanism of Bourget in order increase the feasibility of commercial operation.

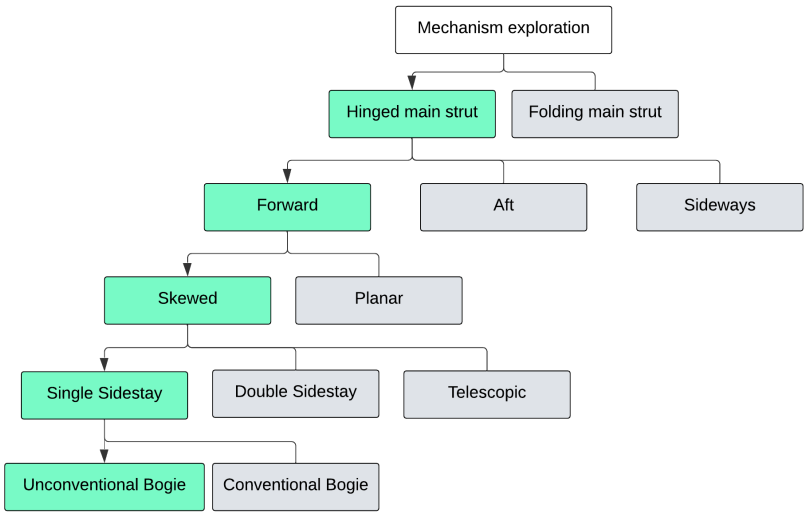

Figure 3.5: Mechanism concept exploration diagram

3.4.1. Planar and skewed retraction

Although forward and aft retraction has been successfully implemented on past aircraft with long landing gears as seen in Chapter 2, an initial choice had to be made. Forward retraction was selected as the preferred mechanism over aft retraction for multiple reasons. The main being that a forward retracting landing gear can be deployed through gravity and aerodynamic assisted free-fall in the case of a hydraulic or actuating power failure. Furthermore, the approximate stowage volume with forward retraction is more aligned with the box structure designed by Voeten. Simple planar retraction was attempted but as can be seen in Figure 3.6, the skewed fuselage causes the gear to retract into the passenger cabin. In order to position the wheels in the designated stowage area the pintle axis is skewed, with the difference schematically show in Figure 3.7.

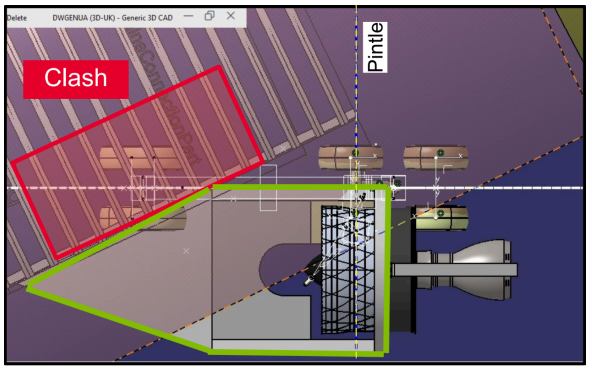

Figure 3.6: Top view: planar retraction

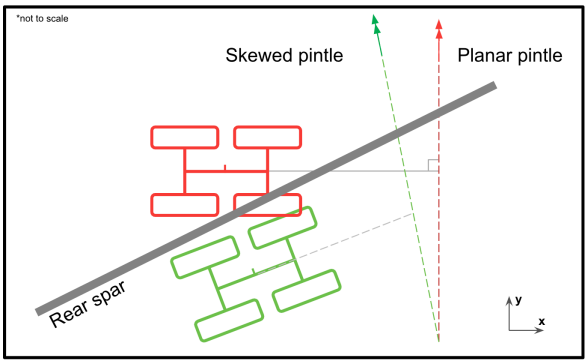

Figure 3.7: skewed pintle vs planar pinle axis schematic

The final location of the skewed bogie is essentially a vector in space and the location can be found numerically. However, since this mechanism was designed graphically, the right combination of angles was found manually and parameterized. Namely, the gear was first rotated about the x axis at the top of the hinge and then once more in its local x-z plane, creating an angle θ_{sd}. Once the final position is

sketched, The pintle axis can be obtained in CATIA by constructing two lines between corresponding bogie axle end-points in their extended and retracted stated, and adding a normal plane to each line. Using the intersect command it is then possible to find the intersection of these planes and will result in the pintle axis. The suitable sideways retraction angle was found to be 25°. Any less the the forward outboard wheel penetrates rear spar. Any more and bogie is positioned more parallel to the rear spar. Skewing the angle too much increases the acute angle which increases complexity and out-of-plane stresses.

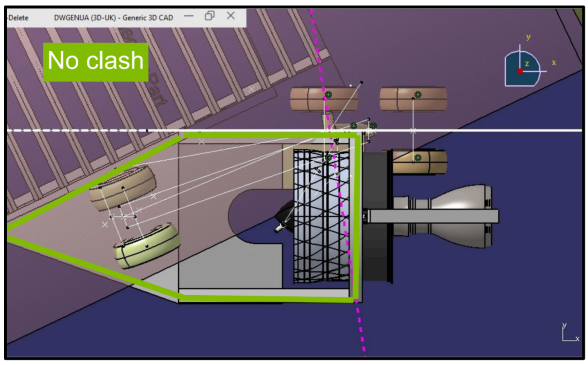

Figure 3.8: Top view: skewed retraction

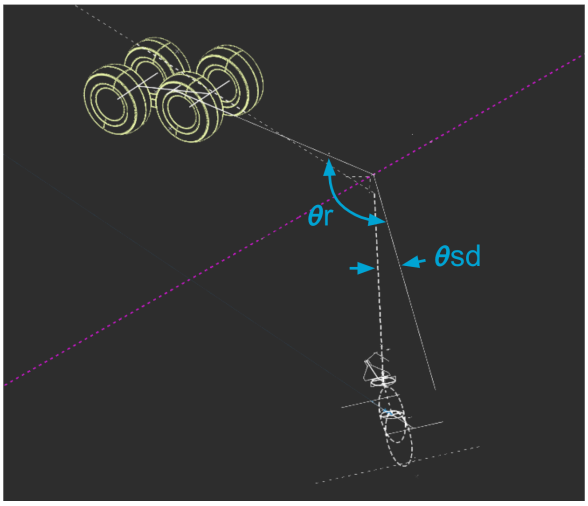

Figure 3.9: Parametric sideways angle and retraction angle definition

3.5. Component kinematics

With the retraction concept defined the next step was to add structural members to the mechanism. The aim was to start with the most dependent and critical components required for the gear to function and cascade down to less dependent components.

3.5.1. Sidestay & Crossbrace

As the name suggests, the function of a sidestay on a conventional aircraft is to counteract sideloads. During the exploration phase, a folding sidestay was chosen as it is operationally simple and commonly found on almost all aircraft in some shape or form. On most modern transport aircraft the sidestay is orientated perpendicular to the aircraft center line. However, on the Flying-V the fuselage longitudinal axis is swept with respect to the global longitudinal axis, therefore a systematic approach had to be taken to obtain a sensible initial guess. From a Kinematic perspective the following parameters were varied in the model:

- Main leg attachment point z-position
- Engine attachment point x-position
- Engine attachment point y-position
- Sidestay apex

The initial placement of the sidestay was oriented at a 45°angle in order to take up 50 percent of the side loads and braking loads. It was then attached to the bottom third of the main fitting and on the outside face of the engine mounting structure. This was chosen to provide maximum load triangulation. The apex was placed at 30% of the sidestay length from the main fitting. Due to the skew of the main leg a simple folding joint is not an option. Therefore, a universal joint was implemented that provides two degrees of rotational freedom by means of a revolute connection between the universal joint to the sidestay and a cylindrical connection between the universal joint and the main gear leg.

Varying engine structure attachment height

The universal joint attached to the engine structure, is referred to in this report as point S. As can be seen in Figure 3.10 attaching this point higher on the box than in Figure 3.12, results in the sidestay sweeping

upward. This penetrates the upper surface and clashes with the design requirement of keeping the inlet flow undisturbed. It was observed that a lower attachment point is preferable. This comes potentially at a future cost of more complicated attachment structure near the edge as opposed to in the middle of the box structure.

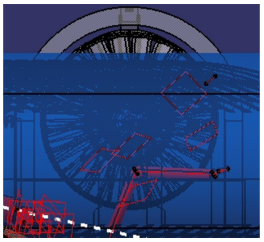

Figure 3.10: Z = 1000mm

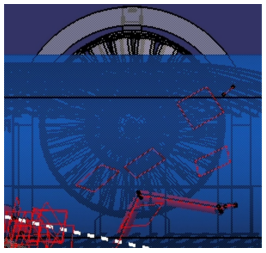

Figure 3.11: Z = 500mm

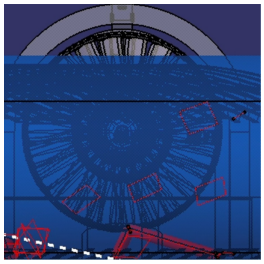

Figure 3.12: Z = 50mm

Varying engine structure attachment height

Varying Node S along the x-axis of the box structure affects the sweep of the sidestay in the z-x plane. When comparing different positions in Figure 3.13 and Figure 3.14 it can be seen that moving the attachment point forward causes the apex to drop below the engine box structure. By pulling it back, the apex moves inboard and the sidestay levels with the box structure. However, moving the attachment too far back reduces the structural triangulation efficiency and potentially clashes with the bottom of the engine fairing.

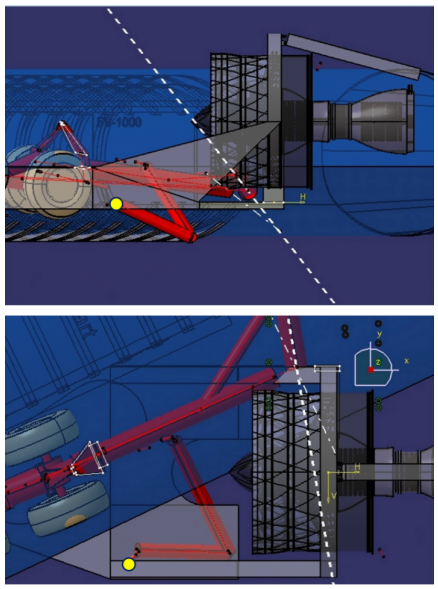

Figure 3.13: Fwd position X = 28900mm

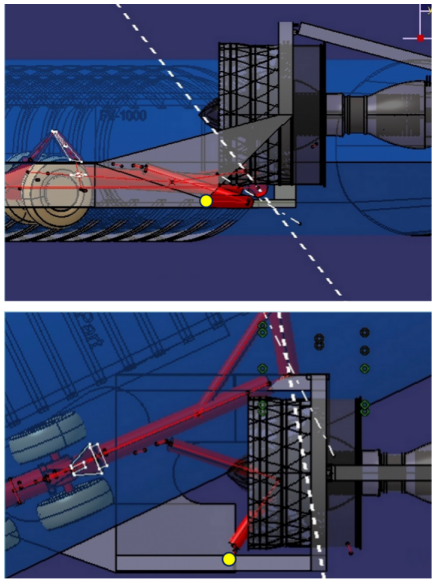

Figure 3.14: Aft position X = 30750mm

Varying sidestay apex

The apex point affects the figures below show the effects of varying sidestay apex on the sweep of the sidestay in it's retracted state. For an apex of 0.3 seen in Figure 3.15, the apex swing inboard past the wall of the box structure. By increasing the length of the upper sidestay member, the folding point occurs more inboard and also moves the point slightly upwards.

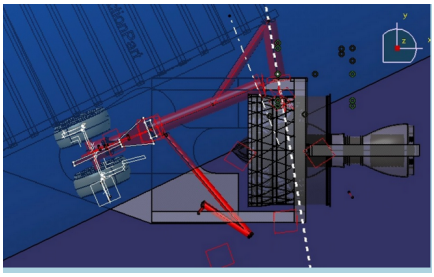

Figure 3.15: High z-attachment point

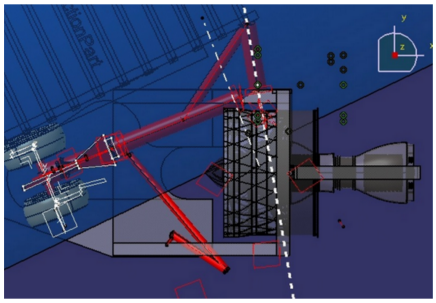

Figure 3.16: Low z-attachment point

3.5.2. Bogie mechanism determination

With the wheels positioned in the designated stowage and fixed wheel spacing determined earlier in Section 3.3.1, the bogie kinematic mechanism was investigated. An A330 bogie, seen in Figure 3.17, which resembles almost all conventional bogies was tested first and it was observed that even at higher-than-average bogie fold angle, that the forward tires clashed with the upper surface. Moving the assembly downwards was deemed not unacceptable given the bulbous nature of the bogie and the resulting large fairing. A flat-packing concept was then pursued as seen in Figure 3.18. Flat-packing can be achieved by various means as covered in Chapter 2.

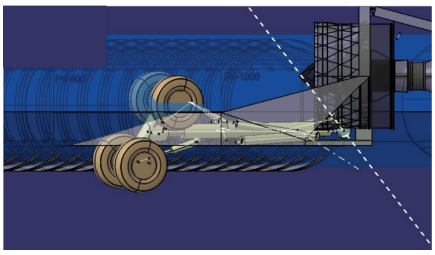

Figure 3.17: Conventional bogie

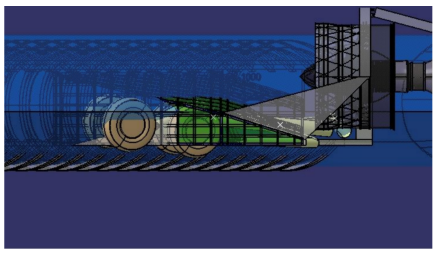

Figure 3.18: Flat-packed bogie

Key points to mention:

- Simple design is desired with simple hinged retraction.
- Space is to be kept around possible hinges and points of rotation to allow space for oversized bearings
- Allow clearance in wheel well not only to allow for tire expansions but also motions in flight

3.5.3. Final mechanism

With the flat-packed bogie designed, the mechanism was iterated in order to obtain the optimal clearances and minimize fairing size. These were checked by simulating the entire mechanism using Kinematic connections in CATIA. The results of the final kinematic design as well as the evaluation of the landing gears features with respect to the design considerations can be found in the results section **??**

4

Weight Estimation Methodology

The following chapter describes the methodology behind the development of the so-called Landing Gear Mass Module (LGMM). This includes an explanation of the framework, the geometry generation, the analytical methods used to calculate stress, the optimizer and the method to obtain a total weight landing gear weight.

4.1. Module framework

The Landing Gear Mass Module (LGMM) as it is called in this report, comprises the set of related functions, classes and variables that were developed during this study to calculate the weight of the landing gear. In line with the research objective, the module is required to be integrated into a larger landing gear tool developed by the Future Projects Office. As a result several criteria need to be met to ensure the code fits into the existing framework.

- The module must be able to handle and inherit data from other modules within the library
- The module shall adhere to the formatting conventions of the existing tool framework
- The module shall not use external third-party python modules
- The code shall be readable and commented for future work at FPO

In terms of functionality the module is considered an analysis tool able to size the structural components and output a set of processed data including the total landing gear weight based on an initial geometry. Meanwhile, the methodology is based on the work by Chai and Mason explained earlier, but has been adapted to the needs and objectives of this thesis. The flow diagram of LGMM is pictured in Figure 4.1. The various blocks are explained below:

1. **Geometry generation:** a landing gear geometry is discretized into nodes and beams using an internal 1D FEM class.
2. **Resolution of Forces:** a layout analysis checks the turnover angle and static loads and applies the external loads in order to obtain the reaction forces.
3. **Internal stress calculations:** The reaction forces are fed into the Tube Class which calculates the buckling and bending stress acting on each beam
4. **Beam sizing:** The stress ratios are fed into a minimize function that obtains the minimum tube thickness per loadcase required to satisfy the critical buckling or stress safety factor
5. **Mass generation:** The critical loads are determined per beam and processed to obtain a final landing gear weight alongside useful processed data

As touched upon, LGMM inherits attributes, classes and data from other modules in the overall landing gear tool. These are highlighted in pink and include the `Aircraft` class which feeds the Flying V overall aircraft parameters, `1DFEM` which discretizes the geometry into beams and `Loadcase` which calculates the ground loads. It is also important to note that the landing gear tool was in active development which dictated the approach to building up LGMM. To ensure bugs stay isolated from the rest of the code global unit tests had to be run before committing new code. This made sure that the data flow for the entire tool worked as expected and was not altered by changes made in LGMM. It also increases the confidence in the smaller steps and assumptions used. This includes communicating changes with co-developers and ensuring the coding architecture is appropriate.

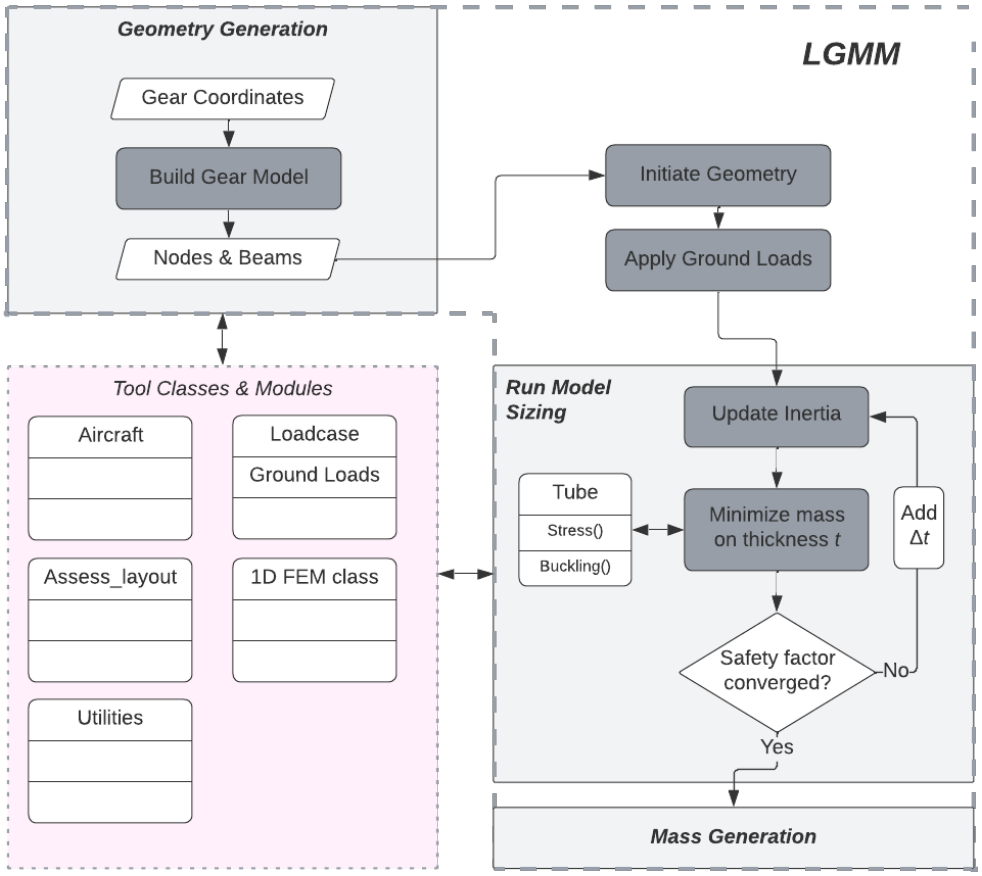

Figure 4.1: Flow chart sizing process

The dark grey boxes represent code that was programmed from scratch, whereas the classes in the pink box are inherited functions and modules. The landing gear of a Flying V may be unconventional as a system but when broken down into beams it can be approached and verified by looking first at 1D beams, then 2D beams and finally 3D beams. When transitioning from textbook examples to landing geometries consistent checks had to be conducted with experts within FPO to serve as sensibility checks on values. The overall aim of LGMM is to obtain a weight estimate using as much physics-based data as possible. The mass generation block is shown below in Figure 4.1.

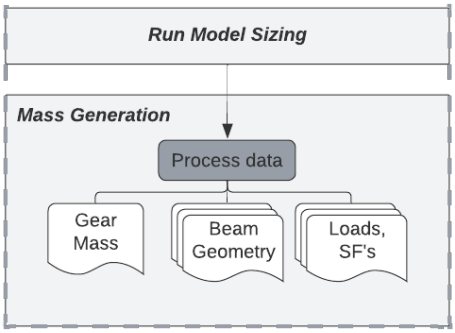

Figure 4.2: Mass generation block

4.2. Baseline geometry generation

With a feasible baseline MLG obtained from the kinematic design process in Chapter 3, a geometry can now be generated. The steps and assumptions are explained in the following section and include beam

discretization and the definition of the degrees of freedom for each node.

4.2.1. Geometry discretization

The CAD model can be represented as a stick model as shown in Figure 4.3. The local datum for the landing gear is point E located at the center of the bogie-gear pivot axis. The remaining points are measured relative to point E. The coordinates from the right and left baseline gear are shown in Table 4.1 and Table 4.2, respectively. It is assumed that all primary structures are directly connected to each other, when in reality there exists joints, offsets and lugs. This is not a limitation of the code but a decision to enable rapid geometry generation. Furthermore, joints and offsets are considered as detailed design components and thus their improper sizing at a preliminary stage could influence the results.

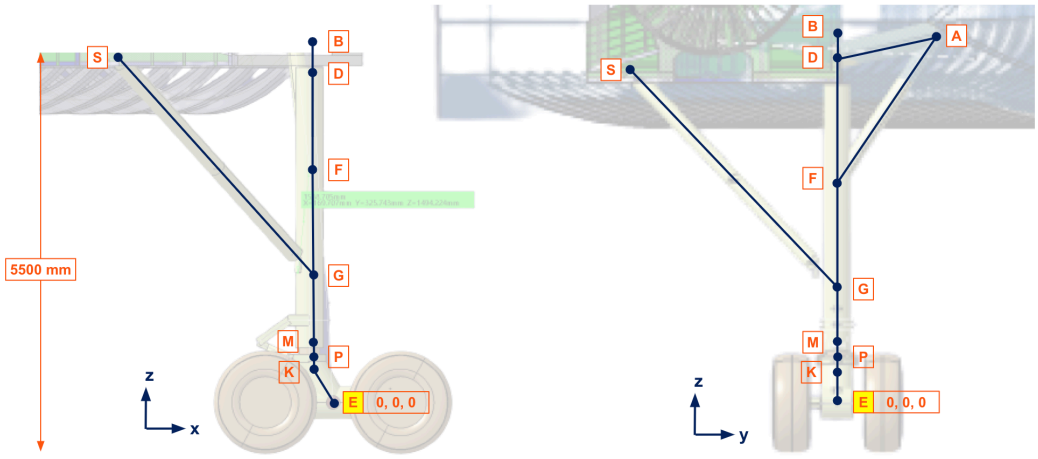

Figure 4.3: Baseline Flying V Right MLG stick diagram

Table 4.1: Right gear coordinates

Node	x [mm]	y [mm]	z [mm]
E	0	0	0
K	-346.4	0	600
P	-346.4	0	705
M	-346.4	0	801
G	-346.4	0	2100
S	-3146.4	-3100	5025
F	-346.4	0	3395
D	-346.4	0	4900
A	-605.7	1524.1	5662.9
B	-346.4	0	5325

Table 4.2: Left gear coordinates

Node	x [mm]	y [mm]	z [mm]
E	0	0	0
K	-346.4	0	600
P	-346.4	0	705
M	-346.4	0	801
G	-346.4	0	2100
S	-3146.4	3100	5025
F	-346.4	0	3395
D	-346.4	0	4900
A	-605.7	-1524.1	5662.9
B	-346.4	0	5325

4.2.2. Degrees of freedom

An important next step is to assign the degrees of freedom (DoF's) to each node as this is crucial to obtain a solution to the stiffness matrix. Therefore, the translation and rotation along the x, y and z axis for each node need to be defined. The degrees of freedoms for node G and node S, which make up the sidestay, as well as the datum node E are given as an example in Table 4.3. The sidestay is made up of a spherical joint, at Node S, which represents the attachment into the engine structure and a universal joint, Node G, at the attachment into the main fitting. The reason the sidestay is prevented form rotating along it's own longitudinal axis is so that it takes up the bending moments. This is common for sidestays as can be visualized in the literature review..

Table 4.3: Degrees of freedom for datum and sidestay nodes

Node Name	Translation			Rotation		
	δ_x [-]	δ_y [-]	δ_z [-]	θ_x [-]	θ_y [-]	θ_z [-]
node E	Free	Free	Free	Free	Free	Free
node G	Fixed	Fixed	Fixed	Fixed	Free	Free
node S	Fixed	Fixed	Fixed	Free	Free	Free

The DoF's for Node A and Node B are also crucial to the solution because they interface between the main landing gear leg and the airframe. Node B is the inboard joint attaching to engine structure and is modelled as a pure spherical joint. Node A which attaches to the rear spar, is defined as a spherical joint with an additional degree of freedom along the pintle axis. This makes the system statically determinate. Assuming that a spherical joint with a linear bearing is more complex in construction it was decided to place this bulkier joint closer to the main structure. In reality, this decision should be clarified based on the final desired loadpath.

4.2.3. Beam properties

With the nodes defined, LGMM is able to construct and assign the relevant properties to each beam. It is assumed that all beams are circular tubes with an inner and outer diameter. Each beam must be assigned an inner diameter such that beam inertia is initialized. This is important for the correct functioning of the minimize mass function. The inner diameters for the baseline MLG are chosen as 80% of the outer diameters digitally measured on a A330 landing gear. Given that the A330 is a lighter aircraft this assumes that the initial inner diameters are sufficiently undersized but still in the correct order of magnitude. Beam names in the form of strings are also assigned and used extensively as keys for the parsing of data in the later phases. The naming of class variables as strings is an example of convention that was kept consistent across the entire landing gear analysis tool. The inner diameter of the main fitting is set by the shock-absorber piston diameter. Finally, the secondary axis, which used by the model to align the local and global axis systems. For this model it is assumed the secondary x-axis runs through the longitudinal axis of the beam.

Table 4.4: FV1000 beam discretization definition

Beam	Name	Node 1	Node 2	Inner diameter [mm]
EK	kink	E	K	400
KP	kink_to_piston	K	P	400
PM	piston_to_lower_cylinder	P	M	330
MG	lower_cylinder_to_sidestay	M	G	380
GS	sidestay	G	S	220
GF	sidestay_to_cross_brace	G	F	380
FD	upper_main_fitting	F	D	380
FA	crossbrace	F	A	220
DA	outboard_to_inboard_pintle	D	A	380
DB	outboard_pintle	D	B	380

The material assumed for all beams in this model is 300M steel with properties shown in Table 4.5, as it is exceptionally stiff and widely used in modern landing gears [21, 19]. In reality however, composites could soon become more even on primary load-bearing structures.

Table 4.5: 300M steel physical properties [39]

	$E[GPa]$	$\rho[kg/m^3]$	$\sigma_y[MPa]$	$\sigma_c[MPa]$
300M Low-alloy steel	200	7833	1586	1703

The cross-section of the beams modelled in the Tube class is shown in Figure 4.4. The beam geometry is initialized by assigning the inner diameter and selecting an initial thickness, from which the outer diameter can be calculated.

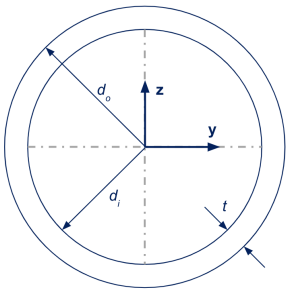

Figure 4.4: Tube cross section notation

This allows for the calculation of the physical properties such as the moment of inertia and surface area using Eqs. (4.1) – (4.4).

$$I_{yy} = I_{zz} = \frac{\pi}{64}\left(d_o^4 - di^4\right) \quad (4.1)$$

$$I_{xx} = I_{zz} + I_{zz} \quad (4.2)$$

$$A = \frac{\pi}{4}\left(d_o^2 - d_i^2\right) \quad (4.3)$$

$$J = \frac{\pi}{32}\left(d_o^4 - d_i^4\right) \quad (4.4)$$

It can be seen from these equations that properties of the beam are beam are a function of the thickness. By changing the thickness, the moment of inertia of the beam changes, which is a key relationship used in the minimize function.

With the node DoF's, beam properties and external loads defined the sizing function is able to resolve the reaction and internal forces on a given beam. As an example, a simple cantilever beam is loaded with an external force acting at the free-end as shown in Figure 4.5 to visualize the results of 1DFEM class. The colored arrows represent the fixed degrees of freedom, in this example the beam is fully-fixed in all directions. The magenta arrows at Node A represent the reaction forces and the magenta arrow at Node B represents the external force. The quivers are scaled proportionally to force therefore offering quick visual verification. The internal moment can also be plotted in yellow as can the deflection and shear. The 1DFEM classes resolves forces as the names suggest using the Finite-Element Method covered in Chapter 2.

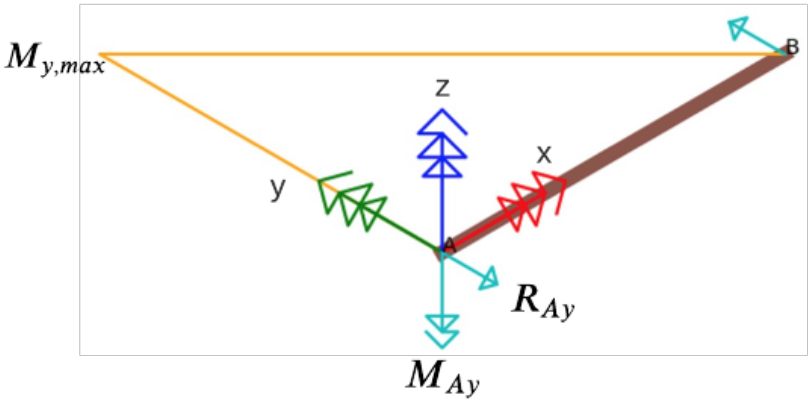

Figure 4.5: Plotting capability of internal 1DFEM Class

4.3. External loads

Referring to the LGMM flow diagram in Figure 4.1, the sizing function inherits the external loads from an internal Loadcase library. This library which is part of the the overall framework contains numerous loads used by FPO. Bookkeeping of loads is crucial because in an industrial setting loads are imported from various departments. To keep in line with this methodology and to isolate different assumptions, the ground loads for this study were calculated from scratch rather than using existing loads. The following ground loads are then to be implemented and inherited for sizing [14]:

- Taxi CS25.491
- Turn CS25.495
- Braked2point C25.493
- Pivot CS25.503

These are a function of the static load per MLG, F_s. The static load per MLG is computed using Equation 4.5 and influenced by the Flying V MTOW and gear layout [18].

$$F_S = \frac{W}{(A/2C + BL_{cg}/T)} \tag{4.5}$$

(4.6)

However, given that this study concerns the landing gear at component level, the MTOW of the aircraft remains constant. As such the static force, calculated to be 127.5 tons on one leg is also constant throughout all further analysis. The remaining variables used to calculate the ground load equations seen in Figure 2.5, are shown below in Table 4.6. It is important to mention that for bogied landing gear ground loads are usually applied at the axle [3]. However as tyre-deflated load cases are not covered (which would result in additional torque around the bogie beams) the external forces will be applied at the bogie pivot point as was done by Chai and Mason [24].

Table 4.6: Load factors and parameters used to calculate external ground loads

Variable	Definition	Turn	Brake2Point	Pivot	Taxi
n_y	loadfactor along y [-]	0.5	-	-	-
n_z	loadfactor along z [-]	1	1	1	1.7
μ	friction coefficient [-]	0	0.8	0.8	0
K_{piv}	pivot coefficient [-]	-	-	1.33	-
d_p	bogie pitch [mm]	-	-	1981	-
d_i	bogie track [mm]	-	-	1397	-
L_{cg}	x cg location [m]	32.4	32.4	32.4	32.4
B	wheelbase [mm]	tbc	tbc	tbc	tbc
T	track [m]	12.2	12.2	12.2	12.2
W	MTOW [t]	260	260	260	260
A	x nose to cg [m]	tbc	tbc	tbc	tbc
C	x main gear to cg [m]	tbc	tbc	tbc	tbc

4.4. Calculating stress

The Tube class contains the stress function and the buckling function. Both are developed from the ground-up and inherit the beam properties from the 1DFEM class. The stress class then assigns physical attributes such as the elasticity, shear modulus, yield stress and the starting inner diameter and wall thickness. The stress function outputs its results to the update_inertia function which is called by the optimizer. The update inertia function calculates the outer diameter (which is a function of the inner

diameter and thickness) as well as the various moments of inertia. The tube class also includes the mass function.

The stress in a thin-walled tube is calculated by taking into account combined loading due to axial load and bending. The stress due to axial load is given by Equation 4.7.

$$\sigma_{axial} = \frac{P}{A} \tag{4.7}$$

The shear stress is a function of the Torsion, T_x, the beam geometry and the internal shear. The normal stress is function of the geometry, the axial stress and the internal bending moments. These equations are derived from classic mechanics of material literature but have tailored adapted for thin-walled tubes [24].

$$\tau_{shear} = \frac{1}{\pi r_{avg} t} \cdot \left(\frac{T_x}{2r_{avg}} \pm \sqrt{V_y^2 + V_z^2} \right) \tag{4.8}$$

$$\tau_{normal} = \sigma_{axial} + \left(\frac{1}{\pi r_{avg}^2 t} \pm \sqrt{M_y^2 + M_z^2} \right) \tag{4.9}$$

Von Mises yield criteria was selected as a design criteria because it is a reliable standard within structural analysis meaning that there are simple textbook examples available for verification. Furthermore, it has been used by Chai and Mason in their landing gear tool as well as the engine box-structure study by Voeten. Von mises stress is calculated with Equation 4.10

$$\sigma_{mises} = \sqrt{\tau_{normal}^2 + 3\tau_{shear}^2} \tag{4.10}$$

As will be explained in the Optimizer Setup, a target safety factor of 1.5 is selected in accordance with argumentation provided by Schmidt and Chai and Mason based on the fact that it has been used in the design of successful landing gears. However, for future detailed design it should be noted that a safety factor does not protect against fatigue. Von Mises stress and buckling criteria are used for the classification of whether a load is critical or not [21, 24].

4.5. Calculating buckling

The lateral deflection that can cause long slender beams to become unstable is called buckling. Given that the Flying V baseline LG is considered to have an unconventionally legs, it is important to give this failure mode attention.

It is assumed that all beams in the tube class are ideal columns. This means that the load is applied at the centroid of beam cross-section. When load is applied it is assumed that the beam will buckle about it's principal axis with the least moment inertia. The critical load at which the column begins to buckle, P_{cr}, depends

$$\sigma_{cr} = \frac{\pi E}{(L/r)^2}$$

The formula also doesn't take into account fillet radii, blend radii or corner breaks. For future studies such details would influence stress concentrations and also the structural analysis of the beams.

$$r_g = \sqrt{\frac{I_{min}}{A}} \tag{4.11}$$

$$SR = \frac{L_{effective}}{r_g} \tag{4.12}$$

The modulus of elasticity is assigned by the user in the *Geometry Generation* function and the tube class inherits the length and moments of inertia from the Beam class. For a cylindrical beam all moment's of inertia are equal due to the symmetric nature of the cross-section. However, if LGMM is further expanded to include an I-beam, for example, then an additional action needs to be added to select the least moment of inertia.

The slenderness ratio of the beam SR is akin to the the aspect ratio of a wing and is measure of the beams flexibility. It is an important value to find out because it dictates which buckling equation to use in the function. Figure 4.6 visualized the regions in green which are covered by LGMM.

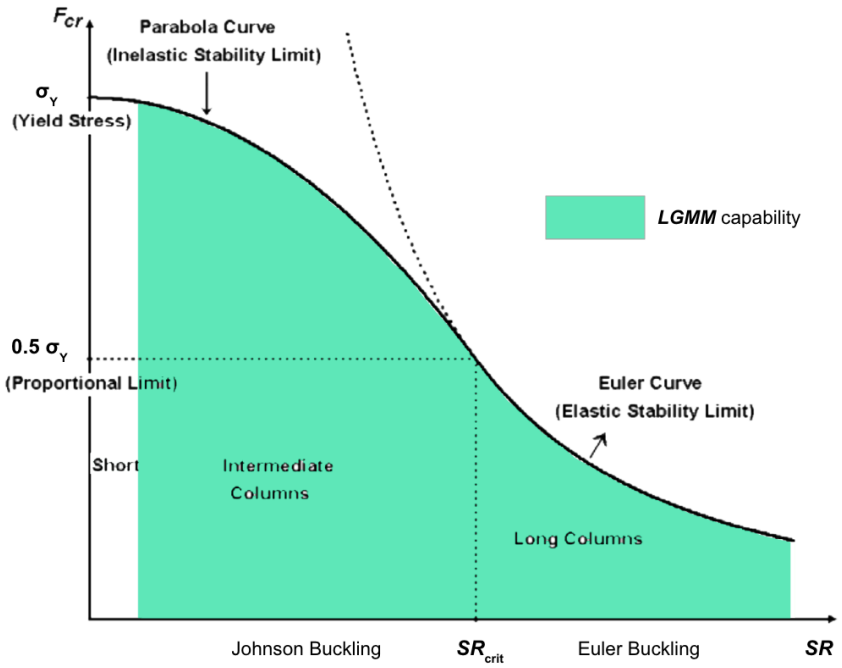

Figure 4.6: Diagram showing elastic and inelastic buckling regions adapted from [40]

The addition of a function that takes into account intermediate columns is not explicitly used by previous reference models such as Chai and Mason. They only take into account long columns and as such this function should be able to accurately capture a broader selection of columns.

Using the beam properties the critical aspect ratio can be calculated using Equation 4.13. The correct approximation of the curve above is then approximated with the conditions in Equation 4.14[31].

$$SR_{crit} = \sqrt{\frac{2\pi^2 E}{\sigma_{yield}}} \tag{4.13}$$

$$\sigma_{cr} = \begin{cases} \frac{\pi^2 E}{(SR)^2} & \text{if } SR > SR_{crit} \\ \left[1 - \frac{(SR)^2}{2\cdot(SR_{crit})^2}\right] \sigma_Y & \text{if } SR < SR_{crit} \end{cases} \tag{4.14}$$

The critical buckling stress is then used as an input when called by the optimizer. Additionally, it is assumed that post-buckling and creep is not take into account. Furthermore all loads act through the longitudinal axis of the beam.

4.6. Optimizer setup

In order to obtain a structurally efficient beam, the tube must be as light as possible while being able to sustain the highest possible combined loading whether that be through stress or buckling. The following section explains the strategy behind the cost function and the imposed constraints.

4.6.1. Cost function

As formalized in Equation 4.15, the objective of the cost function is to minimize the sum of the mass of the beams, which essentially means minimizing the landing gear structural mass. The mass is a function of the thickness, variable x. The thickness is constrained between t_{min}=0.001 and t_{max}=0.9. The maximum thickness is trivial while the minimum thickness was chosen as relatively low in order to avoid overestricting the results. The large range requires a sensibility check at when evaluating the geometry results. A specific algorithm is not selected in Scipy h within the thickness boundaries and such that the stress and buckling constraints are not violated. In other words, the aim is to minimize the total mass of a landing gear structure for a unique loadcase. An initial thickness mass is calculate for an initial thickness x. The function then increases the thickness and updates the inertia of the beam. With a new inertia a new stress and buckling value can be found.

This minimize function is called oncd for each loadcase. Meaning that for this study the function is called 4 teams, resulting in four minimum masses per component, the maximum mass per beam is considered the critical mass and will make the final structural mass. More on in this in later chapter. The optimizer workflow described by Equation 4.15, the objective function is to minimize mass for a beam i

$$\begin{aligned} \text{min} \quad & f(x) = \sum_{i=1}^{n} \text{mass}(x_i) \\ \text{s.t.} \quad & t_{min} \leq x \leq t_{max} \\ & \frac{1.0}{FS_{target}} - R_s \geq 0 \\ & \frac{1.0}{FS_{target}} - R_b \geq 0 \end{aligned} \tag{4.15}$$

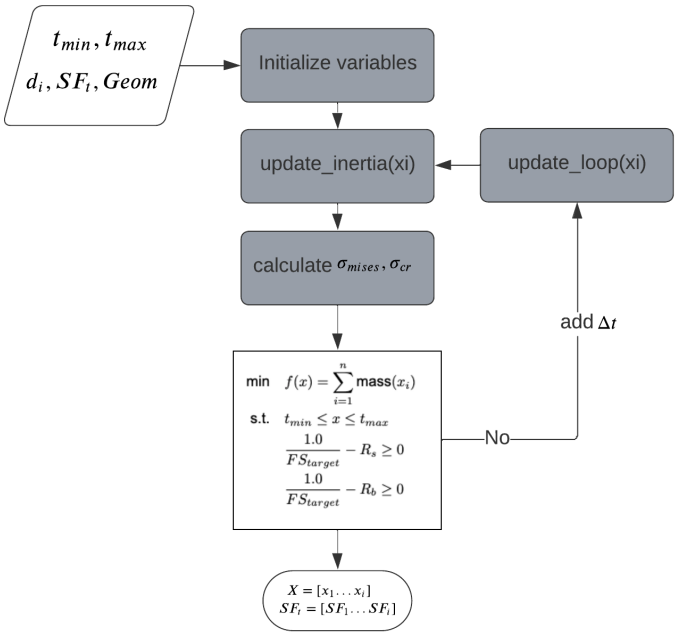

Figure 4.7: Optimizer flow diagram

4.6.2. Optimizer constraints

The conditional constraint $R_s(x_i)$ is the stress ratio between ”actual” stress calculated during the loop, σ_{mises} and the allowable material stress σ_{yield}. If the stresses on a beam are negligible then the ratio is set to 0 to avoid divide by zero error.

$$R_s(x_i) = \begin{cases} 0.0 & \text{if } \sigma_{mises} <= 100 \\ \sigma_{mises}/\sigma_{yield} & \text{otherwise} \end{cases} \tag{4.16}$$

Similarly, $R_b(x_i)$ is the stress ration between the ”actual” stress σ_{axial} and the allowable stress σ_{cr}. In this instance the allowable stress is calculated and the actual stress is given by the material properties. When the axial forces are positive, the beam is under tension or therefore the stress ratio is set to zero because buckling is not applicable. If there is no load on the beam then the stress ratio is set to zero aswell to avoid division errors.

$$R_b(x_i) = \begin{cases} 0.0 & \text{if } \sigma_{axial} > 0 \\ 0.0 & \text{if } \sigma_{axial} = 0 \\ \sigma_{axial}/\sigma_{cr} & \text{if } \sigma_{axial} < 0 \end{cases} \tag{4.17}$$

When the optimizer has converged it outputs the converged thickness, the buckling safety factor and the stress safety factor for each beam. From this the mass and outer diameter can be derived. The optimizer obtains the results for a single loadcase, therefore it needs to be run 4 times for the four loadcases investigated in this study in order to obtain a final landing gear weight.

4.7. Critical load cases

At this stage in the method LGMM has produced 4 data sets for 4 different loadcases. That means that there are four possible thicknesses and four possible masses for each beam. In line, with the sub-research question it is vital to determine for each beam which loadcase is critical. By doing so it is possible to find out for each beam which loadcase produces the highest combined loading thus results in the highest mass.

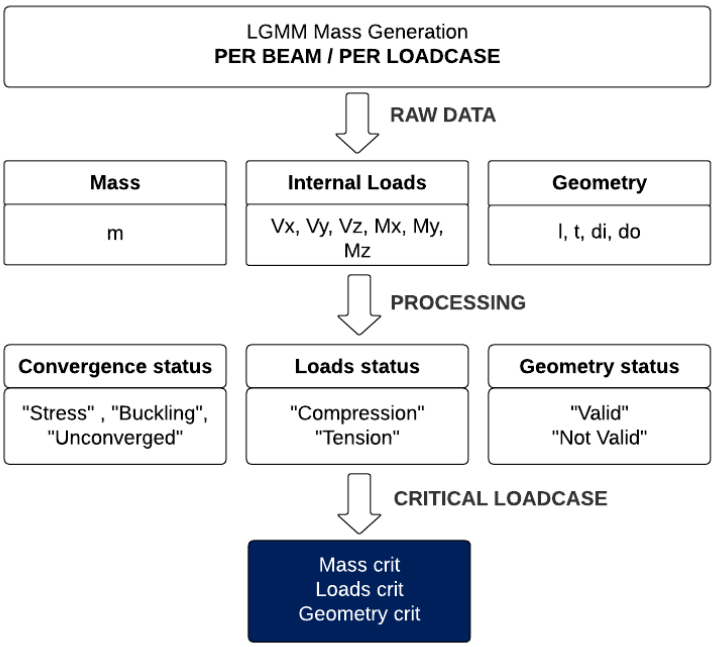

Figure 4.8: Results data flow diagram

A loadcase is considered critical for a beam if the following for conditions are met:

1. Geometry of the beam is valid
2. Convergence to von mises or buckling is reached
3. Loadcase corresponding to the largest beam mass

Of course the above are not independent conditions because, convergence is tied to a valid geometry. For example, it is observed that beams that don't reach convergence are overzized meaning the step thickness of 1mm is applicable. However, 1mm is below the required thickness for a valid geometry so both convergence and valid geometry are tied.

The conditions above are checked for every combination of beam and loadcase analysed. If the conditions are met a 1 is assigned and otherwise 0. The critical loadcase can then be identified based on where a beam has a three ones. This is schematically shown below with the reference data for the Flying V.

4.8. Weight estimation method

The following section breaks down the methodology required to obtain a final main landing gear and subsequent aircraft landing gear weight. For this study, the weight of a single main landing gear, $W_{MLG/2}$ is a summation of the structure, the bogie assembly and the control systems, as expressed in Equation 4.18.

$$W_{MLG/2} = W_{structure} + W_{bogie} + W_{controls} \tag{4.18}$$

This breakdown differs slightly from other methodologies implemented for example by Chai and Mason. Chai and Mason compute the weight of the bogie structure (beam and axle) and the rolling stock (wheels, brakes, tires) separately. For this study, as will be explained in Section 4.8.2, the bogie assembly is derived *including* the bogie structure.

1. Run LGMM to compute mass per beam per loadcase

2. Obtain mass per beam corresponding to critical loadcase
3. Obtain raw primary structural weight representing summation of all critical masses
4. Apply secondary mass and modelling error correction factors
5. Obtain total structural weight
6. Separately compute bogie mass as a function of MTOW
7. Derive control systems mass using statistical component breakdown
8. Sum structural, bogie and control mass to obtain single main landing weight

4.8.1. Structural weight

Once the sizing function computes the required thickness of the material in order to meet the failure criteria, the mass per beam can then be straightforwardly calculated using Equation 4.19. Here area, A is computed using the known inner and outer diameter and the density of 300M steel is used as seen in Table 4.5.

$$W_{LGMM} = \sum m_{i,crit} = \sum \rho_i A_i l_i \tag{4.19}$$

Having computed the mass for each beam per loadcase, the tool then extracts the highest mass per beam as this corresponds to the critical loadcase. Following the sensibility check explained earlier, the mass of the ”worst-case” beams are then summed to calculate the raw total primary structural, mass W_{LGMM}. This value does not represent the overall structural weight however because it only accounts for cylindrical tubes that make up the primary structural beams. In reality the landing gear structural weight, $W_{structure}$, also includes secondary components as given by Equation 4.20.

$$W_{structure} = W_{LGMM} + W_{st,secondary} \tag{4.20}$$

The secondary components include the torque links, fittings, pins, oleo seals, metering tubes, and bearings among others. They are assumed to account for 25% percent of the overall structural weight [24]. This breakdown can be expressed with Equation 4.21 and Equation 4.22

$$W_{LGMM} = 0.75 \cdot W_{structure} \tag{4.21}$$
$$W_{st,secondary} = 0.25 \cdot W_{structure} \tag{4.22}$$

Plugging these expression back into Equation 4.20 makes it possible to calculate the overall structural weight as a function of the known output. This can be seen in Equation 4.24

$$W_{structure,0} = \frac{4}{3} \cdot W_{LGMM} \tag{4.23}$$

During the A310 validation case, discussed in detail in the next chapter, it was found that the method presented so far under sizes the structure by 33%. This model error calibration factor is therefore multiplied by Equation 4.24 to obtain

$$W_{structure} = K_{correction} \left(\frac{4}{3} \cdot W_{LGMM} \right) \tag{4.24}$$

4.8.2. Bogie assembly weight

The structural weight derived from the LGMM computation, in Equation 4.24, does not take into account in is not configured to be able to calculate the structural weight of the the bogie. The assumptions can be seen in (section on tool assumptions). Since the current study concerns changing the landing gear topology for an aircraft with constant MTOW it was deemed suitable to determine the bogie weight as an assembly comprising the wheels, tires, brakes, bogie beam and axle. This so-called bogie assembly, has been derived emperically.

a constant K_{bogie} is calculated in order to derive the bogie weight based on known data. Using the mass breakdown in Figure 2.17, K_{bogie} is the ratio between bogie weight and MTOW. This means that the bogie weight can be calculated based the MTOW of an aircraft.

$$W_{bogie} = K_{bogie} \cdot W_{MTOW} \tag{4.25}$$

Using the A310 as a reference since it provides the most reliable data the constie. $1510kg/142000kg = 0.010634$. It is difficult to verify this ratio as being encompassing for all aircraft especially with the lack of public bogie weight breakdowns. However, a relatively comprehensive study on bogie weight for a similar-sized transport aircraft resulted in $K_{bogie} = 0.007521$ [41]. The authors claim that their weight estimates correspond to statistical data available to them. Various bogie factors are tabulated in Table 4.7. At the moment it is difficult to rationally choose one calibration factor over another. Therefore the average is taken as a middle ground and used in subsequent calculations.

Table 4.7: Bogie factor calibration

Approximation	K_{bogie}	$W_{bogie}\,[kg]$
Conservative	0.01060	2756.0
Middle-ground	0.00906	2355.6
Optimistic	0.00752	1955.5

4.8.3. Total landing gear weight

The final weight component missing from Equation 4.19 is $W_{controls}$, which comprises items such as actuators. Given the scope of the study and since these components are considered detailed design, they have not been calculated analytically. Statistically, these make up 12% of the main landing gear weight, $W_{MLG/2}$ [17]. Using this it is possible to rewrite Equation 4.18 into the expression seen below:

$$W_{MLG/2} = W_{structure} + W_{bogie} + 0.12\,W_{MLG/2} \tag{4.26}$$

$$= \frac{W_{structure} + W_{bogie}}{0.88} \tag{4.27}$$

With the gear weight for a single Flying V main landing gear computed, it is possible to estimate the mass of the overall landing gear component group. As stated in the research objective the nose-landing gear weight is not computed as different set of loadcases are typically sizing cases. These load cases like towing and steering have not been implement yet in the LGMM. Therefore, the Nose-landing gear weight is calculated using the statistical equation from Raymer [8]:

$$W_{NLG} = 0.032 K_{\mathsf{np}} W_l^{0.646} N_l^{0.2} L_n^{0.5} N_{\mathsf{nw}}^{0.45} \tag{4.28}$$

$$= 1255.66\,kg \tag{4.29}$$

This can now be straightforwardly inserted in the expression for the overall landing gear group weight, W_{NLG}

$$W_{LG} = \left(2 \times W_{MLG/2}\right) + W_{NLG} \tag{4.30}$$

5

Verification & Validation

The following chapter outlines the steps taken to gain confidence in the weight estimation methodology described in the previous chapter. This covers the use of unit testing to verify separate functions and classes and the application of the complete methodology on conventional landing gear to evaluate the performance of LGMM.

5.1. Unit testing

Extensive unit testing was used as a verification for two main reasons. The first reason being that module was being developed in parallel to other modules as part of the the overall landing gear analysis tool. Unit testing minimizes the number of bugs during major code commitments and ensures proper data flow between modules and libraries. Secondly, since new functions are being developed, a systematic approach is required to ensure that each unit of code performs as expected and de-bugging occurs during each added step of complexity. These steps are roughly categorized into stress testing, optimizer testing and weight estimation testing.

5.1.1. Stress

In order to verify the combined stress the internal loads and beam geometry calculations were tested first. The accurate computation of shear V and bending moments M by the 1DFEM class, was first tested for simple 1D Beams with two nodes. Next, the same unit tests were applied on a 2D problem containing multiple nodes or multiple beam diameters. Finally, 3D problems and a simple internal nose-landing-gear geometry was tested. The nose-landing gear consisting of a simple beam and drag brace was also tested for different degrees of freedom, which helped gain confidence in correct DoF behaviour during the geometry generation stage. In addition to unit tests, rapid visual verification of reaction loads and internal loads was possible by verifying that the plotted diagrams behaved as expected. An example of this can be seen in Figure 5.1.

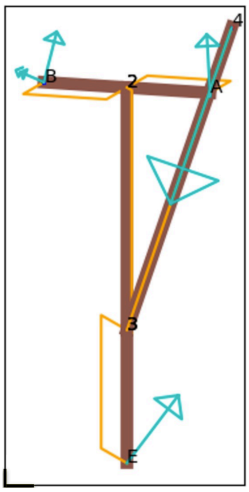

Figure 5.1: NLG internal and reaction loads from 1DFEM

Once sufficient confidence was gained, the relevant stress values σ_{shear}, $\sigma_{bending}$ and σ_{mises} were tested for the same 1D, 2D and 3D cases where applicable. Additional unit tests were added to test tosion in isolation and specific textbook examples were obtained to independently test von mises stress. As the stress calculation class was built from scratch, unit tests proved invaluable to ensure that the geometry and loads from the 1DFEM were inherited correctly. Bugs relating to data output and sign conventions were also addressed. Buckling was tested first tested for accuracy for short beams and long beams and then also for physical behaviour like the distinction between tension and compression.

Finally, the coupling of the stress class and the loadcase class was verified by running the Aircraft class for two variations of the 737-200 seen in Figure C.3 and comparing against the results tabulated in the book by Lomax as seen in Figure C.2 and Figure C.1.

5.1.2. Optimizer verification

The optimizer, which aims to solve the minimize mass function, calls the stress and geometry and therefore was also verified on simple thin tubes and eventually on a simple NLG. First, the optimizer is tested to verify the correct sizing of a beam for stress. Looking at Figure 5.2 a simple cantilevered beam is purposefully undersized for stress through a combined moment and axial internal force. It is undersized because of a calculate safety factor of 1.02 which confirms that the vonmises stress is equal to the yield strength of the material and hence does not satisfy the 1.5 safety factor requirement. After running the optimizer it can be observed in the second column of the same figure that the thickness is increased to a point where the safety factor for stress is now 1.5. This means the optimization problem is satisfied. Furthermore, it can be seen that the buckling safety factor increased from 8.62 to 12.18 which confirms the expected physical behaviour as as a higher moment of inertia increases the radius of gyration and therefore increases the force required to destabilize a column, thereby making the column more resistant to buckling. In order to test if the optimizer is able to size for buckling instead of stress, the beam cross-section is kept concept but the beam length increased to increase the slenderness ratio. The beam was confirmed to be oversized due to a buckling safety factor of 3.75. Upon running the optimizer the beam converged to a buckling safety factor of 1.5 and the stress safety factor decreased to 4.22.

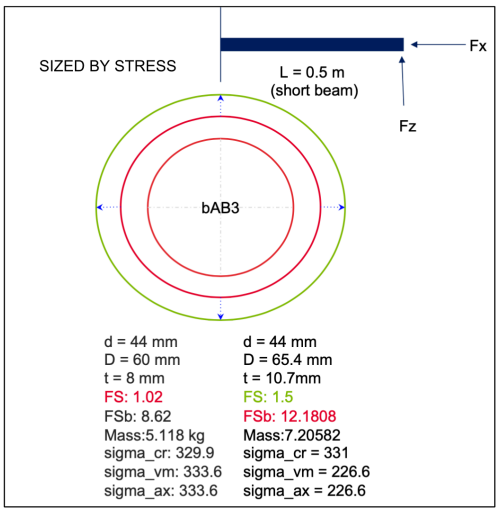

Figure 5.2: Sizing for stress

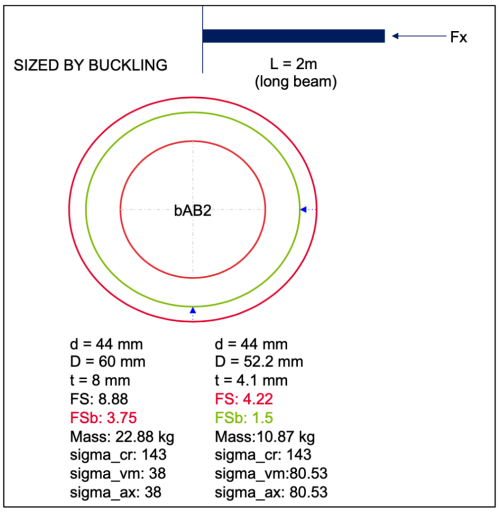

Figure 5.3: Sizing for buckling

These simple beam tests were part of a series of unit tests that confirmed that the optimizer is able to increase and decrease the thickness of a beam with a given inner diameter for both stress and buckling. Additional functionalities of the code were also tested to ensure that the optimizer results are correctly interpreted. The unit tests were then expanded to the simple NLG in Figure 5.1 to check if the optimizer can handle multiple beams. Further complexity was added by skewing the pintle BA in the NLG. As expected the weight increased since the attachment points experience out-of-plane loads.

5.2. Validation data determination

With the individual functionalities verified the module must be validated for a LG topology of a comparable commercial aircraft with a four-wheel bogie. Following a prolonged search, no suitable public landing gear data was found for a direct reference aircraft such as the A350. This can be attributed to the closely guarded nature of mass values on manufacturers proprietary data. Fortunately, suitable publicly available data was found for the A310-200 landing gear [42]. The two mass values available are the weight of a single MLG and that of the MLG Bogie assembly, 2710kg and 1510kg respectively. The legitimacy of the FedEx manual has been further verified by comparing the indicated FedEx MLG weight of 6110 kg to the A300B2 MLG weight given by Schmidt of 6186 kg.

As mentioned, LGMM does not have the capability yet to calculate the bogie beam axle weight. Therefore, the structural weight of the A310 without the structure of the bogie needs to be extracted in order to validate the mass output from LGMM. The first step in this extraction can be achieved by assuming the same MLG component mass breakdown found in Table 11.3 in [17]. The B707 mass breakdown is chosen because it has the closest MTOW, ranging from 111 tons on the B707-121 to 150 tons on the B707-320C, compared to the MTOW of 142 tons of the A310-200 [5]. On the B707, 38% of the MLG is rolling stock, 50% is structure and 12% is controls. Applying these percentages to the first given weight of 2710kg for single A310-200 MLG results in the breakdown shown in Figure 5.4. This estimated structural mass is verified against an actual source which puts the A310-200 % of structural weight of 3 landing gear units at 2.02 % MTOW [43]. The weight of two estimated structural MLG units is 2710 kg which amounts to 1.9 % of MTOW. Thereby confirming the breakdown is reasonable. With the Rolling stock weight now known, the structural weight of the bogie beam of 480 kg can be derived by subtracting the rolling stock weight from the bogie beam assembly weight. This breakdown is visualized in Figure 5.5.

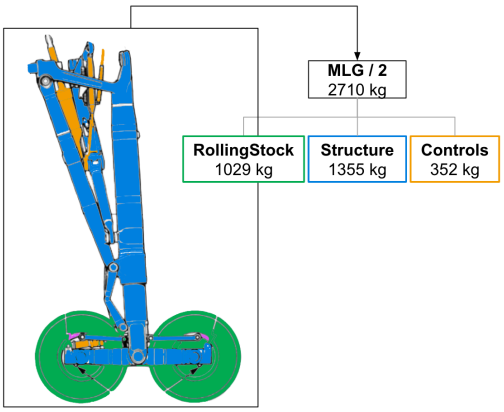

Figure 5.4: A310 MLG breakdown

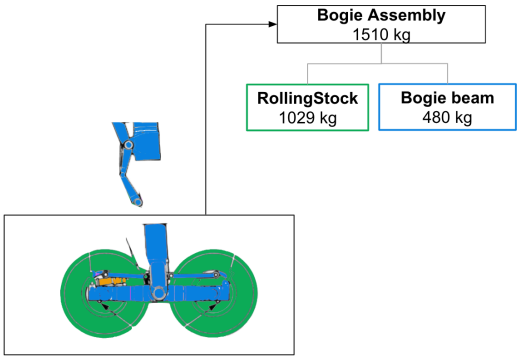

Figure 5.5: A310 Bogie breakdown

With the bogie structural weight derived, this value is subtracted from the overall structural mass to obtain an upper structural weight of 874 kg. This value, broken down in Figure 5.6 is defined as the target mass to be reproduced by LGMM in an ideal case.

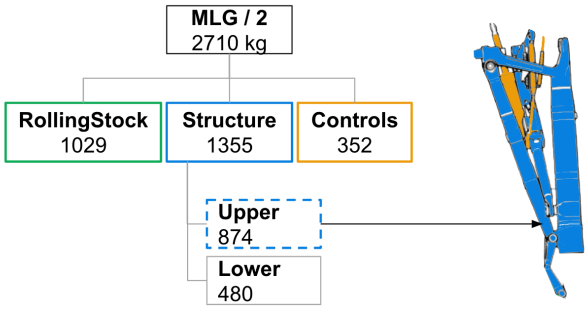

Figure 5.6: A310 derived component mass breakdown diagram.

5.3. Validation model initiation

The parameters in Table 5.1 were used to calculate the external loads acting on the gear. It is important to note that the MLG and NLG track were incorrectly initialized. The NLG track and MLG are 625 and 927 mm respectively. This error doesn't influence the static load distribution and therefore only influences the Ground Pivot load since it is a function of the bogie size as recapped in Figure 2.5. The implications of this on the validation quality will discussed at the end of the chapter. **??** presents the beams and nodes used to generate the geometry of the A310 landing gear. The inner diameter was approximated as being 80% of the outer diameter that was digitally measured. This ensured a reasonably undersized starting diameter while still be in the same order of magnitude. The beams discretized and overlayed in Figure 5.7 with the original source material from Roskam found in Appendix A.

Table 5.1: A310-200 input data to LGMM

Variable	Value	Unit			
W_{MTOW}	142.0	$10^3 kg$	mlg_track	1397.0	m
MAC	6608.0	m	nlg_track	927.0	m
$x_{MAC1/4}$	19948.0	m	gear_track	9600.0	m
h_{hfdz}	4689.0	m	aftcg_mac	0.41	$\%MAC$
x_{MLG}	21890.0	m	cg_z	0	m
x_{NLG}	6671.0	m			

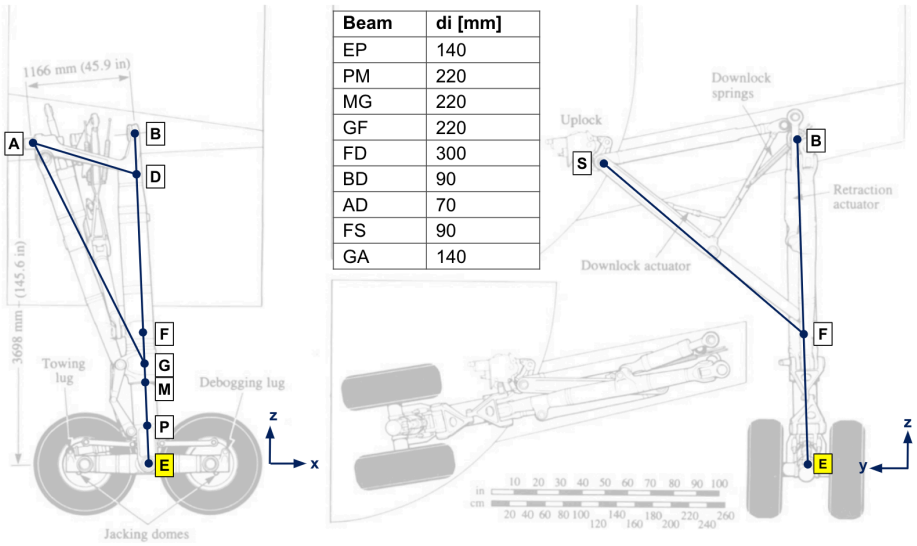

Beam	di [mm]
EP	140
PM	220
MG	220
GF	220
FD	300
BD	90
AD	70
FS	90
GA	140

Figure 5.7: A310 nodes definition, image adapted from Roskam [13]

The degrees of freedom for nodes which are not fully-free are shown in Table 5.2. The data source also mentions that the pintle attachments are spherical joints. Furthermore, from images it can be deduced that node F at the sidestay is a universal joint.

Table 5.2: Degrees of freedom for datum and sidestay nodes

Node	Translation			Rotation		
	δ_x [-]	δ_y [-]	δ_z [-]	θ_x [-]	θ_y [-]	θ_z [-]
node E	Free	Free	Free	Free	Free	Free
node G	Fixed	Fixed	Fixed	Fixed	Free	Free
node S	Fixed	Fixed	Fixed	Free	Free	Free
node A	Free	Fixed	Fixed	Free	Free	Free
node B	Fixed	Fixed	Fixed	Free	Free	Free

5.4. Validation results

The total weight of the A310 landing gear is computed by running the sizing function and then processing the critical load cases to obtain overall landing gear weight. The following section will evaluate the critical loadcases, mass and internal loads for selected beams to evaluate the performance of LGMM. The raw data for one beam, the dragstay, is shown to serve as an explanation of how critical loads and mass is determined. The remaining raw data can be found in Appendix D.

5.4.1. Dragstay

Table D.3 is split into 3 sets of rows each corresponding to the sizing results for the mass, convergence and geometry criteria as introduced in Section 4.7. It can be observed that the Taxi condition was unconverged but it is in close proximity to 1.5. This could signify that there are significant loads acting there, but when looking at the sized geometry it can be seen that barely any thickness was added implying that the initial diameter of 140mm was already enough to sustain the loads. Turn loadcase is discarded as sizing case as it doesn't see any loads as seen by the red "unconverged status" in Figure 5.8. However, the sizing function converged and produced a valid geometry for both the pivot and brake2point loads. However, it can be seen that the mass for the Brake2point case is the highest. This suggests that beam under the Brake2point had the highest combined loading. This is confirmed when comparing the internal loads in **??** in **??** . It can be seen that although the Pivot loadcase induces a significant internal bending moment around the X and Z axis, it is the shear in X direction from the Braked2point case that introduces the most combined loading.

Table 5.3: Beam GA: dragstay results on A310-200 Main Landing Gear

Load case	sizing_mass	Mass [kg]
Taxi	0	7
Brake2point	1	57
Pivot	0	13
Turn	0	7
Load case	sizing_convergence	Sizing criteria: (stress ratio, buckling ratio)
Taxi	0	Unconverged: (1.5748), (0.0)
Brake2point	1	Stress: (1.5), (0.0)
Pivot	1	Stress: (1.5), (0.0)
Turn	1	Stress: (1.5), (0.0)
Load case	sizing_geometry	Condition: (inner_d, outer_d, t)
Taxi	0	Invalid: (140.0, 141.4, 0.7)
Brake2point	1	Valid: (140.0, 151.1487, 5.6)
Pivot	1	Valid: (140.0, 142.4402, 1.2)
Turn	0	Invalid: (140.0, 141.4, 0.7)

The mass generator therefore labels the Braked2point case as critical and selects 57kg as the com-

ponent mass to be used in the overall summation. The dragstay on the A310, as the name suggest is designed to counteract drag loads. The observations gathered from these results thus far support this function. These are visualized in Figure 5.8.

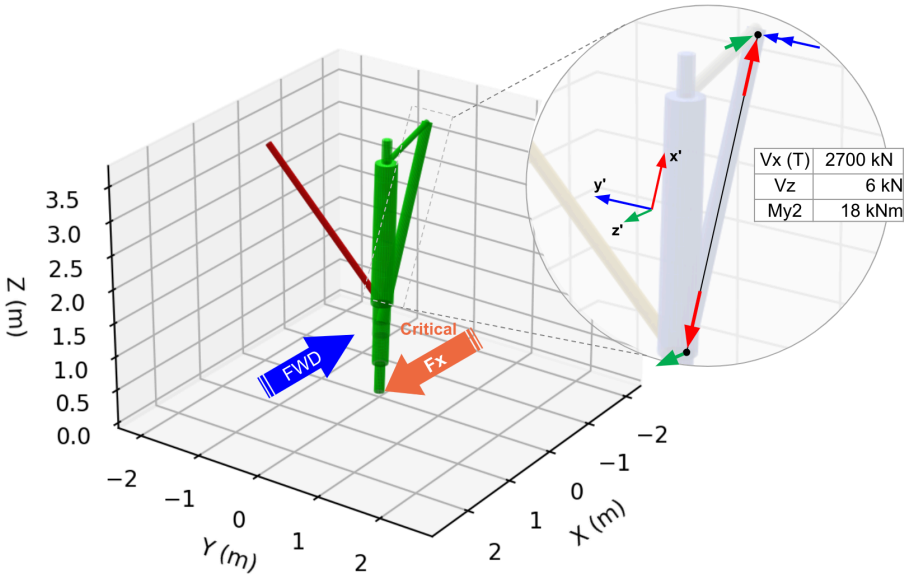

Figure 5.8: A310 Dragstay internal loads

5.4.2. Sidestay

The sidestay is another distinct component with the function to counteract side loads. The turn loadcase was determined to be the critical loadcase. Looking at the Figure 5.9, it can be seen that the only force acting through the beam is a compressive shear force corresponding to approximately 74% of MTOW. Once again, looking at the sizing results in Table D.5 it can be seen relatively clearly that out of the four loadcases only the Turn loadcase converged. Looking at the internal loads in Table D.4 it is clear during a Turn the beam only experiences a shear force in the local X axis, which in global coordinates is the Y axis. With these observations the loadcase is deemed valid and therefore the critical mass is carried further.

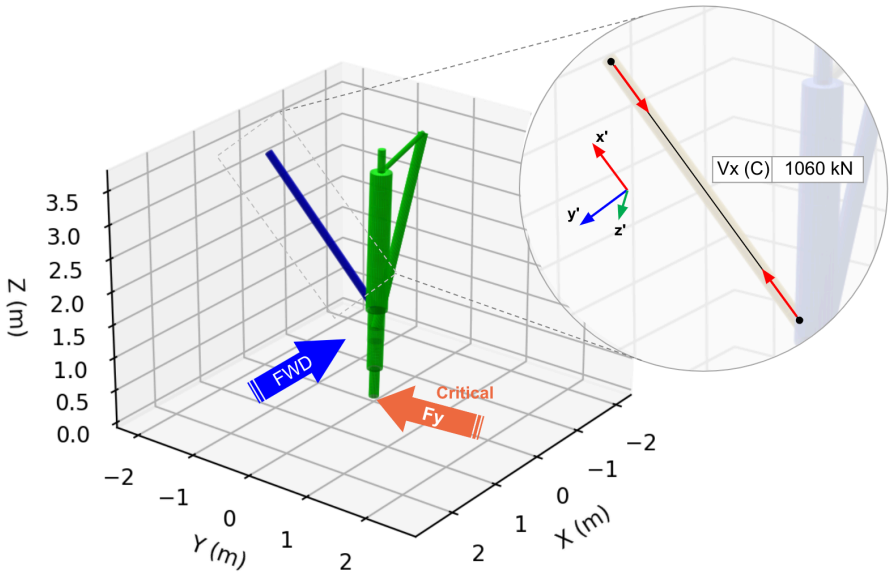

Figure 5.9: A310 Sidestay internal loads

5.4.3. Upper Main fitting

The main fitting converged for all loadcases as can be deduced by the green color. This is expected as it's the main structural member. Observing the internal loads it can be seen that the main fitting experience higher axial loads during the braking load case of 3210 kN than during the taxi bump of 1600 kN. The external load also induces a large internal bending moment at Node F, which cetainly contributes to the stresses.

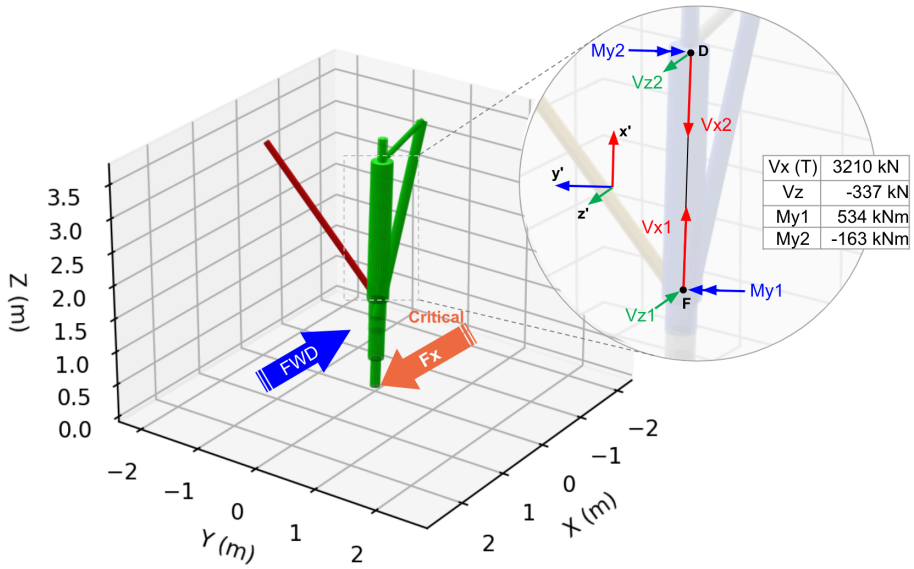

Figure 5.10: A310 Upper main fitting internal loads

5.4.4. Lower Piston

The critical loadcase for lower piston is pivoting. Looking at Figure 5.11 it can be seen that the external torque produces significant bending moments about the longitudinal axis. This critical loadcase is deemed to be a valid conclusion because typically a torque limiter is located in the exact spot where the maximum torque as seen in this case is also present. Furthermore it can be seen that the sidestay is over designed for this loadcase.

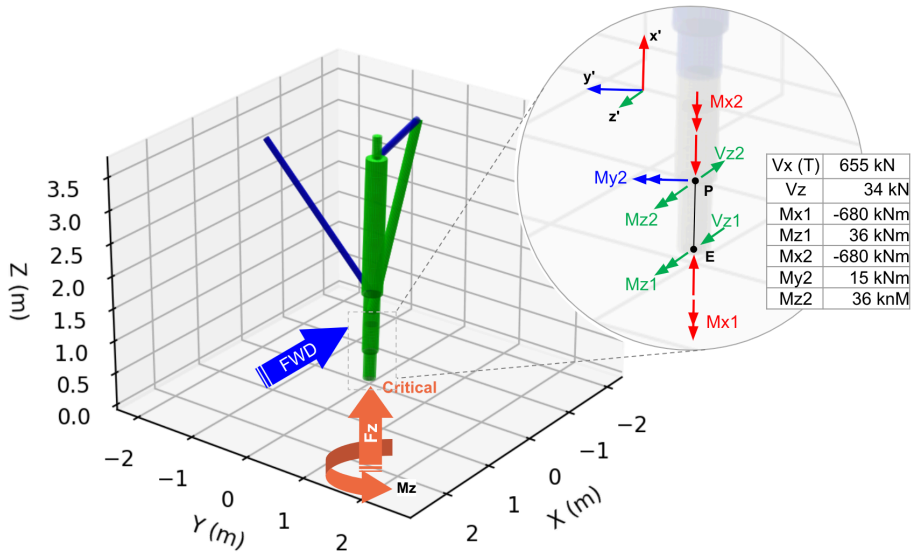

Figure 5.11: A310 Lower Piston internal loads

5.5. Weight validation

With the critical loads determined and validated it is possible to sum the critical masses of the remaining components the make up the landing gear in Table 5.4. The final raw structural mass, W_{LGMM} comes out to 489 kg. When multiplied by 4/3 to account for secondary components at total upper structural mass of 656 kg is computed. Referring back to Section 5.2, the target upper structurla mass of an actual A310 MLG is 872 kg. LGMM is therefore under-predicting the mass by approximately 32%. This error can most likely be attributed to either the empirical assumptions used or certain components not being sized properly due to the lack of dynamic loads being taken into account. It is also known from looking at data from publicly available maintenance documents for a popular narrowbody airliner and a popular widebody airliner that the sidestay + locking mechanism as a percentage of single landing gear weight is between 6 - 12 %. In this calculation it comes out to 4.7 when including the secondary component %. Based on these conclusions an error correction factor of K = 4/3 is to be used for estimation the Flying V MLG.

Table 5.4: critical mass for A310-200 MLG components

Beam	Name	mass [kg]
EP	pointE_to_piston	45
PM	piston_to_cylinder	32
MG	cylinder_to_dragstay	15
GF	dragstay_to_sidestay	28
FD	sidestay_to_uppercylinder	153
BD	aftpintle_to_uppercylinder	24
AD	forwardpintle_to_uppercylinder	39
FS	sidestay	96
GA	dragstay	57
	Sum	489

6

Results

The following chapter presents the kinematic design and the overall mass estimation of the MLG for the the Flying V as an output of the Landing Gear Mass Module (LGMM). The baseline LG and its components are evaluated and a sensitivity study is conducted on the leg length, sidestay and cross-brace.

6.1. Refined baseline landing gear

The Baseline landing gear is the result of the refinement of the previous MLG design of Bourget. The new baseline serves as the input geometry for the LGMM. The following section explains the retraction sequence and evaluates the baseline gear against the design requirements and considerations set at the beginning of the Kinematic design process. The kinematic sequence is visualised in Figure 6.1.

1. **Weight-on-wheels:** This is the state of the landing gear when it is resting the ground at gate or holding position. The shockabsorber is 80% compressed with a stroke if 454 mm.
2. **Sidestay Unlock:** The wheels-are free in the air and shock absorber fully extended. At a positive rate-of-climb the sidestay ”unlocks” thereby enabling the folding kinematics to begin.
3. **Bogie flatpacking:** As the retraction sequence progresses, the bogie is pitched counter-clockwise by means of actuation, to enter a flat-packed stated
4. **Stowage:** The gear is now up-locked and its stowed state, signalling the end of the sequence.

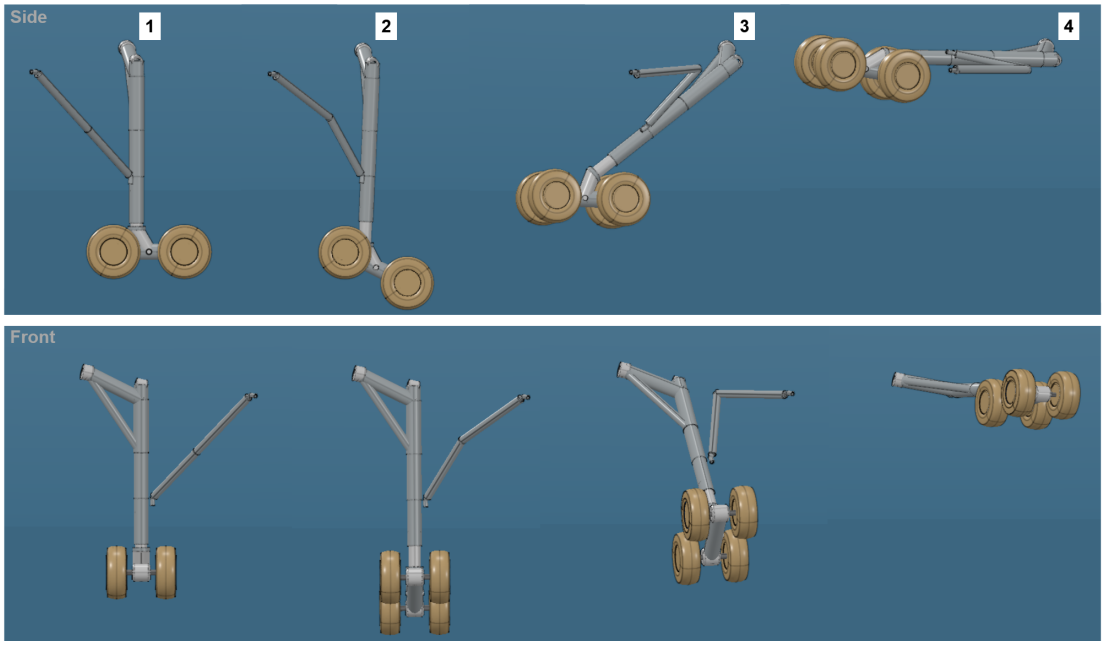

Figure 6.1: Side view and front view retraction sequence of right FV1000 Baseline MLG

6.1.1. Evaluating design considerations

1. **Compactness:** A flatpacked bogie is enabled through the the addition of a 10 °kink from the lower piston to the bogie hinge point. The stowed gear is stowed such that the contour of upper surface of the wing is undisturbed. In the stowed state the beam folding angles are inline with the design requirements.

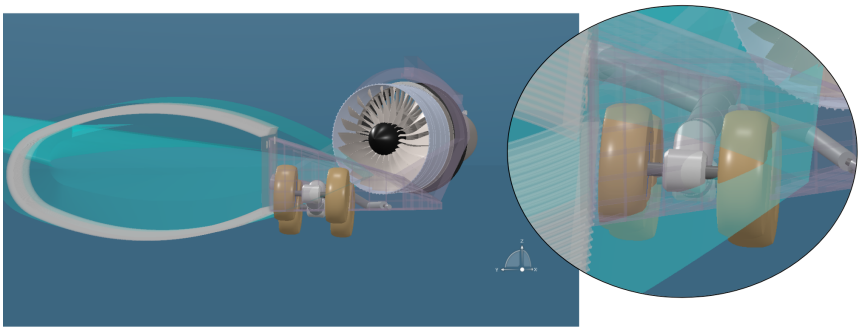

Figure 6.2: Critical Sidestay loadcase

2. **Complexity:** The skewed pintle axis enables the gear to fold in parallel to the rear-spar. The skew angle is unconventional and likely requires more complicated spherical joints due to increased local stresses. However, the universal joint and spherical joint at the sidestay are conventional. Added complexity is expected to actuate the bogie into flatpacked position but it is something that has been done before on the C-141 starlifter. The long sidestay also is expected to add challenges to a rather large lock-unlock mechanism which has not been modelled. The torque-link on the other hand can be designed in a conventional manner.
3. **Structural efficiency:** Node A is attached to the rear spear which is main structural member on the aircraft. Node B is attached by design to be below the right engine structural column, allowing for future integration. Finally, the sidestay is attached to a rigid engine box structure. The engine can be removed freely during maintenance.

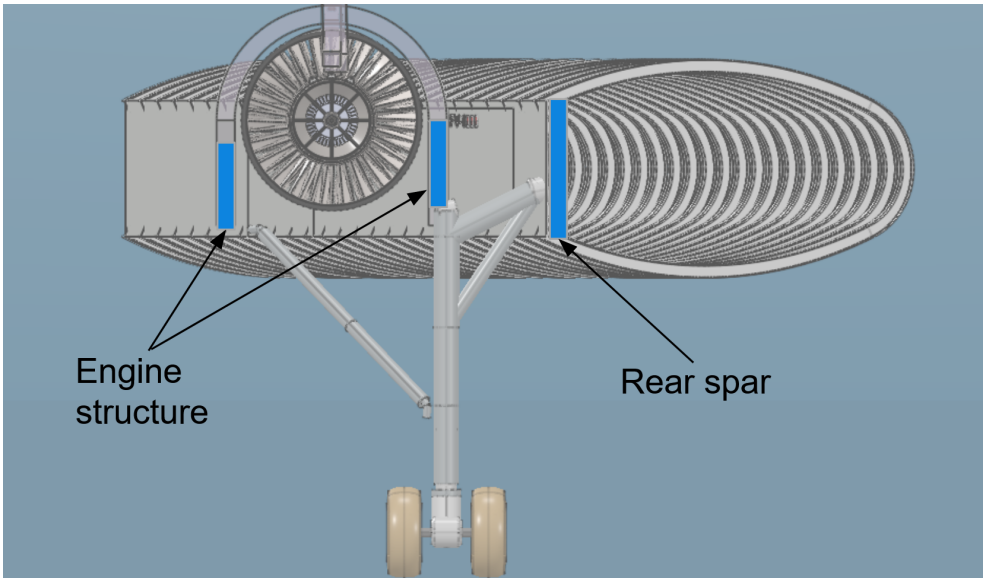

Figure 6.3: Landing gear and structural interfaces

4. **Risk:**

   Tyre failure envelopes for different modes described in Chapter 2, have been loaded into the 3D model. Looking at Figure 6.4, the left mode is the flailing strip. Sensitive sensors, aerodynamic aids

or appendages should be clear of the area in purple below the engine structure. The middle image shows the tire burst pressure envelope, fuel and hydraulic lines in the vicinity should be taken into account. The right most image shows the tire debris envelope. It can be seen that the entire trailing edge of the bottom surface is in the trajectory of large debris. Typically this can be certified with increased material thickness however, exposed sub-systems should be certified as well. Finally, it can be seen that the engine inlet is protected by the mounting structure.

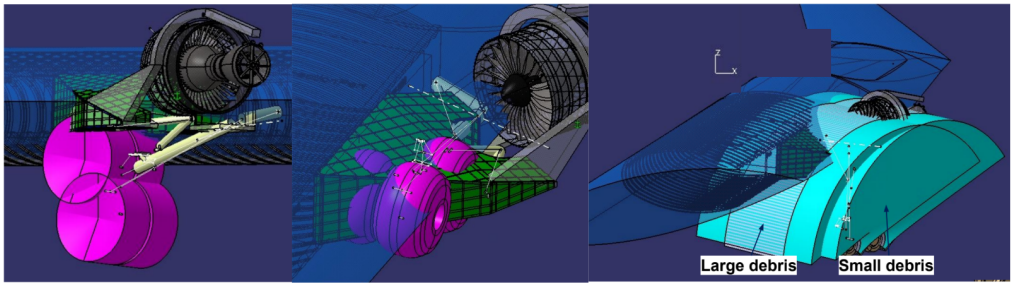

Figure 6.4: Tire failure zones of vulnerability a: Flailing thread, b: Tire burst pressure c: Tire debris

6.2. Critical load results

The following section presents the results of sizing module of LGMM with a focus on the critical loads. The ground loads are generated for the baseline aircraft in Table 3.4. Looking at the calculated ground loads in Table 6.1 it can be seen that the Taxi bump case induces an external force almost equivalent to the MTOW of the aircraft.

Table 6.1: Baseline MLG calculated external ground loads

Loadcase	$Fx_r\,[kN]$	$Fy_r\,[kN]$	$Fz_r\,[kN]$	$Mx_r\,[kN]$	$My_r\,[kN]$	$Mz_r\,[kN]$
Taxi	0	0	2500	0	0	0
Brake	1020	0	1275	0	0	0
Pivot	0	0	1250	0	0	1950
Turn	0	-970	1940	0	0	0

After running LGMM the internal loads and critical loadcases are known. These will be presented in detail for the dragstay, sidestay and kink. Focusing on the sidestay in Figure 6.6, it can be seen Brake2point is clearly the critical loadcase.

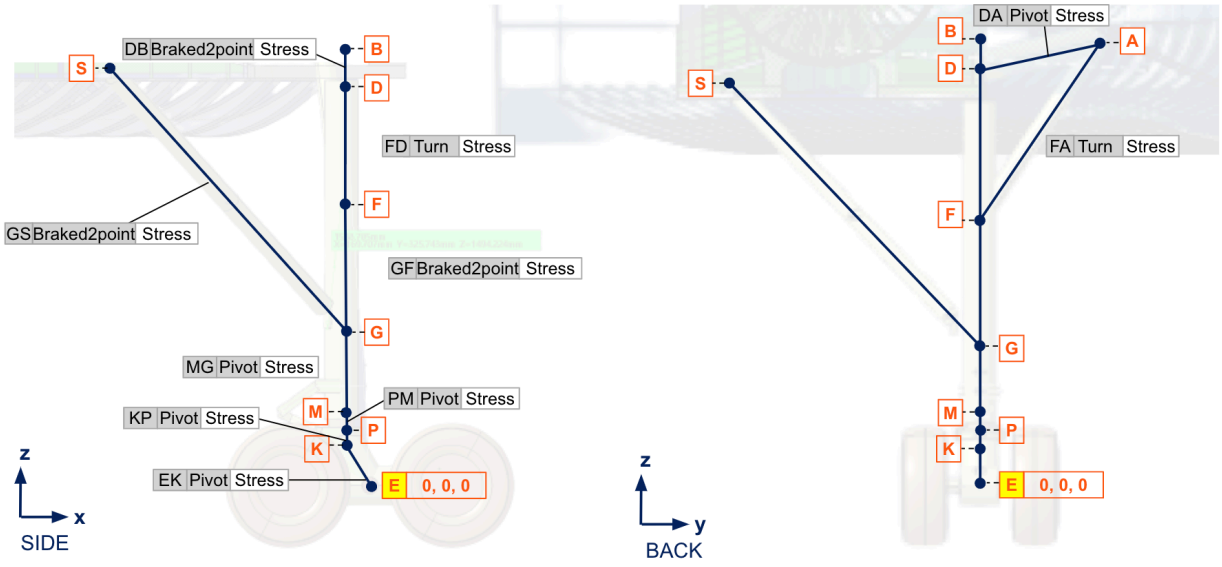

Figure 6.5: Critical loadcases for the Flying V Baseline MLG

6.2.1. Sidestay

The critical loadcase for the baseline sidestay is identified as the Brake2point. Looking at the internal loads, the sidestay is carrying solely tension forces of a high magnitude. Compression on the sidestay from the other loadcases is apparently not sufficient to trigger a buckling response. Therefore, it is likely that these loadcases are inadequate to properly size the sidestay.

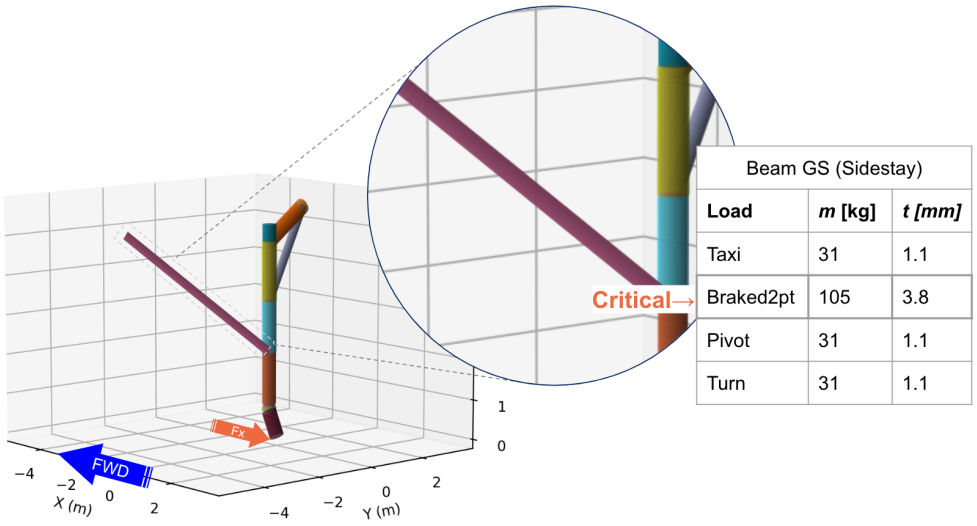

Beam GS (Sidestay)		
Load	***m* [kg]**	***t* [mm]**
Taxi	31	1.1
Braked2pt	105	3.8
Pivot	31	1.1
Turn	31	1.1

Figure 6.6: Critical Sidestay loadcase

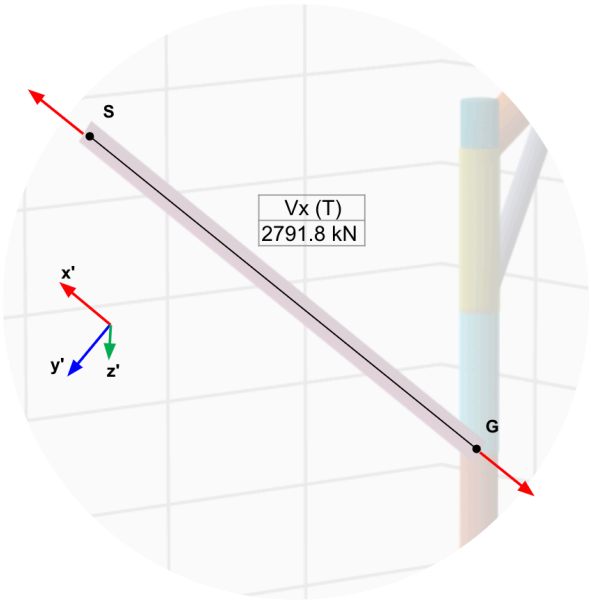

Figure 6.7: Sidestay internal loads on the Flying V Baseline MLG

6.2.2. Crossbrace

When looking at the results for the Crossbrace it must firstly be noted that the sizing loadcases are not the same for the left and right gear. For the right gear the sizing loadcase is Turn while for the left gear it is braking. While Turning is results in the highes loads, the difference with Braking is minimal, so it will be interesting to see what the sensitivity study shows.

Both beams experience significant loads during all loadcases (contrary to the Sidestay) with equally high shear force experienced during braking. However, during turning the right gear sees 3.6 times higher moment about the beams local longitudinal axis, XX times higher in the Y axis and Z axis. As Node 2 of the crossbrace represents at interface point with the airframe structure, these internal loads are important to consider.

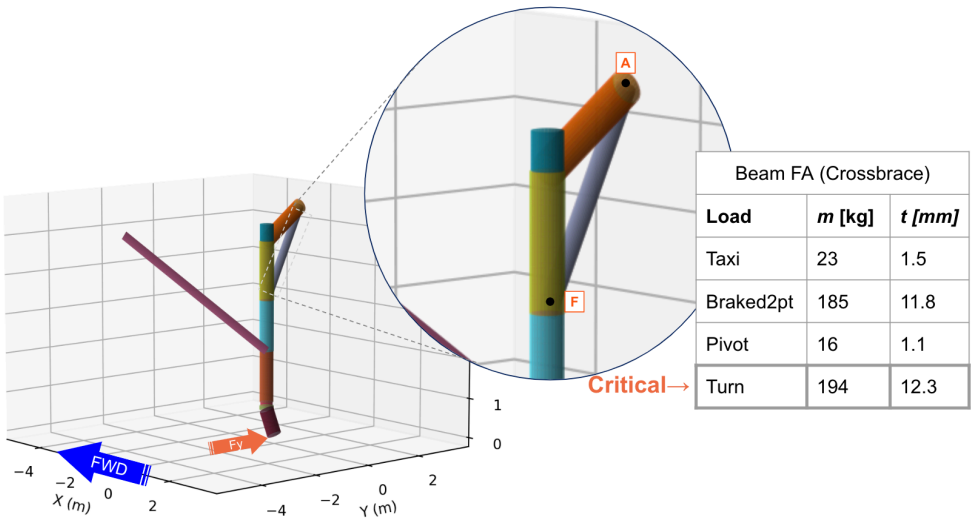

Beam FA (Crossbrace)		
Load	***m* [kg]**	***t* [mm]**
Taxi	23	1.5
Braked2pt	185	11.8
Pivot	16	1.1
Critical→ Turn	194	12.3

Figure 6.8: Critical loadcases for the Flying V Baseline MLG

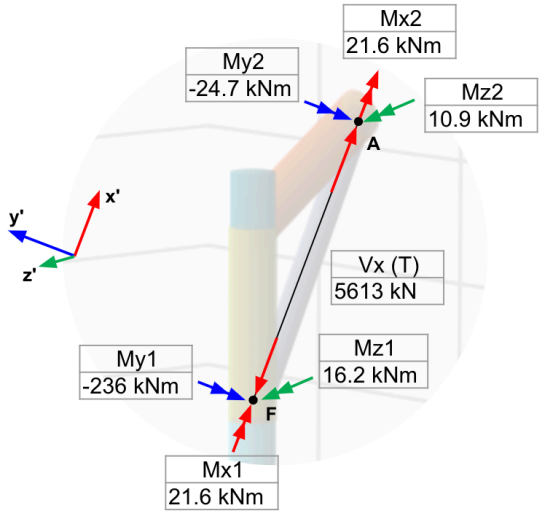

Figure 6.9: Crossbrace internal loads for the Flying V Baseline MLG

6.2.3. Pintle

The Pintle is the beam that connects the two pivoting axis. As a landing gear designer this is a key component and thus should be given attention. The sizing results point to the Pivot being the critical loadcase, due to a very large moment experienced due to the interal torque resulting from the pivot load.

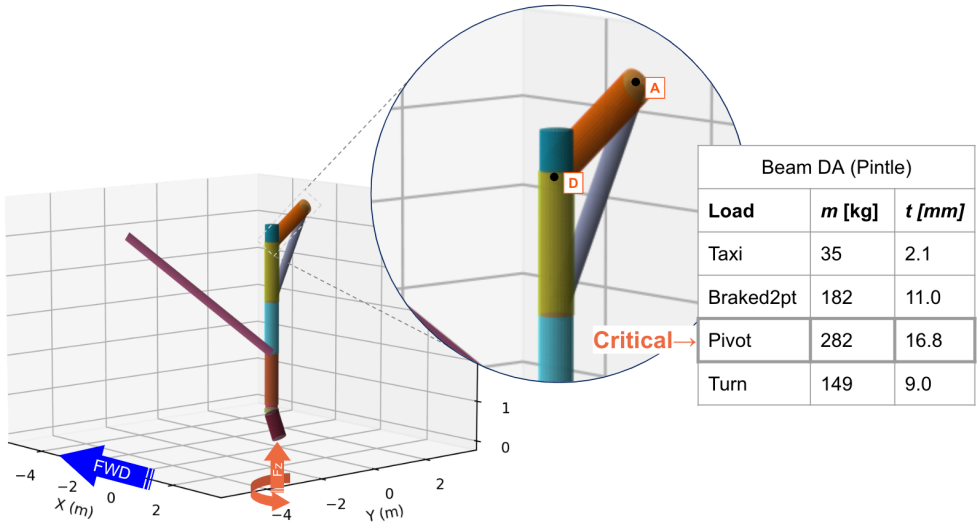

Beam DA (Pintle)		
Load	***m* [kg]**	***t* [mm]**
Taxi	35	2.1
Braked2pt	182	11.0
Critical→ Pivot	282	16.8
Turn	149	9.0

Figure 6.10: Critical loadcases for the Flying V Baseline MLG

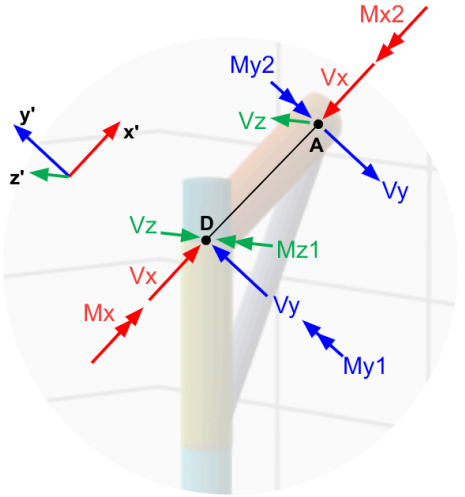

	(kN)
Vx	-422
Vy	1166.7
Vz	-236
Mx1	69
My1	403
Mz1	2011
Mx2	69
My2	3.6
Mz2	0

Figure 6.11: Critical loadcases for the Flying V Baseline MLG

6.3. Mass overall landing gear

The mass of the overall landing gear is one of the main desired outputs. The mass of the overall gear is obtained by adding up the maximum mass per beam for both the left and right gear. This represents the geometry of the beams required to overcome the induced loads. For the baseline forward retracting landing gear with a hfdz of 6225m, the maximum masses are shown in the table below.

6.3.1. Component mass results

Table 6.2: Right Beam results for baseline FV1000 main landing gear

Beam name	Length [m]	thickness [mm]	mass [kg]
kink	0.693	11.72	82.28
kink_to_piston	0.105	12.60	13.43
piston_to_lower_cylinder	0.096	17.68	14.52
lower_cylinder_to_sidestay	1.299	13.81	173.91
sidestay	5.100	3.76	105.45
sidestay_to_cross_brace	1.295	21.91	280.60
upper_main_fitting	1.505	28.03	423.51
crossbrace	2.745	12.33	193.55
outboard_to_inboard_pintle	1.724	16.77	282.26
outboard_pintle	0.425	14.47	59.71
			1629.22

Table 6.3: Left Beam results for baseline FV1000 main landing gear

Beam name (left)	Length [m]	Thickness [mm]	Mass [kg]
kink	0.693	11.72	82.28
kink_to_piston	0.105	12.60	13.43
piston_to_lower_cylinder	0.096	17.68	14.52
lower_cylinder_to_sidestay	1.299	13.81	173.91
sidestay	5.100	3.75	105.42
sidestay_to_cross_brace	1.295	21.91	280.57
upper_main_fitting	1.505	25.84	388.40
crossbrace	2.745	11.77	184.31
outboard_to_inboard_pintle	1.724	16.43	276.40
outboard_pintle	0.425	14.47	59.71
			1578.95

6.3.2. Single main landing gear weight

The overall weight of the primary upper gear structure for the Baseline Flying V with a strut length of = 1629.22 kg.

To account for the secondary mass such as fittings, oleo mechanisms and torque links, this value is multiplied by 4/3. This results in total upper weight of

For a single main landing gear, $W_{MLG/2}$:

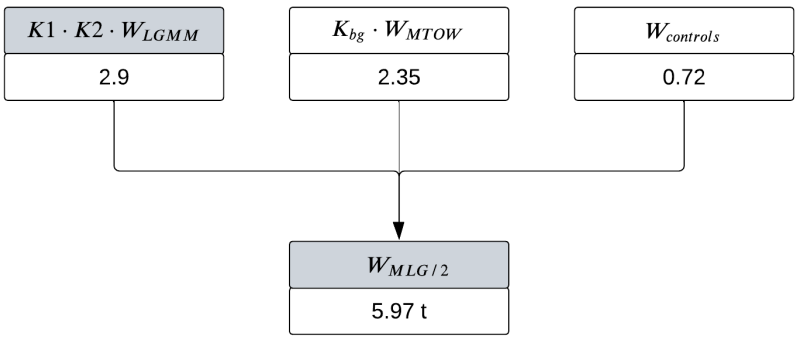

Figure 6.12: Critical loadcases for the Flying V Baseline MLG

With the assumption that controls make up 12% of the remaining weight the following equation can be plugged back into Equation 4.18 to obtain the following expression

Therefore the entire main landing gear weight can be calculated by multiplying the single gear weight by 2, giving the result seen in

6.3.3. Total aircraft landing gear weight

With the gear weight for a single Flying V main landing gear computed, it is possible to calculate the mass of the overall landing gear component group. As stated in the research objective the nose-landing gear weight is not computed because different set of loadcases, like towing and steering, are usually sizing and have not been implement in LGMET. Therefore, the Nose-landing gear weight is calculated using the statistical Equation 4.28 seen earlier. Assuming a NLG strut length of 3.7m from Bourget and 2 nose-wheels a purely statistical NLG weight of 1255.66 kg is calculated.

Therefore the total landing gear weight for the Baseline Flying V can now be obtained as seen in Figure 6.13 .

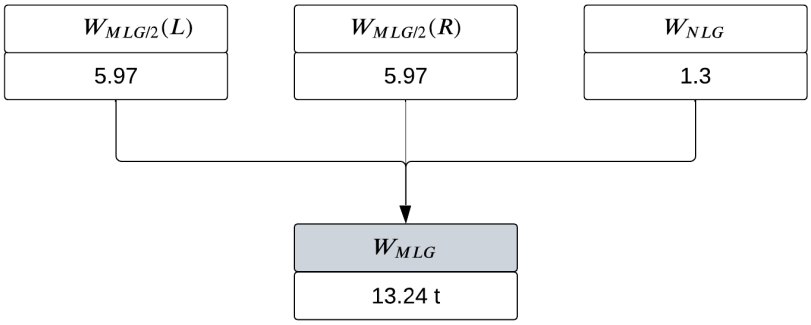

Figure 6.13: Critical loadcases for the Flying V Baseline MLG

With a final main landing gear weight calculated it is now possible to compare it to existing commercial airlines. Table 6.4 presents the relevant mass data for various aircraft. The A310-200 is included as it's the main validation case for the tool and the B707-320 is included as comparison for the A310-200 to ensure that different landing gear manufacturers are compared. The DC10-30, A340-200/300 and A340 500 were the only commercial long haul aircraft for with which sufficient mass data was found. Some data was found for the B777 however the nose-landing gear is missing hence the overall LG weight can't be confirmed.

Table 6.4: Landing gear mass data compared to the baseline Flying V Landing Gear

AC	$MTOW\,[t]$	$W_{LG}\,[kg]$	%MTOW	$W_{MLG/2}\,[t]$	$W_{NLG}\,[t]$	Source
FV1000 (Corr.)	260.0	13.24	5.09	5.97	1255.66	-
FV1000 (Uncorr.)	260.0	11.5	4.44	5.15	1255.66	-
B707-320	141.4	5.77	4.08	-	-	Schmidt [5]
A310-200	142.0	6.11	4.30	2.71	690	FedEx [42]
DC10-30	252.0	11.7	4.65	4.62	832	Schmidt [5]
A340 200/300	275.0	8.92	3.24	3.67	759	Airbus MFP [44]
B777-300	299.0	N/A	3.68 - 4.32	4.54	N/A	Yourkowski [45]
A340 500	380.0	15.43	4.06	4.97	1333	Airbus MFP[46]

The FV1000 with a MTOW of 260t fits in between the A340 and the DC10. Compared to the DC10 with a lower MTOW than the FV1000, the LG is 22% heavier and the MLG alone is 42% heavier. The difference against the A340 200/300 is even greater, showing that the FV1000 LG is 61 % heavier. In general, the A340 seems to carry quite a structurally efficient landing gear as its %MTOW is 0.8% lower than the rest of the aircraft in the table. Nonetheless there are numerous factors that can influence the comparison even between conventional aircraft. It's interesting to observe that the Flying V LG weight is 7% lighter than the A340-500 whilst also carrying a relatively similar amount of passengers. With the A340-500's range of 9000 nm and the FV's targeted A350-1000's range of 8700nm, the landing gear weight when compared in that light is more reasonable. Nevertheless, the FV's significantly higher weight as a percentage of Maximum Take Off Weight can't be ignored. According to Schimdt who has published the most most recent and arguably most comprehensive textbook on Landing Gear design to date, claims that conventional transport aircraft have a %MTOW of 4% on average. The literature also claims that aircraft like the 777 have landing gear with "exceptionally high structural efficiency" are within 8% of this 4% mark. Which would mean either a 3.68 or 4.32 %MTOW. With that remark it would be safe to assume that the FV1000 landing gear structure designed during this thesis can not yet be considered exceptionally structurally efficient.

It is clear that quite a few assumptions have been made in calculating the weight of the landing gear and that not all components of this weight calculation were based on physics. The raw structural weight is more likely undersized than oversized but what there is the chance that the bogie weight or controls could be overpredicted. This is also a phenomena described by Schmidt as common during preliminary design.Then there is also the argumentation new technologies which exist on the newest generation of aircraft and how they could influence the final weight. These considerations are discussed next.

6.3.4. Influence of correction factor

The correction factor that was calculated in Equation 4.24 was based on the knowledge that LGMM undersized the validation structure of the A310. Upon review of the code it was discovered that the Turn loadcase for the A310 was incorrect which could have contributed to lower combined loads and thus lower structural weight. It is therefore possible that the correction factor is overly conservative. However, even without the correction factor and assuming that LGMM was computing the structural weight correctly, the FV1000 still demonstrates a %MTOW that is higher than comparable aircraft.

6.3.5. Influence of new technologies

1/3 of the landing gear structure consists of secondary components which for this study and equivalent analytical sizing tools have been computed empirically. These statistical assumptions may not be an accurate representation of what would be possible with current advancements in systems and materials. For example, the A330 Landing gear by Safran included Titanium components and it's not unreasonable to assume that advancements have been made on the A350-900 landing gear.

6.3.6. Comparison with statistical methods

The results are also to be compared to the statistical weight estimation which was the original catalyst for this thesis. Bourget used Equation 6.1, found in the book by Raymber, to calculate the first landing gear estimate. The equation is based on the regression analysis of 11 aircraft and variables must be inserted as imperical units.

$$W_{mlg} = 0.0106 \cdot k_{mp} \cdot W_l^{0.888} \cdot N_l^{0.25} \cdot L_m^{0.4} \cdot N_m^{0.321} \cdot N_{mss}^{-0.5} \cdot V_{st}^{0.1} \tag{6.1}$$

Table 6.5 shows three cases of weight estimations. FV1000—Baseline represents the quasi-analytical weight estimation which is the subject of this thesis. FV1000—Bourget represents the statistical weight estimation with correction factor conducted by Bourget. FV1000 —Raymer presents the statistical weight estimation without correction factor.

Table 6.5: Comparing mass estimation methods for baseline Flying V

Case	$MTOW[t]$	$W_{LG,total}\,[kg]$	% MTOW	$W_{MLG/2}\,[kg]$
FV1000 (Base LG)	260.0	13.24	5.53	6565.0
FV1000 (Bourget)	260.0	12.3	4.73	5400.0
FV1000 (Raymer)	260.0	11.62	4.47	5185.0

It can be clearly seen that the quasi-analytical method calculates a weight for the single main landing gear to be 21% higher than Bourgets and 26% higher than a pure statistical weight estimation. Given the differences in methods and assumptions this result implies that statistical methods so far undersize the landing gear weight for baseline Flying V with 5.5 floor-to-ground height.

6.4. Sensitivity study scope

The weight so far has only been calculated for the baseline gear with the assumption that this is a feasible representation of the Flying V landing gear. However, as expected in early-stage designs, future designers are likely to change the topology to account for a new kinematic concept, a shift in gear position or change in aircraft height. In order to provide early insights that could help guide future design studies a sensitivity study is conducted that focuses on the landing gear at component-level.

The sensitivity analysis for this thesis captures the sensitivity of gear and component raw structural mass, W_{LGMM}, to changes in aircraft height from ground, $hfdz$. Height-from-ground was chosen for two reasons. Firstly, it is a relevant overall-aircraft parameter from which additional insights could benefit other multidisciplinary studies ranging from outer wing design to emergency evacuation. Secondly, the landing gear strut length is a common design variable found in literature which provides data for comparison.

The overall-aircraft parameter $hfdz$ is connected to the landing gear system-parameter through Point E. This means that landing gear height can be changed by adding or subtracting the appropriate vertical displacement, Δ_z, on Point E which would then cascade down to transform the remaining coordinates. By fixing which nodes do or don't translate it's possible to run LGMM for various topology "cases". The two main components that will be varied alongside leg length are the sidestay and dragstay. The different cases are summarized below.

- V-LCS: Varying Gear Length, Sidestay and Crossbrace
- V-LC: Varying Gear Length and Crossbrace
- V-LS: Varying Gear Length and Sidestay
- V-C: Varying Crossbrace on baseline gear
- V-S: Varying Sidestay on baseline gear

For the "fixed leg - varying component study" the upper and lower vertical displacement limits of the sidestay and dragstay are bound by physical constraints. The following sub-sections will explain the Δ_Z boundaries and corresponding geometric results for each change in topology. Note that L_{leg} is the summation of the DB, FD, GF, MG, PM, KP and EK. All aircraft interface nodes such as Node S, Node A and Node B are assumed with unchanged coordinates. All degrees of freedoms are also remain unchanged to the baseline.

For example looking at Figure 6.14, node G is limited in the upward direction by Node F and in the downward direction by the piston and torque link. Likewise, Node F of the crossbrace is limited in the upward direction by the pintle beam and in the downward direction by Node G of the sidestay attachment point. With these limits defined an equal distribution of taken in either direction.

VLCS: Varying leg length, sidestay and crossbrace
For this case the leg length, sidestay and crossbrace move together proportionally. The leg length drives the displacement as it extends or compresses relative to the baseline. It is physically limited moving upwards by Node F eventually clashing with the Node B of the pintle. It is limited downwards by the longest leg length investigated in the study by Bourget [7].

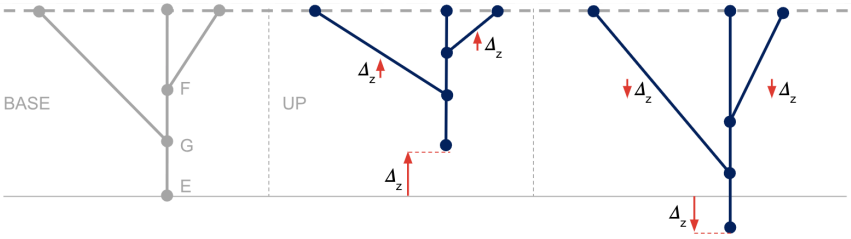

Figure 6.14: V-LCS: Vary Leg + Crossbrace + Sidestay

Table 6.6: V-LCS: Vary Leg + Crossbrace + Sidestay

$\delta_z\,[mm]$	700	350	175	0	-650	-1950	-2600
$hfdz\,[mm]$	7325	6975	6800	6625	5975	4675	4025
$L_{sidestay}\,[m]$	5.53	5.31	5.20	5.10	4.76	4.29	4.19
$L_{crossbrace}\,[m]$	3.35	3.04	2.89	2.74	2.24	1.58	1.58
$L_{leg}[m]$	6.12	5.77	5.59	5.42	4.77	4.36	5.01

Looking at the results in Figure 6.15, it is observed that reducing the gear length by more than 650mm has no effect on the overall structural mass. Beyond 650mm the sidestay and crossbrace structures are almost horizontal and therefore limited capacity to carry vertical loads. Presumably this causes the spike in upper main fitting load. Increasing the length all else equals causes a linear increase in weight due to an increase in length of the upper main fitting. The crossbrace weight increases slightly with increase leg length presumably due to increased moments which are a critical loadcase for this component. Overall an increase in 342 kg/m can be derived from linear-regression. Therefore if the gear is shortened weight savings are expected but the cross brace and sidestay attachments will need to be placed sperately.

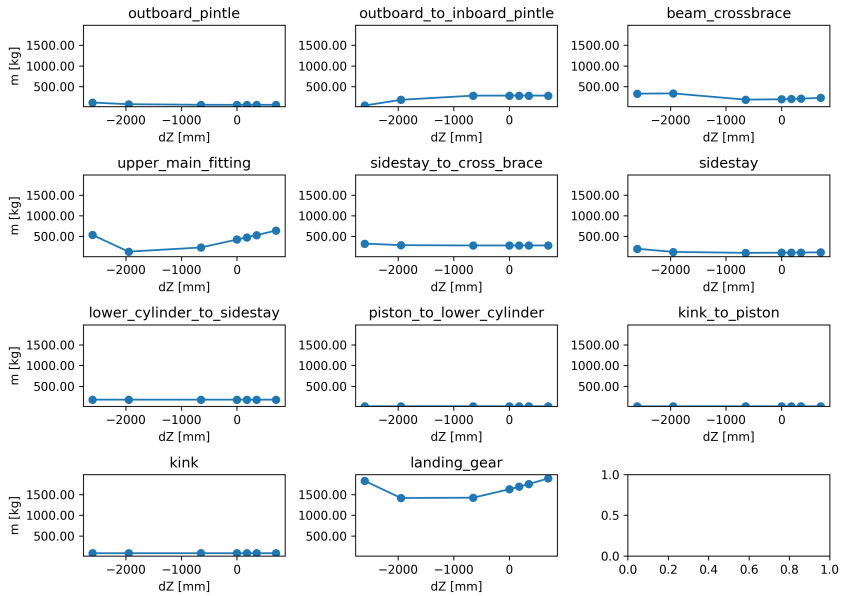

Figure 6.15: Vary Leg + Crossbrace + Sidestay component mass plots

V-LC: Varying gear length and crossbrace

For this case the sidestay is fixed relative to the leg. Meanwhile the vertical displacement is applied to the crossbrace and gear length. Meaning that as aircraft height from ground increases, the leg length increases and the crossbrace length increases as seen in Figure 6.16 while the sidestay length stays the same.

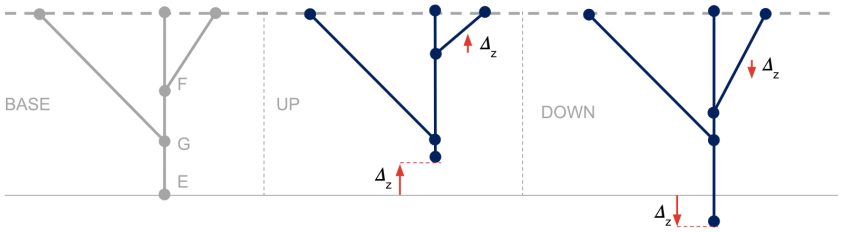

Figure 6.16: V-LC: Vary Leg + Crossbrace, sidestay fixed

Table 6.7: V-LC: Vary Leg + Crossbrace, sidestay fixed

$\delta_z[mm]$	700.0	460.0	230.0	0.0	-466.7	-933.3	-1400.0
$hfdz$ [mm]	7325.0	7085.0	6855.0	6625.0	6158.3	5691.7	5225.0
$L_{sidestay}[m]$	5.10	5.10	5.10	5.10	5.10	5.10	5.10
$L_{crossbrace}[m]$	3.35	3.14	2.94	2.74	2.37	2.04	1.77
$L_{leg}[m]$	6.12	5.88	5.65	5.42	4.95	4.48	4.22

At a component-level results in Figure 6.17 show a linear trend for the main fitting, sidestay, lower cylinder. Decreasing the landing gear length has no effect on the crossbrace mass. However, it is observed that the pintle beam experiences an increase in weight when the leg length is reduced, presumbably since the crossbrace isn't able to trinagulate the loads as efficiently and thereby takes on more of the loads. From an overall mass perspecitve, the slope is linear 351 kg/m and thus higher than the V-LCS Case.

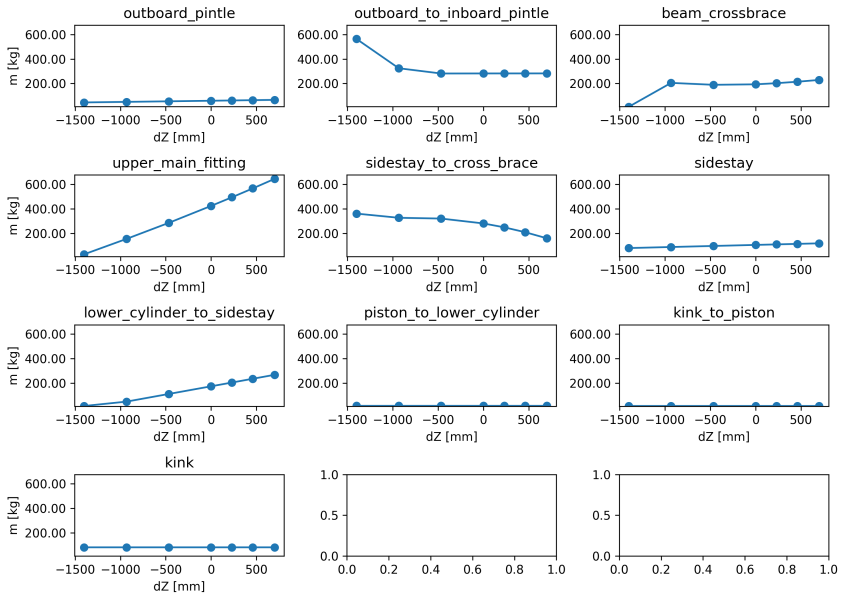

Figure 6.17: V-LC: Vary Leg + Crossbrace component mass plots

V-LS: Varying Gear Length and Sidestay

Conversely, in this case as the aircraft from ground height increases the sidestay length increases and the crossbrace length stays the same. When the ground height decreases, the sidestay length decreases.

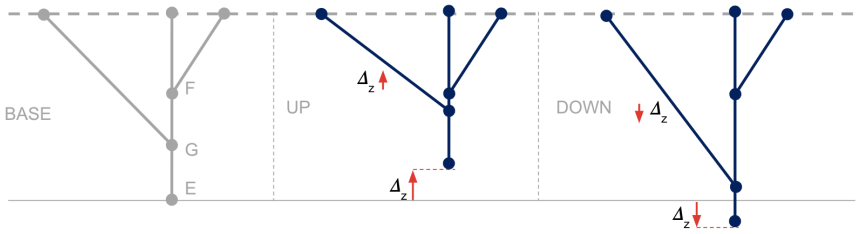

Figure 6.18: VLS: Vary Leg + Sidestay, crossbrace fixed

Table 6.8: VLS: Vary Leg + Sidestay, crossbrace fixed

$\delta_z[mm]$	700.0	460.0	230.0	0.0	-430.0	-860.0	-1300.0
$hfdz$ [mm]	7325.0	7085.0	6855.0	6625.0	6195.0	5765.0	5325.0
$L_{sidestay}[m]$	5.53	5.38	5.24	5.10	4.88	4.69	4.52
$L_{crossbrace}[m]$	2.74	2.74	2.74	2.74	2.74	2.74	2.74
$L_{leg}[m]$	6.12	5.88	5.65	5.42	4.99	4.56	4.13

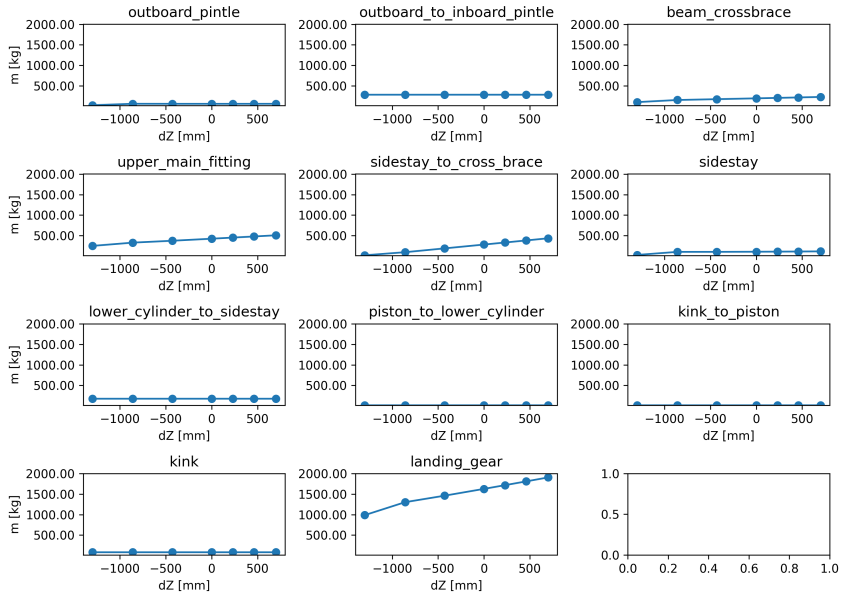

Figure 6.19: V-LS: Varying Gear Length and Sidestay mass plots

According to the results the pintle mass is not sensitive to sidestay increase or decrease. Furthermore, the sidestay mass itself does not experienced large net increase between Δ_Z -430 and 700. The difference is 10 kg. Since the sidestay mass is undersized anyways, this small absolute change is expected and can be improved by fixing the sidestay analysis. Furthermore, it was observed that the critical loadcase for the main fitting changes from Braked2point to Turning. This is potentially implying a more efficient load distribution to the sidestay and could be the cause for increased weight savings. At an overall aircraft level changing the sidestay position has the highest impact on overall landing gear weight as evidenced by a linear slope of 439 kg/m. This implies that the gear weight is most sensitive to changes in sidestay position than crossbrace position. This potentially due to the fact the sidestay is the most ”out of plane” member. The inclusion of more loads may shine more light on exactly which parameters cause this sensitivity.

V-S: Varying Sidestay only

For this case the leg length is fixed and the sidestay attachment point G is moved up and down along the leg. The crossbrace doesn't change.

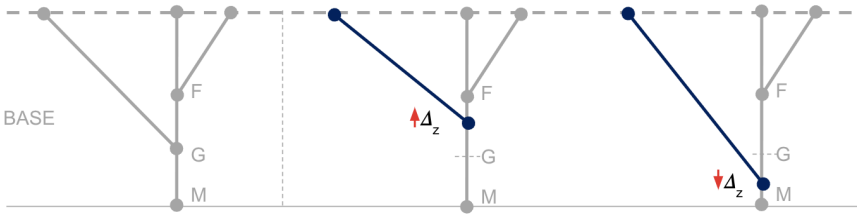

Figure 6.20: V-S: Varying Sidestay

Table 6.9: V-S: Varying Gear Length and Sidestay only

$\delta_z[mm]$	700.0	466.7	233.3	0.0	-400.0	-800.0	-1200.0
$L_{sidestay}[m]$	5.53	5.38	5.24	5.10	4.88	4.69	4.52
$L_{crossbrace}[m]$	2.74	2.74	2.74	2.74	2.74	2.74	2.74
$L_{leg}[m]$	5.42	5.42	5.42	5.42	5.42	5.42	5.42

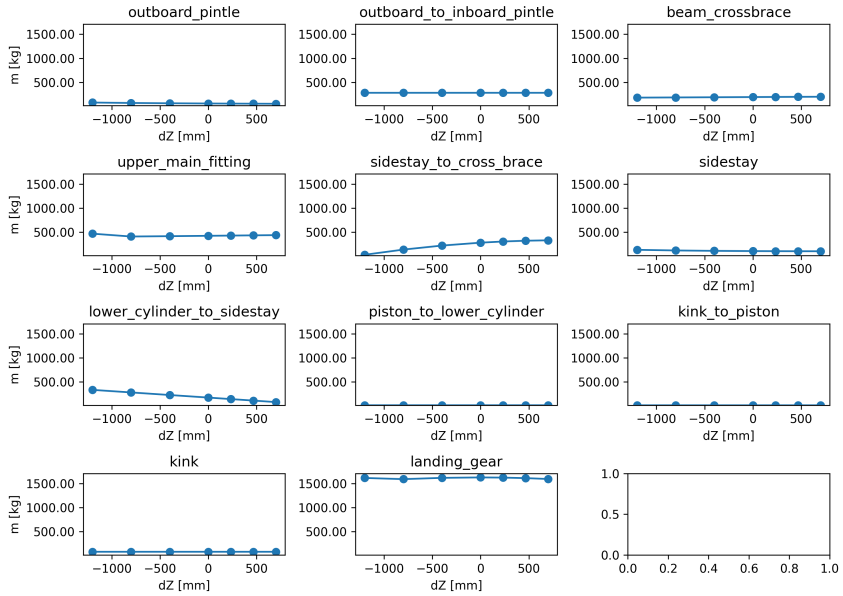

Figure 6.21: V-S: Varying Sidestay mass plots

Looking at Figure 6.23 below, the overall small net change is most likely explained by the fact that the sidestay, given the studied loadcases, doesn't experience substantial stresses. This was already observed during the sizing of the default gear in the previous chapter whereby the sidestay only experiences tensile loads. This was contrary to expectations.

V-C: Varying Crossbrace

For this case the leg length is fixed and the crossbrace attachment point F is moved up and down along the leg. The sidestay doesn't change.

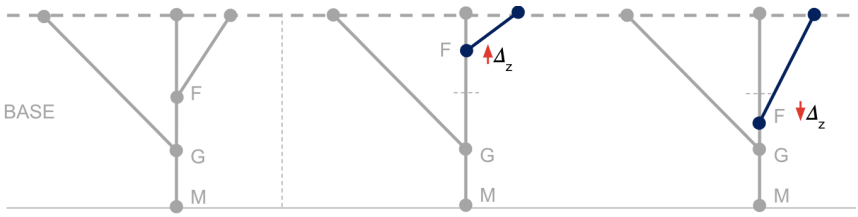

Figure 6.22: V-C: Varying Crossbrace

Table 6.10: V-C: Varying Gear Length and Sidestay

$\delta_z[mm]$	1900.0	1260.0	633.0	0.0	-466.7	-933.3	-1400.0
$L_{sidestay}[m]$	5.10	5.10	5.10	5.10	5.10	5.10	5.10
$L_{crossbrace}[m]$	4.45	3.85	3.29	2.74	2.37	2.04	1.77
$L_{leg}[m]$	5.42	5.42	5.42	5.42	5.42	5.42	5.42

Moving the crossbrace upwards between a Δ_Z of -933 to -1400 significantly increases pintle mass. This is presumably because the pintle now takes up the loads of the crossbrace . Starting at Δ_Z 1260 the pintle weight increases 37% from 281 kg to 386 kg. And then another 260% from 386 kg to 732. The two significant jumps correspond to switch from Braked2point as a critical loadcase to Turning. Between Δ_Z -466 and 1260, the mass is relatively unchanged, and increasing from 1260 to 1900 results in an increase of over 385 kg. Meaning there is an optimal range for crossbrace placement.

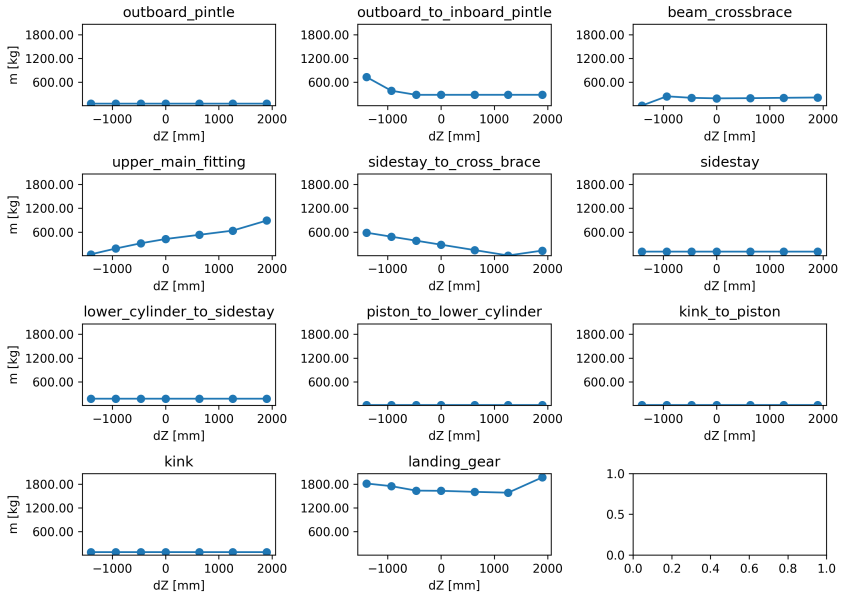

Figure 6.23: V-S: Varying Crossbrace mass plots

6.4.1. Conclusions

The gear length weight sensitivities obtained in the sensitivity study are summarized in Table 6.11. For reference the A310 weight sensitivity has also been included and it is noticeably lower. For reference, Chai and Mason expect a sensitivity of 40 pounds per inch which equals 730 kg/m [24].

Table 6.11: Overall strut length sensitivity results

	kg/m
V-LCS	343
V-LC	352
V-LS	439
V-LCS A310	227

To give an example of how reduction in leg length may affect weight savings it is assumed that an articulated bogie is added which reduces the effective strut length by about 570mm. Applying this the relations as shown in Figure 6.24 shows that weight savings of 1.2 tons are possible by only reducing the structural weight by 21 %. While the absolute numbers should be taken with caution, this observation combined with the significantly higher savings predicted by Chai and Mason point to the significant weight effects of a shorter landing gear.

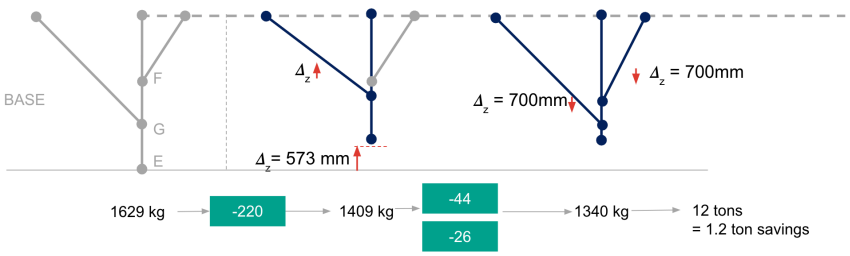

Figure 6.24: Possible weight savings through articulated bogie

7

Conclusion

The aim of this study is to increase the fidelity of the weight estimation of an operationally-feasible Flying V main landing gear by maximising the use of fundamental physics-based analysis methods. This arises from the need to facilitate future multidisciplinary studies which require more accurate weight methods to construct more accurate structural and aerodynamic models, thus aiding in better evaluating aircraft performance and making informed design choices. The research question is approach by first determining what is required for a feasible gear. This is achieved by first refining the landing gear kinematic mechanism by taking into account operational and design considerations which are based on safety regulations and industry practices. The new baseline geometry is then initiated as a beam model and fed into a mass estimation module that is developed and integrated into an existing larger landing gear analysis library. A sizing function is then run to calculate the minimum thickness required per beam to sustain a set of sizing ground loads. The resulting data is processed to identify the critical loads per each beam which is used to calculate a total structural mass for the upper primary structural components.

The kinematic mechanism is refined in order to address a combination of complexities from the previous landing gear mechanism which do not align with considerations of a commercially-feasible landing gear. Following a concept exploration phase, a forward retracting mechanism is chosen with a skewed hinge axis that is capable of positioning the wheels parallel to the rear spar and inside the engine mounting box-structure. A kink is added below the shock absorber in order to offset the bogie pivot point from the leg centerline, which allows the bogie assembly to pack flat inside the stowage bay. As a result, the more compact package significantly reduces the fairing required on the lower surfaces of the Flying V trailing edge while not interfering with the upper contour. The kinematic mechanism is simulated in 3DEXPERIENCE to verify that the modelled components fold realistically and adhere to the recommended design requirements. Finally, the tire failure modes are evaluated for the first time by visually identifying zones of vulnerabilities that may call for additional reinforcement. The resulting new baseline landing gear is considered operationally feasible compared to the predecessor but additional components need to be added such as the torque link, actuators and locking mechanisms in order to fully validate the gears feasibility under all circumstances. Nonetheless, it provides increased understanding of the design space at a system level surrounding the engine and airframe. Furthermore, it provides a more realistic geometry of primary components to be used in the subsequent weight estimation process.

The total landing gear weight is an output of the so-called Landing Gear Mass Module (LGMM) which is a set of functions and classes that were developed during the course of this thesis. The internal forces of the discretized landing gear beam model are calculated using an existing FEA class and fed into a developed stress analysis class capable of calculating the Von Mises and critical buckling stress of each beam. The stress calculations are entirely based on the forces and beam physical properties. A sizing function then makes use of a minimize optimizer to converge to a desired target safety factor of 1.5 from which a critical loadcase and subsequent mass per beam can be found. In accordance with the Class 2.5 weight estimation method, the secondary components weights are computed by deriving the bogie assembly and controls weights from empirical relationships based on statistics. Furthermore, a correction factor is applied to the primary structural mass to account for the undersizing performance of the model. During analysis it was determined that the final weight of a single MLG comes out to 6 tons of which 48% is the structural weight, 40% is the bogie assembly and the remainder being the controls. With a total landing gear of 13.24 tons, the FV1000 landing gear amounts to 5.09 % of the MTOW. This is noticeably is higher than what experts consider structurally efficient gears which range between 3.2 and 4 % of

MTOW. The new mass estimate is also higher than the previously empirically computed mass of 12.3 tons and corresponding % of MTOW of 4.73.

As the cabin-to-floor height of Flying V is the subject of interest in future studies, a sensitivity study was conducted to evaluate the effects of changing the gear length, sidestay and cross-brace attachment positions on the weight of the components and the overall gear. The overall trend points to a linear relationship between weight increase as function of changing the leg length. This is likely attributed to the linear nature of the ground loads. When decreasing the leg length proportionally together with the sidestay the weight sensitivity comes out to 440 kg/m. This is only accounts for the structural weight but is still short of sensitivities in literature that point to up to 700 kg/m. Nonetheless, given the general undersizing performance of LGMM, the overall trend of a large sensitivity to gear length is observed.

Overall the goal of the study is to add knowledge and insights to the FV landing gear at component-level and its effects on the integration into the surrounding environment. The new kinematic design is evidence of a potential mechanism that full-fills key design considerations in the scope of the available design space. The mechanism aims to implement as many tried and tested features of past gear designs however the addition of complexities within the pintle and bogie design should remind future designers that that the landing gear mechanism is influenced by the aircraft structure and aerodynamic performance needs. Nonetheless, the primary structure of the main landing gear experiences many of the same critical ground loadcases except for the sidestay which behaves in a different function as expected. The Flying V landing gear is unconventionally long due to the pitch and roll wingtip strike requirements and this was reflected in the overall higher total landing mass as percentage of MTOW.

8

Future Recommendations

Following this study it was observed that a weight estimation tool can be implemented on Flying V landing gear and that the structural mass of primary components can be estimated using physics-based methods and validated using conventional landing gear data. However, accurately calculating secondary components, adding loads and modelling remaining key kinematic components are still required to refine the weight estimate and in turn better understand the weight effects during the entire aircraft design process. It is important to continue iterating on the landing gear design in order to eventually achieve an optimal weight that doesn't detract from the Flying V's performance gains as well as to ensure the Flying V can safely operate compared to reference aircraft. The follow sections aims to list a few recommendations that could aid future build on the current study or apply the lessons learned from this study.

- Currently it is assumed that the primary components in the kinematic mechanism are capable of being actuated and locked in position. However, with enough complexity any mechanism can be achieved so the question isn't whether it is possible but rather at what cost. Preliminary actuator power requirements could be a logical next step to estimate the weight of the required actuators which from a initial observation face a large mass and are provided with a short lever arm. The estimated weight can be used to replace the statistical "controls" percentage which was used in this study.
- Dynamic loads and static landing loads were not considered in the sizing of the beams. And while ground loads do provide a good sizing loads for conventional aircraft based on statistic, the study shows that certain components like the shock-absorber and sidestay are most likely sized by landing or dynamic loads. And although the shock-absorber doesn't interface with other Flying-V stuctures, it is heavily influeced by aircraft roll rate, pitch rate, landing speed and other top-level performance characteristics. This in turn influences the shock absoberdiameter which could influence the entire geometry of the landing gear and thus the weight.
- Once multi-body model of the Flying V exists the Spin-up and spring-back forces should be derived for a flexible gear and support structure. It is expected that large slenderness of the gear can be susceptible to oscillations. Off-center buckling should also be considered as a next step as well as the investigation of different beam cross-sections since the all-tubular assumption is a simplification applicable to early design phases.
- The leg length is major driver of mass and so it is in the interest of the Flying V to reduce the leg length as much as possible. The leg length currently is limited by the wingtip strike clearance during a pitch-roll requirements. If these requirements can't be negotiated through flight control adjustments then there are complexities that can be added to reduce the effective leg length. These include a shortening mechanism, as seen on the 737-10, Concorde or A330, jump strut or articulating bogie. Another alternative could be a folding outer wing tip which draws inspiration from Bourgets dihedral study and the 777-X.
- Finally, although the Landing Gear Mass Module is rapid at calculating the weight estimate for variations of a given geometry. Practical implementation at FPO during the validation process showed that the LGMM geometry generation function is not mature enough to be used independetly. If the designer is not familiar with landing gears then there are not enough fail-safes in the code to ensure that the geometry is iniated properly. Further documentation or robustness needs to be added if the code is to be further integrated in to the overall landing gear analysis library.

References

[1] Rico Luman et al. *Global aviation outlook: delayed but persuasive recovery despite new turbulence*. Tech. rep. ING Bank, Apr. 2022.

[2] J. Benad. “The Flying V - a New Aircraft Configuration for Commercial Passenger Transport”. In: *Deutscher Luft- und Raumfahrtkongress* (2015), pp. 1–8. URL: http://www.dglr.de/publikationen/2015/370094.pdf.

[3] Michael C. Niu. *Airframe Structural Design*. Burbank: Conmilit Press Ltd., 1988.

[4] F.R. Shanley. *Weight-strength analysis of aircraft structures*. 2nd ed. Los Angeles, California: Dover publications inc., 1960.

[5] Robert K. Schmidt. *The Design of Aircraft Landing Gear*. Burbank: SAE International, 2021.

[6] D.W Young. “Proceedings of the Institution of Mechanical Engineers , Part D: Journal of Systems and Control Engineering”. In: *Proceedings of the Institution of Mechanical Engineers , Part D: Journal of Systems and Control Engineering* (1986), pp. 75–92.

[7] G Bourget. “The effect of landing gear implementation on Flying V aerodynamics, stability and controllability”. In: (2020). URL: http://resolver.tudelft.nl/uuid:599eca91-6200-4d29-8dd7-e4e7060703e1.

[8] Daniel P. Raymer. *Aircraft Design: A Conceptual Approach*. Reston, Virginia: American Institute of Aeronautics and Astronautics (AIAA), 2018.

[9] P. Beaudet et al. “Failure Analysis Case Histories of Canadian Forces Aircraft Landing Gear Components”. In: *AGARD Conference Proceedings 484*. Povoa de Varzim, Portugal: AGARD, 1990, Article 1 Page 1.

[10] R C J Voeten. “Flying-V A design methodology for un-conventional engine mounting structures”. PhD thesis. Delft University of Technology, 2022. URL: http://resolver.tudelft.nl/uuid:8ae4ad77-43d6-44d4-ae34-bb3b118587dd.

[11] G J de Zoeten. “Comparative Flight Performance Evaluation of the Flying-V and a Reference Aircraft”. PhD thesis. Delft University of Technology, 2022.

[12] T. Cappuyns. *Handling Qualities of a Flying V Configuration*. Delft: Delft University of Technology, 2019.

[13] J. Roskam. “Airplane design, part IV, layout design of landing gear system”. In: *Roskam aviation &engineering corp. 1st* (1986).

[14] EASA. *Certification Specifications for Large Aeroplanes CS-25*. 3rd ed. Cologne, Germany: European Aviation Safety Agency, 2007.

[15] Pedro Albuquerque et al. *Evaluation of Structural Loads*. Tech. rep. December 2014. Lisboa: Técnico Lisboa, 2012. DOI: 10.13140/2.1.4615.3288.

[16] G. Kempf et al. “Development of Undercarriage Design Loads”. In: *AGARD Conference Proceedings 484*. Povoa de Varzim, Portugal: AGARD, 1990, Article 4 Page 1. DOI: 10.1002/9781118352700.

[17] Norman S. Currey. *Aircraft Landing Gear Design - Principles and Practices*. Marietta, Georgia: American Institute of Aeronautics and Astronautics (AIAA), 1988.

[18] Ted Lomax. *Structural Loads Analysis for Commercial Transport Aircraft Theory and Practice*. Reston, Virginia: American Institute of Aeronautics and Astronautics (AIAA), 1996.

[19] S. F. N. Jenkins. “Landing gear design and development”. In: *Proceedings of the Institution of Mechanical Engineers, Part G: Journal of Aerospace Engineering* 203.1 (1989), pp. 67–73. DOI: 10.1243/PIME{_}PROC{_}1989{_}203{_}055{_}01.

[20] H. Wentscher et al. “The Design, Qualification and Maintenance of Vibration-Free Landing Gear”. In: *AGARD Report 800*. March. 1996, Article 5 Page 5.

[21] Peijun Wu. “A Physics-based Approach to Assess Critical Load Cases for Landing Gears within Aircraft Conceptual Design”. PhD thesis. 2019, p. 289. DOI: 10.4233/uuid.

[22] J.R. McGehee et al. *Analytical Investigation of the Landing Dynamics of a Large Airplane with a Load-Control System in the Main Landing Gear*. Tech. rep. 2. 1979, pp. 301–310. DOI: 10.1016/0021-8928(76)90067-8.

[23] Camille Parat et al. “Design and stiffness analysis of an overconstrained landing gear retraction mechanism with four side-stays”. In: *Proceedings of the Institution of Mechanical Engineers, Part G: Journal of Aerospace Engineering* 233.12 (2019), pp. 4421–4435. DOI: 10.1177/0954410018824509.

[24] Sonny T. Chai et al. *Landing Gear Integration in Aircraft Conceptual Design*. Tech. rep. Blacksburg: Virginia Polytechnic Institute and State University, 1996.

[25] Condor. *Ein Fahrwerkwechsel bei einem Flugzeug*. [Online; accessed September 07, 2022]. 2020. URL: https://www.condor.com/de/blog/ein-fahrwerkwechsel-bei-einem-flugzeug/.

[26] J. Miller. *Convair B-58 Hustler: The World’s First Supersonic Bomber*. 1st ed. Hinckley, England: AeroFax, 1985.

[27] Ali Elham et al. “An Advanced Quasi-Analytical Weight Estimation Method for Airplane Lifting Surfaces Ali Elham”. In: 3571. Bad Goegging and Manching: Society of Allied Weight Engineers, Inc., 2012.

[28] A. Elham et al. “Development and implementation of an advanced, design-sensitive method for wing weight estimation”. In: *Aerospace Science and Technology* 29.1 (2013), pp. 100–113. DOI: 10.1016/j.ast.2013.01.012. URL: http://dx.doi.org/10.1016/j.ast.2013.01.012.

[29] Michael C. Niu. *Synthesis of Subsonic Airplane Design*. 1st ed. Delft, Netherlands: Delft University Press, 1982.

[30] Paul R. Kraus. “An Analytical Approach to Landing Gear Weight Estimation”. In: *29th Annual Conference of SAWE, Inc.* Washington D.C: SAWE, 1970.

[31] Richard G. Budynas. *Shigley’s Mechanical Engineering Design 9th Edition*. New York: McGraw-Hill, 2011.

[32] W J Oosterom. “Flying-V Family Design”. PhD thesis. Delft University of Technology, 2021. URL: http://repository.tudelft.nl/..

[33] C Busch et al. “Homogeneous reporting of Pavement Classification Number (PCN) in an Airport Pavement Management System”. In: *… of the International Conferences on the …* January 2013 (2013). URL: https://www.ntnu.no/ojs/index.php/BCRRA/article/view/2614.

[34] Angeliki Armeni et al. “Preliminary evaluation of the ACR-PCR system for reporting the bearing capacity of flexible airfield pavements”. In: *Transportation Engineering* 8.May (2022), p. 100117. DOI: 10.1016/j.treng.2022.100117. URL: https://doi.org/10.1016/j.treng.2022.100117.

[35] Technial Data Support et al. *A330 Aircraft Characteristics Airport and Maintenance Planning*. Blagnac Cedex: Airbus S.A.S, 2005.

[36] D.R. Brill. *ACR/PCR Overview*. Federal Aviation Administration, 2020.

[37] Technial Data Support et al. *A350 Aircraft Characteristics Airport and Maintenance Planning*. Blagnac Cedex: Airbus S.A.S, 2005.

[38] LNVL. *eAIP EH-AD-2 EHAM — AMSTERDAM/SCHIPHOL*. https://eaip.lvnl.nl/web/2023-04-06-AIRAC/html/eAIP/EH-AD-2.EHAM-en-GB.html. Accessed 01/11/23. 2023.

[39] Battelle Memorial Institute. *Metallic Materials Properties Development and Standardization (MMPDS-17)*. Battelle Memorial Institute, 2022.

[40] Behrooz Farshi et al. “Buckling analysis of structural steel frames with inelastic effects according to codes”. In: *Journal of Constructional Steel Research* 65.10-11 (2009), pp. 2078–2085. DOI: 10.1016/j.jcsr.2009.04.018.

[41] A. Nuti et al. “Design of a Fuselage-Mounted Main Landing Gear of a Medium-Size Civil Transport Aircraft”. In: *Aerotecnica Missili & Spazio* 97.2 (2018), pp. 85–95. DOI: 10.1007/bf03405803.

[42] FedEX. *Airbus A300-600/A310-200 Airframe Systems*. 2001.

[43] Jacques Veaux. *New design procedures applied to landing gear development*. 1988. DOI: 10.2514/3.45678.

[44] AIRBUS S.A.S. *A340-200/-300 Facility Planning Manual Maintenance Facillity Planning MFP*. Tech. rep. Blagnac Cedex, 2002.

[45] Swanee Yourkowski. *777 Tour Facts Data*. 2003.

[46] AIRBUS S.A.S. “A340-500/-600 Facility Planning Manual Maintenance Facility Planning MFP”. Blagnac Cedex, 2002.

[47] Chris Brady. *The Boeing 737 Technical Guide*. Lulu.com, 2011.

[48] Ministere des Armees. *AIP AD-2 LFML — MARSEILLE PROVENCE*. https://www.dircam.dsae.defense.gouv.fr/images/Stories/Doc/MIAC1/miac1_marseille_lfml.pdf. Accessed 01/11/23. 2023.

A

Additional Kinematic Visualizations

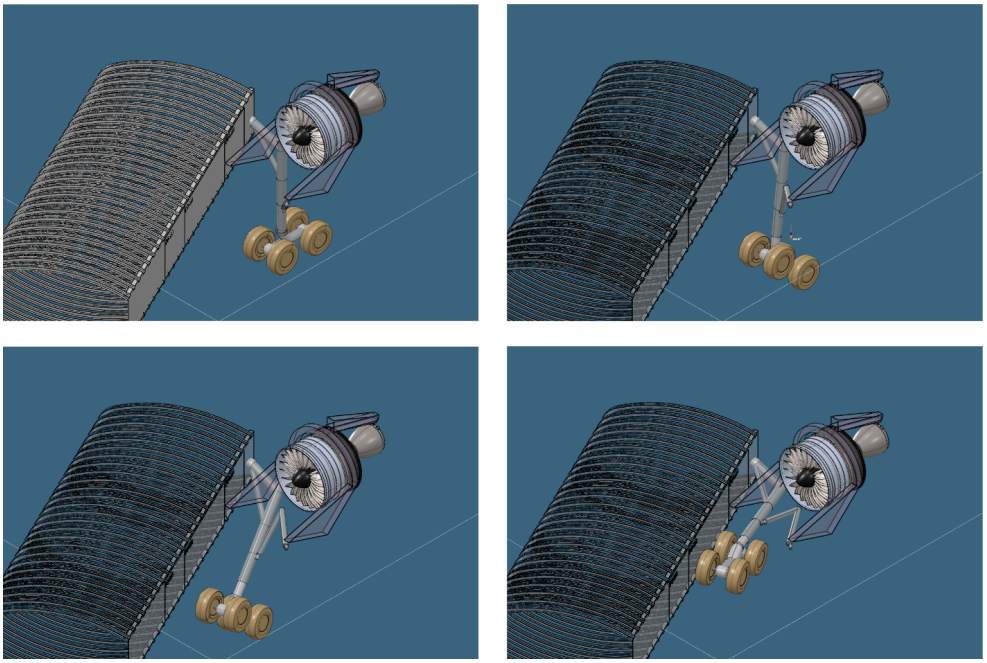

Figure A.1: Baseline MLG Kinematic with engine frame and fuselage

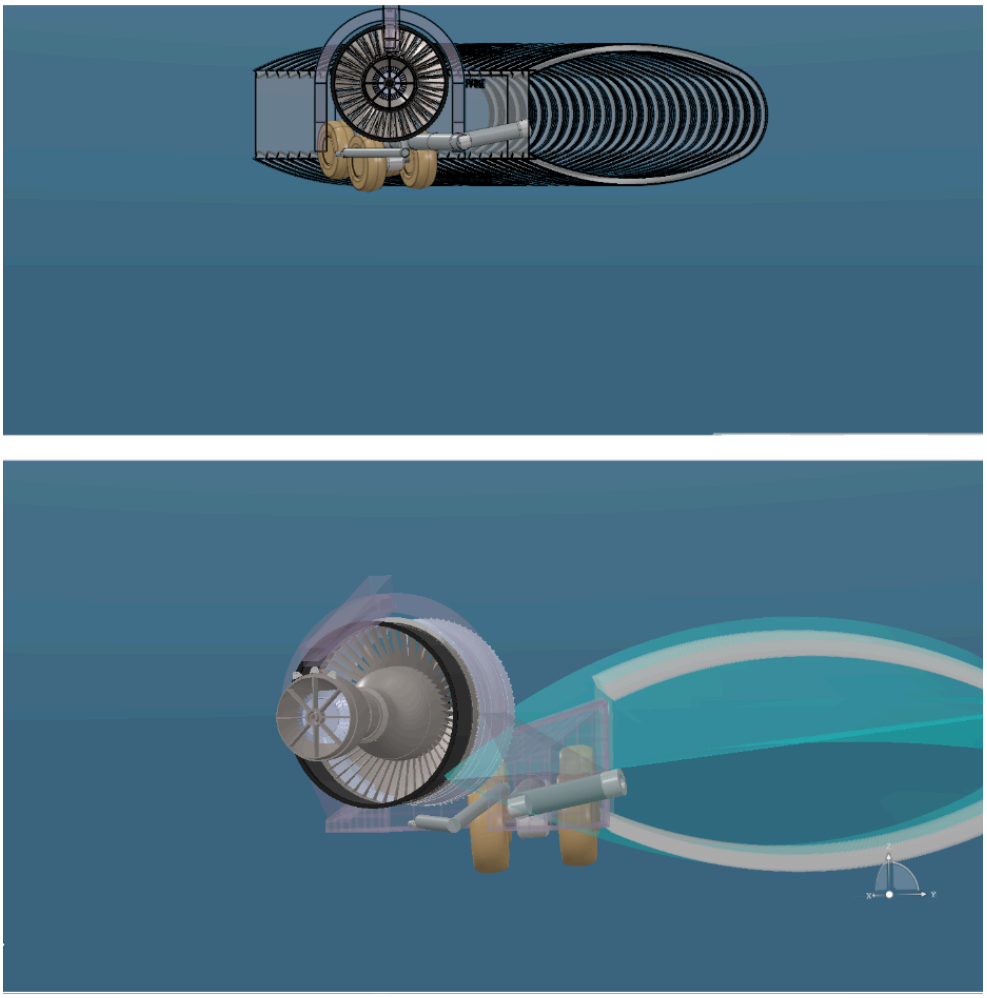

Figure A.2: Baseline MLG back-view stowed position

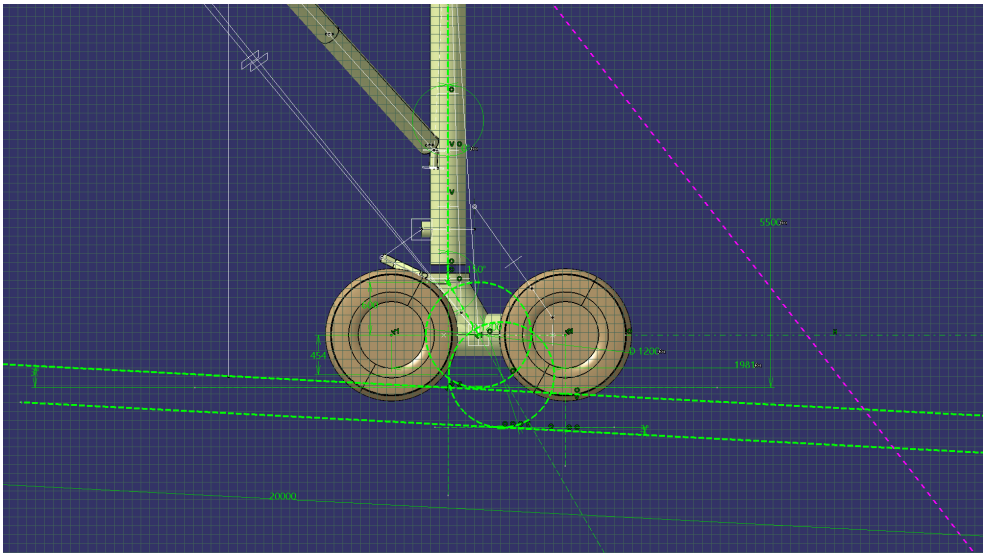

Figure A.3: Paramterized Bogie sketch

B

Baseline Flying V

B.1. Input for LGMM

```
# Define Baseline Aircraft
ac_flyingv = Aircraft(mac=18740.,
                      mac_ch25_x=25770.,
                      hfd_z=6625.0,
                      mlg_x=32400.,
                      geartrack=12200.,
                      mlg_track=1397.,
                      nlg_track=710.,
                      nlg_x=6500.)

ac_flyingv.mlg_wtb = {'tyre_n': 8, 'tyre_code': '1400x530R23PR40'}
ac_flyingv.nlg_wtb = {'tyre_n': 2, 'tyre_code': '1050x395R16PR28'}

ac_flyingv.bogie_pitch = {'fwd_bogie_pitch': 1981.}
ac_flyingv.name = 'FV1000_kinked'

mtow_loadcase = Loadcase(mass=260000,
                               fwd_cg_x_mac_k=None,
                               aft_cg_x_mac_k=0.575,
                               cg_z=0,
                               casename='MTOW')

ac_flyingv.add_loadcase(mtow_loadcase)
```

C

Lomax validation

Table 7.5 Turn radius for ground turn conditions calculated using Eq. (7.58) assuming the following constants: c = 562.3 in., T = 206 in., and n_y is the lateral load factor developed during the turn

	n_y, limit	W, lb	CG, % mac/100	A, in.	E, in.	V_{MGs},[a] lb limit	V_{MG},[b] lb limit
Design ground turn condition	0.50	143,000	0.28	527.55	102.2	67,081	102,554
Overweight operation	0.428	150,500	0.28	527.55	102.2	70,600	102,554

Figure C.1: Table 7.5 Turn radius for ground turn conditions calculated using Eq. (7.58) assuming the following constants: c = 562.3 in., T = 206 in., and n y is the lateral load factor developed during the turn [18]

Table 7.1a Design ground loads for right main gear only of a cargo airplane with a lateral unbalance

Weight cond.	W, lb	CG, % mac/100	M_{unbal}, in.-lb	BL_{cg}, in.	A, in.	E, in.
MTW	120,000	0.25	500,000	4.17	411.8	110.0
MLW	105,000	0.34	500,000	4.76	423.9	110.0

C, in. = 450.0 T, in. = 210.0

Cond. type	n_z	n_y	Coefficient friction	V_{MGr}, lb ult.[a]	D_{MGr}, lb ult.[a]	S_{MGr} lb ult.[a]
Main gear loads at maximum taxi weight (MTW)						
Two-point braked roll	1.0	0	0.80	93,600	74,900	0
Three-point braked roll	1.0	0	0.80	72,500	58,000	0
Unsymmetrical braked roll	1.0	0	0.80	78,300	62,600	7,000
Reversed braked roll	1.0	0	0.55	85,900	−47,200	0
Ground turn	1.0	−0.50	0	133,100	0	−66,500
Taxi/takeoff	2.0	0	0	171,800	0	0
Pivot	1.0	0	0.80	85,900	0	0
Towing	1.0	0	0	85,900	27,000	0

Figure C.2: Table 7.1a Design ground loads for right main gear only of a cargo airplane with a lateral unbalance [18]

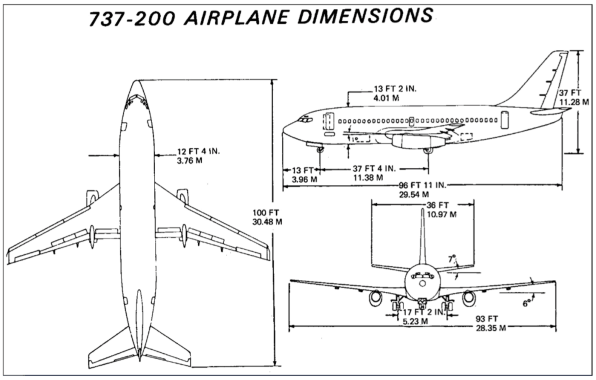

Std Weights (kg):		
Max. ramp	44361	52615
Max. take-off	**44225**	**52390**
Max. landing	40687	46720
Max. zero-fuel	38555	43091

Undercarriage:		
Track (m)	5.23	5.23
Wheelbase (m)	10.46	11.38
Turning radius (m)	17.20	17.58
No. of Nose Wheels	2	2
Nose Wheel Diameter (Inches)	24	24
Nose Wheel Tread Width (Inches)	7.75	7.75
Nose Tyre Pressure (psi)		
No. of Main Wheels	4	4
Main Wheel Diameter (Inches)	40	40
Main Wheel Tread Width (Inches)	14.5	14.5
Main Tyre Pressure (psi)	133	183

Std Weights (kg):		
Max. ramp	44361	52615
Max. take-off	**44225**	**52390**
Max. landing	40687	46720
Max. zero-fuel	38555	43091

Figure C.3: 737-200 Aircraft Characteristics [47]

D

A310 Validation Loads

D.1. Drag stay raw results

Table D.1: Beam GA: dragstay internal loads results on A310-200 Main Landing Gear

Loadcase	V_{x1}	V_{y1}	V_{z1}	V_{x2}	V_{y2}	V_{z2}
Taxi	311603.7	2.47E-10	861.2	311603.7	2.47E-10	861.2
Brake2point	2712055.7	1.90E-09	6352.4	2712055.7	1.90E-09	6352.4
Pivot	138991.5	-20657.05	706.9	138991.5	-20657.05	706.9
Turn	239293.2	-1278.60	386.3	239293.2	-1278.60	386.3

Loadcase	M_{x1}	M_{y1}	M_{z1}	M_{x2}	M_{y2}	M_{z2}
Taxi	1.36E-10	-1.14E-13	3.83E-10	1.36E-10	2437.0	-3.1616E-10
Brake2point	8.92E-10	0	2.55E-09	8.92E-10	17976.6	-2.8122E-09
Pivot	-6050.542429	2.67E-12	-17254.15826	-6050.542429	2000.3	41203.06
Turn	-1146.159042	5.68E-13	-3268.468857	-1146.159042	1093.1	349.83

Table D.2: Beam GA: dragstay internal loads results on A310-200 Main Landing Gear

Loadcase	V_{x1}	V_{y1}	V_{z1}	V_{x2}	V_{y2}	V_{z2}
Taxi	311603.7	2.47E-10	861.2	311603.7	2.47E-10	861.2
Brake2point	2712055.7	1.90E-09	6352.4	2712055.7	1.90E-09	6352.4
Pivot	138991.5	-20657.05	706.9	138991.5	-20657.05	706.9
Turn	239293.2	-1278.60	386.3	239293.2	-1278.60	386.3

Loadcase	M_{x1}	M_{y1}	M_{z1}	M_{x2}	M_{y2}	M_{z2}
Taxi	1.36E-10	-1.14E-13	3.83E-10	1.36E-10	2437.0	-3.1616E-10
Brake2point	8.92E-10	0	2.55E-09	8.92E-10	17976.6	-2.8122E-09
Pivot	-6050.542429	2.67E-12	-17254.15826	-6050.542429	2000.3	41203.06
Turn	-1146.159042	5.68E-13	-3268.468857	-1146.159042	1093.1	349.83

Table D.3: Beam GA: dragstay results on A310-200 Main Landing Gear

Load case	sizing_mass	Mass [kg]
Taxi	0	6.858670421
Brake2point	1	56.85896386
Pivot	0	13.24842997
Turn	0	6.982027023
Load case	sizing_convergence	Sizing criteria: (stress ratio, buckling ratio)
Taxi	0	Unconverged: (1.5748), (0.0)
Brake2point	1	Stress: (1.5), (0.0)
Pivot	1	Stress: (1.5), (0.0)
Turn	1	Stress: (1.5), (0.0)
Load case	sizing_geometry	Condition: (inner_d, outer_d, t)
Taxi	0	Invalid: (140.0, 141.4, 0.7)
Brake2point	1	Valid: (140.0, 151.1487, 5.6)
Pivot	1	Valid: (140.0, 142.4402, 1.2)
Turn	0	Invalid: (140.0, 141.4, 0.7)

D.2. Sidestay raw results

Table D.4: Beam FS: sidestay internal loads results on A310-200 Main Landing Gear

Loadcase	V_{x1}	V_{y1}	V_{z1}	M_{x1}	M_{y1}	M_{z1}
Taxi	0.00	0.00	0.00	0.00	0.00	0.00
Brake2point	0.00	0.00	0.00	0.00	0.00	0.00
Pivot	24407.22	0.00	0.00	0.00	0.00	0.00
Turn	-1059378.22	0.00	0.00	0.00	0.00	0.00

Loadcase	V_{x2}	V_{y2}	V_{z2}	M_{x2}	M_{y2}	M_{z2}
Taxi	0.00	0.00	0.00	0.00	0.00	0.00
Brake2point	0.00	0.00	0.00	0.00	0.00	0.00
Pivot	24407.22143	0.00	0.00	0.00	0.00	0.00
Turn	-1059378.222	0.00	0.00	0.00	0.00	0.00

Table D.5: Beam FS: sidestay results on A310-200 Main Landing Gear

Load case	sizing_mass	Mass [kg]
Taxi	0	2.756
Brake2point	0	2.756
Pivot	0	2.756
Turn	1	96.037
Load case	sizing_convergence	Sizing criteria: (stress ratio, buckling ratio)
Taxi	0	No load: (0.0), (0.0)
Brake2point	0	Unconverged: (0.0), (1513636238968.496)
Pivot	0	Unconverged: (8.3091), (0.0)
Turn	1	Buckling: (6.672), (1.5)
Load case	sizing_geometry	Condition: (inner_d, outer_d, t)
Taxi	0	Invalid: (90.0, 90.9, 0.45)
Brake2point	0	Invalid: (90.0, 90.9, 0.45)
Pivot	0	Invalid: (90.0, 90.9, 0.45)
Turn	1	Valid: (90.0, 117.3642, 13.7)

D.3. Piston Raw Results

Table D.6: Beam PM: piston internal loads results on A310-200 Main Landing Gear

Loadcase	V_{x1}	V_{y1}	V_{z1}	M_{x1}	M_{y1}	M_{z1}
Taxi	-1310240.84	0.00	68689.41	0.00	29494.66	0.00
Brake2point	-666383.25	0.00	592908.35	0.00	254761.07	0.00
Pivot	-655120.42	0.00	34344.71	-680182.70	14747.33	35658.60
Turn	-994855.48	498110.83	52155.33	-8.01	22395.06	-214037.44

Loadcase	V_{x2}	V_{y2}	V_{z2}	M_{x2}	M_{y2}	M_{z2}
Taxi	-1310240.84	0.00	68689.41	0.00	58536.67	0.00
Brake2point	-666383.25	0.00	592908.35	0.00	505443.79	0.00
Pivot	-655120.42	0.00	34344.71	-680182.70	29268.34	35658.60
Turn	-994855.48	498110.83	52155.33	-8.01	44446.43	-424639.61

E

FV Baseline Gear Loads

E.1. External loads

Table E.1: Baseline Left MLG external loads for different ground loads

Loadcase	$Fx_l\,[kN]$	$Fy_l\,[kN]$	$Fz_l\,[kN]$	$Mx_l\,[kN]$	$My_l\,[kN]$	$Mz_l\,[kN]$
Taxi	0	0	2500	0	0	0
Brake	1020	0	1275	0	0	0
Pivot	0	0	1250	0	0	1950
Turn	0	280	560	0	0	0

E.2. Sidestay loads

E.2.1. Right sidestay

Table E.2: Beam GS: Right sidestay internal loads results on FV1000 Baseline Main Landing Gear

Loadcase	V_{x1}	V_{y1}	V_{z1}	M_{x1}	M_{y1}	M_{z1}
Taxi	411146.41	0.00	0.00	0.00	0.00	0.00
Brake2point	2791776.41	0.00	0.00	0.00	0.00	0.00
Pivot	-59.90	0.00	0.00	0.00	0.00	0.00
Turn	-62839.91	0.00	0.00	0.00	0.00	0.00

Loadcase	V_{x2}	V_{y2}	V_{z2}	M_{x2}	M_{y2}	M_{z2}
Taxi	411146.41	0.00	0.00	0.00	0.00	0.00
Brake2point	2791776.41	0.00	0.00	0.00	0.00	0.00
Pivot	-59.90	0.00	0.00	0.00	0.00	0.00
Turn	-62839.91	0.00	0.00	0.00	0.00	0.00

E.3. Crossbrace loads

E.3.1. Right Crossbrace

Table E.3: Beam FA: Right crossbrace internal loads results on FV1000 Baseline MLG

Loadcase	$V_{x1}\,[N]$	$V_{y1}\,[N]$	$V_{z1}\,[N]$	$V_{x2}\,[N]$	$V_{y2}\,[N]$	$V_{z2}\,[N]$
Taxi	762232.81	-5353.10	887.72	762232.81	-5353.10	887.72
Brake2point	5613235.48	-39998.94	42422.65	5613235.48	-39998.94	42422.65
Pivot	22748.66	-18703.13	-2407.78	22748.66	-18703.13	-2407.78
Turn	5413862.29	1919.21	77281.00	5413862.29	1919.21	77281.00

Loadcase	$M_{x1}\,[N]$	$M_{y1}\,[N]$	$M_{z1}\,[N]$	$M_{x2}\,[N]$	$M_{y2}\,[N]$	$M_{z2}\,[N]$
Taxi	2771.27	-13654.31	-13979.73	2771.27	-11217.77	712.94
Brake2point	18772.60	-171673.92	-102397.50	18772.60	-55236.30	7387.75
Pivot	-11478.96	5104.16	-42643.81	-11478.96	-1504.49	8690.74
Turn	21636.22	-236845.48	16168.73	21636.22	-24732.01	10901.05

E.3.2. Left Crossbrace

Table E.4: Beam FA: Left crossbrace internal loads results on FV1000 Baseline MLG

Loadcase	$V_{x1}\,[N]$	$V_{y1}\,[N]$	$V_{z1}\,[N]$	$V_{x2}\,[N]$	$V_{y2}\,[N]$	$V_{z2}\,[N]$
Taxi	762244.54	-5364.79	-897.61	762244.54	-5364.79	-897.61
Brake2point	5611626.36	-40063.68	-42569.40	5611626.36	-40063.68	-42569.40
Pivot	618274.92	79761.20	-17343.42	618274.92	79761.20	-17343.42
Turn	1572975.51	477.32	-23468.17	1572975.51	477.32	-23468.17

Loadcase	$M_{x1}\,[N]$	$M_{y1}\,[N]$	$M_{z1}\,[N]$	$M_{x2}\,[N]$	$M_{y2}\,[N]$	$M_{z2}\,[N]$
Taxi	-2776.98	13674.64	-14006.45	-2776.98	11210.97	718.31
Brake2point	-18801.73	171836.50	-102527.90	-18801.73	54996.09	7435.03
Pivot	-60486.75	46445.06	184991.48	-60486.75	-1157.49	-33929.41
Turn	-6343.84	68922.64	4811.07	-6343.84	4509.45	3500.96

F

Airport PCN classifications

This Appendix contains pavement classifications for Schiphol Airport and Marseille Airport, to be used with ACN-PCN method for determining aircraft-ground compatibility. The PCN's for other Airports can typically be found by searching for the Airport code followed by "AIP" (Aeronautical Information Publication). Note that from 2024 the ACR-PCR method will be used.

Table F.1: ELHAM Schiphol Airport Pavement Classification [38]

RWY	Construction	Type	Subgrade (CBR)	Max tire pressure	PCN
4	Asphalt	Flexible	C	Unlimited	79
22	Asphalt	Flexible	C	Unlimited	79
6	Asphalt	Flexible	C	Unlimited	89
24	Asphalt	Flexible	C	Unlimited	89
9	Asphalt	Flexible	C	Unlimited	89
27	Asphalt	Flexible	C	Unlimited	89
18C	Asphalt	Flexible	C	Unlimited	89
36C	Asphalt	Flexible	C	Unlimited	89
18L	Asphalt	Flexible	C	Unlimited	89
36R	Asphalt	Flexible	C	Unlimited	89
18R	Asphalt	Flexible	C	Unlimited	89
36L	Asphalt	Flexible	C	Unlimited	89

Table F.2: LFML Marseille Airport Pavement Classification [48]

RWY	Construction	Type	Subgrade (CBR)	Max tire pressure	PCN
13L	Concrete	Rigid	B	Unlimited	58
31R	Concrete	Rigid	B	Unlimited	58
13R	Concrete	Flexible	C	Unlimited	70
31L	Concrete	Fleible	C	Unlimited	70